ISSN 2959-0663 (Print)
ISSN 2959-0671 (Online)
ISSN-L 2959-0663

EURASIAN JOURNAL OF CHEMISTRY

2023. No. 1(109)

ISSN 2959-0663 (Print)
ISSN 2959-0671 (Online)
ISSN-L 2959-0663

EURASIAN JOURNAL OF CHEMISTRY

2023

No. 1(109)

January–February–March

March, 30th, 2023

Founded in 1996

Published 4 times a year

Karaganda, 2023

Publisher: **Karagandy University of the name of academician E.A. Buketov**

Postal address: 28, University Str., Karaganda, 100024, Kazakhstan

E-mail: chemistry.vestnik@ksu.kz; irina.pustolaikina@ksu.kz; ipustolaikina@gmail.com

Tel./fax: +7(7212) 34-19-40.

Web-site: http://chemistry-vestnik.ksu.kz

Editor I.N. Murtazina

Computer layout V.V. Butyaikin

Eurasian Journal of Chemistry. — 2023. — No. 1(109). — 89 p.

ISSN 2959-0663 (Print). ISSN 2959-0671 (Online). ISSN-L 2959-0663

Proprietary: NLC "Karagandy University of the name of academician E.A. Buketov".

Registered by the Ministry of Information and Social Development of the Republic of Kazakhstan. Re-registration certificate No. KZ95VPY00063697 dated 30.01.2023.

Signed in print 27.03.2023. Format 60×84 1/8. Offset paper. Volume 11,13 p.sh. Circulation 200 copies. Price upon request. Order № 29.

Printed in the Publishing house of NLC "Karagandy University of the name of acad. E.A. Buketov". 28, University Str., Karaganda, 100024, Kazakhstan. Tel.: +7(7212) 35-63-16. E-mail: izd_kargu@mail.ru

CONTENTS

Министерство информации и общественного развития Республики Казахстан

Комитет информации

СВИДЕТЕЛЬСТВО
о постановке на переучет периодического печатного издания, информационного агентства и сетевого издания

№ KZ95VPY00063697 Дата выдачи 30.01.2023
г.Астана

Название: журнал,EURASIAN JOURNAL Of CHEMISTRY
Язык: английский
Периодичность: 4 раза в год
Собственник: Некоммерческое акционерное общество "Карагандинский университет имени академика Е. А. Букетова"
Тематическая направленность: публикация научных статей по актуальным направлениям фундаментальных и прикладных исследований в области неорганической, органической, физической химии, химической технологии, методики химии
Территория распространения: Республика Казахстан и зарубежные страны
Дата и номер первичной постановки на учет:
23.10.2012, 13110-Ж

Заместитель председателя Есмағұл Ілияс Ізімғалиұлы

PREFACE

ABOUT CHANGING THE TITLE OF THE JOURNAL

Dear Readers, Authors, and Reviewers,

In 2022, the Editorial Board of the "Bulletin of the Karaganda University. Chemistry series" journal decided to change its title to "EURASIAN JOURNAL OF CHEMISTRY" with the aim of further development and promotion at the international level. This decision was supported by the leadership of Karagandy University of the name of academician E.A. Buketov by the Rector′s Order No.1708 dated December 28, 2022.

On January 30, 2023, the journal received a certificate of re-registration of the periodical printed edition No.KZ95VPY00063697 from the Information Committee of the Ministry of Information and Social Development of the Republic of Kazakhstan.

On February 23, 2023, "EURASIAN JOURNAL OF CHEMISTRY" received new ISSN 2959-0663 (Print), ISSN 2959-0671 (Online) from the ISSN International Center.

Today it is our greatest pleasure to introduce the first issue of the "EURASIAN JOURNAL OF CHEMISTRY", which includes 9 articles by the authors from Kazakhstan, Russia, India, Czech Republic and Saudi Arabia.

"EURASIAN JOURNAL OF CHEMISTRY" (ISSN 2959-0663 (Print), ISSN 2959-0671 (Online) continues founded in 1996 "Bulletin of the Karaganda University. Chemistry series" (ISSN 2518-718X (Print), ISSN 2663-4872 (Online) journal. The founder and publisher of the journal is *Karagandy University of the name of academician E.A. Buketov*, Karaganda, Kazakhstan.

The main purpose of the "EURASIAN JOURNAL OF CHEMISTRY" is to provide an authoritative internationally recognized open public platform for publishing the results of scientific research in the field of chemistry for national and international authors.

Journal is published 4 times a year. The subject of the journal includes such sections as: organic chemistry, physical and analytical chemistry, inorganic chemistry, chemical technology. Manuscripts are accepted in English on an ongoing basis in accordance with the IMRAD structure in the form of full research articles, as well as author reviews. Articles are published and distributed according to the Gold Open Access model under Creative Commons Attribution-NonCommercial-NoDerivatives 4.0 International (CC BY-NC-ND 4.0) open license. Rules for authors are presented on the journal website: https://chemistry-vestnik.ksu.kz/regulations

EURASIAN JOURNAL OF CHEMISTRY
Editorial Board

How to Cite: Gopula, V.B., & Pathan, M.K. (2023) Simple and Efficient Method for One Pot Multicomponent Synthesis of 3,4-Dihydropyrimidin-2-(1H)-One Derivatives Catalyzed by Organocatalyst: Benzoic Acid. *Eurasian Journal of Chemistry, 109(1), 6-12.* https://doi.org/10.31489/2959-0663/1-23-8

ORGANIC CHEMISTRY

Article

Received: 1 September 2022 | Revised: 12 January 2023 | Accepted: 12 February 2023 | Published online: 06 March 2023

UDC 547.8

https://doi.org/10.31489/2959-0663/1-23-8

Venkatesh B. Gopula[1*], Mohsin K. Pathan[2]

[1]*Department of Chemistry, Anandibai Raorane Arts, Commerce and Science College, Vaibhavwadi, Dist. Sindhudurg, Maharashtra, India;*
[2]*Department of Analytical Method Development Lab (R&D), Jamjoom Pharmaceutical, Jeddah, Saudi Arabia*
*(*Corresponding author's e-mail: gopulavenkatesh@gmail.com)*

Simple and Efficient Method for One Pot Multicomponent Synthesis of 3,4-Dihydropyrimidin-2-(1H)-One Derivatives Catalyzed by Organocatalyst: Benzoic Acid

The Biginelli reaction is one the useful multicomponent reactions and a very appropriate reaction for the synthesis of 3,4-dihydropyrimidin-2(1H)-ones derivatives. These 3,4-dihydropyrimidin-2(1H)-ones have biological and pharmacological properties which make them a very important class of medicinal chemistry. Although they are an important class of medicinal chemistry, the syntheses of these compounds have been catalyzed by large number of strong Bronsted acids and Lewis acids under thermal conditions. Small organic molecules, organocatalysts, have been used as catalysts for the Biginelli reaction in a small number as compared to Bronsted acids and Lewis acid. Benzoic acid, which is a small organic molecule, although an acid, has never been tested for the synthesis of 3,4-dihydropyrimidin-2(1H)-ones. Benzoic acid is an inexpensive, non-toxic molecule, it has been successfully tested here as a catalyst for the one-pot three component synthesis of 3,4-dihydropyrimidin-2-(1H)-one derivatives via Biginelli reaction between β-keto ester, a variety of aromatic aldehydes and urea or thiourea under thermal conditions using 20 mol% benzoic acid in acetonitrile solvent refluxed for 12 h to give good to high yields. This synthetic method includes inexpensive, non-toxic, easily available benzoic acid as a catalyst and is carried out in a simple operational procedure.

Keywords: organocatalyst, benzoic acid, Biginelli, 3,4-dihydropyrimidin-2-(1H)-one, β-keto ester, aldehydes, urea, thiourea.

Introduction

The Biginelli reaction is one of the multicomponent reactions. It is a very suitable reaction for preparation of the 3,4-dihydropyrimidin-2(1H)-ones. 3,4-Dihydropyrimidinones (DHPMs) are a very important class since the recent discovery of their biological and pharmacological properties, namely antiviral, antitumour, antibacterial, anti-inflammatory and antihypertensive ones. Dihydropyrimidinone cores are also found in many natural products, highlighting important efforts aimed at the synthesis of these heterocycles [1–6]. These DHPMs have become a crucial basis for several calcium channel blockers, antihypertensives, α_{1a}-adrenergic antagonists and neuropeptide Y (NPY) antagonists [7].

Conventionally, Biginelli reactions were performed under strong acidic conditions with heating, and the yields were low to moderate (Scheme 1) [8].

Traditionally, there are several suitable reaction conditions with strong Bronsted acid along with the use of Lewis acid in condensation to more efficiently synthesize these DHPMs molecules; e.g. H_2SO_4 [7], $BF_3{\cdot}Et_2O/CuCl$ [9], $BiCl_3$ [10], $CeCl_3{\cdot}7H_2O$ [11], $Cu(OTf)_2$ [12], $TiCl_4$ [13], LiBr [14], Gallium (III) halides [15], Metal triflimide [16], *p*-toluenesulfonic acid [17], polystyrenesulfonic acid (PSSA) [18], $Cu(OTf)_2$ [19],

$ZrCl_4$ [20], $FeCl_3 \cdot 6H_2O$ [21], $RuCl_3$ [22], $Bi(NO_3)_3 \cdot 5H_2O$–TBAF [23], SmI_2 [24]. In addition to these, the Biginelli reaction has also been reported by using nanomaterials [25–27], nano-composite [28], zeolites [29–31], polymers [32], ultrasonic irradiation [33, 34], microwaves [35–38] and ball milling [39].

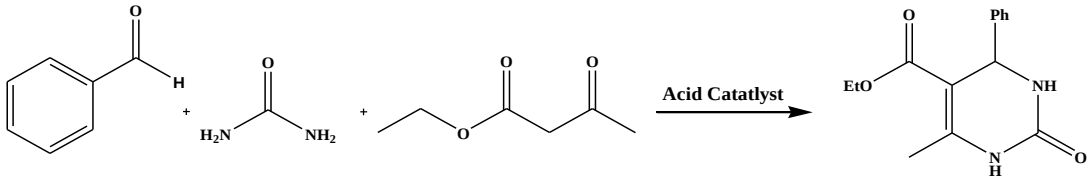

Scheme 1

The use of small organic molecules known as Organocatalysts [40–44] is a very rapidly developing area of synthetic organic chemistry that is replacing the use of metal-based Lewis acids. Organocatalysis offers many advantages for synthetic organic chemistry. In contrast to many transition metal catalysts, most organocatalysts are resistant to air and water, easily handled experimentally, relatively nontoxic, and readily separated from the crude reaction mixture [45]. Given the growing interest in developing green processes and procedures in organic synthesis [46], organocatalysts are considered to be a more eco-friendly and user-friendly alternative to traditional counterparts. Because of these many advantages of organocatalysts, few organocatlysts have been explored in the synthesis of DHPM derivatives such as bakers' yeast [47], hydrazine type [48], oxalic acid [49, 50], citric acid [51], boric acid [52], phenylboronic acid [53], L-proline [54] and Lactic acid [55].

In continuation of our work on new methodologies using organocatalysts [44, 56] in the synthetic organic chemistry we wish to report the efficient use of benzoic acid and a very simple effective approach for the synthesis of 3,4-dihydropyrimidine-2-(1H)-ones derivatives via the Biginelli reaction under thermal conditions having good to high yield.

In addition to those listed above, numerous methods for the synthesis of 3,4-dihydropyrimidin-2-(1H)-one derivatives by the Biginelli reaction are available in the literature. However, few organocatalysts are available for the synthesis of DHPMs. Benzoic acid is cheap, non-toxic and readily available in every laboratory. To our knowledge, so far the potential of benzoic acid as a mild organocatalyst has not been much tested in organic synthesis. We decided to explore the potential of benzoic acid as an organocatalyst for the synthesis of 3,4-dihydropyrimidine-2-(1H)-ones and their thione analogs as well as their derivatives by the Biginelli reaction under thermal conditions.

Experimental

The following reagents were used in this work without additional purification; benzaldehyde, 4-chlorobenzaldehyde, 3-nitrobenzaldehyde, 4-methoxybenzaldehyde, 4-nitrobenzaldehyde, 4-hydroxybenzaldehyde, ethylacetoacetate, methylacetoacetate, benzoic acid, urea, thiourea, acetonitrile, ethanol (loba Chemie), 4-methylbenzaldehyde, 3-methoxybenzaldehyde (Sigma-Aldrich).

The general procedure for the Biginelli reaction is as follows: a solution of the appropriate aldehyde **1** (1.0 mmol), urea or thiourea **2** (1.5 mmol), β-keto ester **3** (1.0 mmol), benzoic acid (20 mol%, 0.2 mmol) in acetonitrile (10 mL) is heated to reflux for 12 h. Then it is cooled to room temperature and poured into ice-water about 50mL. The solid products are filtered, washed with ice water, dried and recrystallized from ethanol to give pure product **4 (a-m)**.

4a. 5-Ethoxycarbonyl-6-methyl-4-phenyl-3,4-dihydropyrimidin- 2(1H)-one, Melting point: Found 206–208 °C (200–202 °C) [57] ^{1}H NMR (DMSO-d6): δ = 9.18 (s, 1H), 7.73 (s, 1H), 7.20–7.30 (m, 5H), 5.14 (s, 1H), 3.98 (q, J = 7.2 Hz, 2H), 2.24 (s, 3H), 1.06 (t, J = 7.2 Hz, 3H). ^{13}C NMR (DMSO-d6): δ = 166.3, 152.1, 147.2, 144.2, 128.1, 127.2, 126.5, 99.0, 58.1, 53.9, 17.9, 14.0. Mass m/z $[M+1]^+$ = 261.11.

4b. 4-(4-Chlorophenyl)-5-ethoxycarbonyl-6-methyl-3,4-dihydropyrimidin-2(1H)-one, Melting point: Found 214–216 °C (210–212 °C) [58]. ^{1}H NMR (DMSO-d6): δ = 9.20 (s, 1H), 7.76 (s, 1H), 7.40 (d, J = 9.0 Hz, 2H), 7.26 (d, J = 9.0 Hz, 2H) 5.16 (s, 1H), 3.95 (q, J = 7.1Hz, 2H), 2.19 (s, 3H), 1.10 (t, J = 7.1 Hz, 3H). ^{13}C NMR (DMSO-d6): δ = 167.1, 151.4, 146.4, 141.9, 130.1, 126.2, 125.5, 98.0, 56.1, 53.6, 19.7, 13.4. Mass m/z $[M+1]^+$ = 295.07.

Results and Discussion

We started our study with the reaction of benzaldehyde, ethyl acetoacetate and urea using benzoic acid as a catalyst under thermal conditions (Scheme 2) as a model reaction and the results are summarized in Table 1.

Initially, the reaction was carried out without a catalyst for an appropriate time and no progress was observed in acetonitrile solvent (Table 1, entry 01). Catalyst 1 mole % was added and the reaction was carried out up to 18 h, the obtained yield was very low (Table 1, entry 05).

The reaction gradually progressed with increasing the amount of catalyst while maintaining the reaction time (Table 1, entries 06 & 07). Due to the gradual development of the reaction, the amount of catalyst was increased to 7.5 mol % to see the reaction development, reducing the reaction time to 15 hours, a yield of 60 % was obtained (Table 1, entry 08). To obtain high and excellent yields, we continued to vary the amount of catalyst (Table 1, entries 09 & 16). The best reaction conditions were obtained using 20 mol% catalyst and the reaction was completed after 12 hours with a yield of 92 % (Table 1, entry 17). To our curiosity, we continued the reaction again up to 15 hours and also increased the amount of catalyst, but there was no any significant improvement in either case (Table 1, entry 18 & 19). In addition to acetonitrile, we also optimized the reaction conditions using different solvents as shown in Table 1. Without using a catalyst none of the reactions progressed to give any product (Table 1, entries 02, 03 & 04). Instead of introducing lower amount of catalyst for solvents water, THF and ethanol, we purposefully used 10 mol% and 20 mol% catalyst for our study. Yields were obtained relatively lower as compared with acetonitrile using 10 mol% catalyst for 15 hours (Table 1, entries 10, 11 & 12). Also, approximately the same results were observed using 20 mol% catalyst for 12 hours (Table 1, entries 13, 14 & 15) as compared with acetonitrile solvent (Table 1, entry 17).

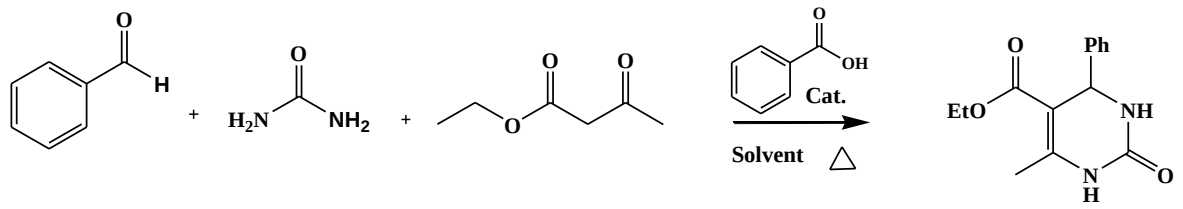

Scheme 2

Table 1

Optimization of the reaction conditions in the synthesis of DHPM[a]

Entry	Solvent	Catalyst (mole %)	Time (h)	Yield[b] (%)
01	CH_3CN	None	18	0
02	H_2O	None	18	0
03	THF	None	18	0
04	EtOH	None	18	0
05	CH_3CN	1	18	20
06	CH_3CN	2	18	30
07	CH_3CN	5	18	46
08	CH_3CN	7.5	15	60
09	CH_3CN	10	15	72
10	H_2O	10	15	20
11	THF	10	15	35
12	EtOH	10	15	30
13	H_2O	20	15	32
14	THF	20	12	65
15	EtOH	20	12	54
16	CH_3CN	15	15	85
17	CH_3CN	20	12	92
18	CH_3CN	20	15	94
19	CH_3CN	25	15	96

[a]Reaction conditions: Benzaldehyde (1.0 mmol), Urea (1.5 mmol), Ethyl acetoacetate (1.0 mmol), catalyst, solvent (10 ml) refluxed for the appropriate time.
[b]Isolated yields.

After obtaining the best reaction conditions; 1.0 mmol of benzaldehyde, 1.0 mmol of ethyl acetoacetate, 1.5 mmol of urea, 20 mol% benzoic acid as a catalyst in 10 ml of acetonitrile refluxed for 12 hrs, in order to explore the scope and generality of the present reaction conditions, various aldehydes and an urea analog, i.e. thiourea were taken for the Biginelli reaction using our optimized reaction conditions (Scheme 3). The results obtained are summarized in Table 2.

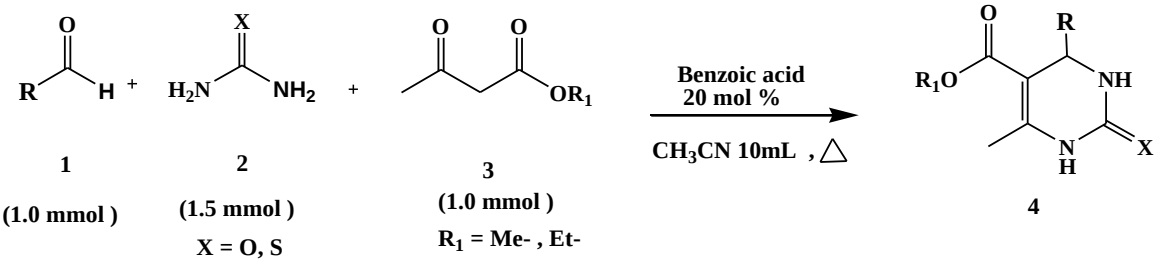

Scheme 3

In addition to the parent benzaldehyde, aldehydes with electron-donating groups such as methyl-, methoxy- and chloro-type groups, also electron withdrawing group such as nitro- were treated with ethyl acetoacetate and urea, resulting in the formation of the corresponding DHPM derivative in 84–92 % yield (Table 2, entries 01–05). The urea analog, i.e., thiourea, was also tested in the same reaction with benzaldehydes bearing chloro-, hydroxyl-, nitro- and methoxy-groups yielding the corresponding product in 82–90 % yield (Table 2 entries 06–10). Reaction with methylacetoacetate showed results similar to the reaction with ethylacetoacetate and gave the corresponding DHPM (Table 2, entries 11–12) in high yield. This reaction was also suitable for aldehydes with α-hydrogen, such as *n*-valeraldehyde (Table 2, entry 13), to give the corresponding DHPM product in good yield, and a significant reduction in yield was observed compared with aromatic aldehydes.

Table 2

Scope of Aldehydes with urea/thiourea and β-keto esters in the synthesis of DHPM derivatives[a]

Entry	Aldehyde 1 (R)	Urea/thiourea 2 (X)	β-keto ester 3 (R_1)	Product 4	Yield[b] %
01	C_6H_5	O	Et	**4a**	92
02	4-ClC_6H_4	O	Et	**4b**	90
03	4-$CH_3C_6H_4$	O	Et	**4c**	84
04	4-$OCH_3C_6H_4$	O	Et	**4d**	87
05	4-$NO_2C_6H_4$	O	Et	**4e**	90
06	C_6H_5	S	Et	**4f**	84
07	4-OHC_6H_4	S	Et	**4g**	82
08	3-$NO_2C_6H_4$	S	Et	**4h**	87
09	3-$OCH_3C_6H_4$	S	Et	**4i**	90
10	4-ClC_6H_4	S	Et	**4j**	86
11	C_6H_5	O	Me	**4k**	86
12	4-ClC_6H_4	O	Me	**4l**	82
13	n-Bu	O	Et	**4m**	72

[a]Reaction conditions: Aldehyde (1.0 mmol), Urea/thiourea (1.5 mmol), β-keto esters (1.0 mmol), benzoic acid 20 mol%, in acetonitrile (10 ml) refluxed for the 12 h.
[b]Isolated yields.

Conclusions

In conclusion, we have developed a simple and efficient method for one-pot three-component synthesis of 3,4-dihydropyrimidinone derivatives from aldehydes with β-keto esters and urea or thiourea using benzoic acid as an organocatalyst by refluxing in acetonitrile in high yields of 72–92 %. This method using benzoic acid as an organocatalyst is very useful to explore diversified aldehydes for synthesizing derivatives of 3,4-dihydropyrimidinones as well as thione analogues, which can play crucial role in the field of medicinal chemistry.

Acknowledgements

We would like to thank Anandibai Raorane Arts, Commerce and Science College, Vaibhavwadi for providing all necessary facilities for conducting this research work.

References

1 Atwal, K. S., Rovnyak, G. C., O'Reilly, B. C., & Schwartz, J. J. (1989). Substituted 1,4-dihydropyrimidines. 3. Synthesis of selectively functionalized 2-hetero-1,4-dihydropyrimidines. *Organic Chemistry, 54*, 5898–5907. https://doi.org/10.1021/jo00286a020

2 Atwal, K. S., Swanson, B. N., Unger, S. E., Floyd, D. M., Moreland, S., Hedberg, A., & O'Reilly, B. C. (1991). Dihydropyrimidine calcium channel blockers. 3. 3-Carbamoyl-4-aryl-1,2,3,4-tetrahydro-6-methyl-5-pyrimidinecarboxylic acid esters as orally effective antihypertensive agents. *Journal of Medicinal Chemistry, 34*, 806–811. https://doi.org/10.1021/jm00106a048

3 Rovnyak, G. C., Atwal, K. S., Hedberg, A., Kimball, S. D., Moreland, S., Gougoutas, J. Z., O'Reyli, B. C., Schwartz, J., Malley, M. F., & Semones, M. A. (1992). Dihydropyrimidine calcium channel blockers. 4. Basic 3-substituted-4-aryl-1,4-dihydropyrimidine-5-carboxylic acid esters. Potent antihypertensive agents. *Journal of Medicinal Chemistry, 35*, 3254–3263. https://doi.org/10.1021/jm00095a023

4 Kappe, C. O. & Fabian, W. M. F. (1997). Conformational analysis of 4-aryl-dihydropyrimidine calcium channel modulators. A comparison of ab initio, semiempirical and X-ray crystallographic studies. *Tetrahedron, 53*, 2803–2816. https://doi.org/10.1016/S0040-4020(97)00022-7

5 Kappe, C. O., Shishkin, O. V., Uray, G., & Verdino, P. (2000). X-Ray Structure, Conformational Analysis, Enantioseparation, and Determination of Absolute Configuration of the Mitotic Kinesin Eg5 Inhibitor Monastrol. *Tetrahedron, 56*, 1859–1862. https://doi.org/10.1016/S0040-4020(00)00116-2

6 Rovnyak, G. C., Kimball, S. D., Beyer, B., Cucinotta, G., DiMarco, J. D., Gougoutas, J., Hedberg, A., Malley, M., McCarthy, J. P., Zhong, R., & Moreland, S. (1995). Calcium Entry Blockers and Activators: Conformational and Structural Determinants of Dihydropyrimidine. *Calcium Channel Modulators Journal of Medicinal Chemistry, 38*, 119–129. https://doi.org/10.1021/jm00001a017

7 Azizian, J., Mohammadi, M. K., Firuzi, O., Mirza, B., & Miri, R. (2010). Microwave-Assisted Solvent-Free Synthesis of Bis(dihydropyrimidinone)benzenes and Evaluation of their Cytotoxic Activity. *Chemical Biology & Drug Design, 75*, 375–380. https://doi.org/10.1111/j.1747-0285.2009.00937.x

8 Kappe, C. O. (2000). Recent Advances in the Biginelli Dihydropyrimidine Synthesis. *New Tricks from an Old Dog. Accounts of Chemical Research, 33*, 879–888. https://doi.org/10.1021/ar000048h

9 Hu, E. H., Sidler, D. R., & Dolling, U. H. (1998). Unprecedented catalytic three component one-pot condensation Reaction: An Efficient Synthesis of 5-Alkoxycarbonyl-4-aryl-3,4-dihydropyrimidi-2(1H)-ones. *The Journal of Organic Chemistry, 63*, 3454–3457. https://doi.org/10.1021/jo970846u

10 Ramalinga, K., Vijayalakshmi, P., & Kaimala, T. N. B. (2001). Bismuth (III)-catalyzed Synthesis of Dihydropyrimidones: Improved protocol conditions for the Biginelli Reaction. *Synlett, 6*, 863–865. https://doi.org/10.1055/s-2001-14587

11 Bose, D. S., Fatima, L., & Mereyala, H. B. (2003). Green Chemistry Approaches to the Synthesis of 5-Alkoxycarbonyl-4-aryl-3,4-dihydropyrimidin-2(1H)-ones by a Three-Component Coupling of One-Pot Condensation Reaction: Comparison of Ethanol, Water, and Solvent-free Conditions. *The Journal of Organic Chemistry, 68*, 587–590. https://doi.org/10.1021/jo0205199

12 Paraskar, A. S., Dewkar, G. K., & Sudalai, A. (2003). $Cu(OTf)_2$: a reusable catalyst for high-yield synthesis of 3,4-dihydropyrimidin-2(1H)-ones. *Teterahedron Letters, 44*, 3305–3308. https://doi.org/10.1016/S0040-4039(03)00619-1

13 Maiti, G., Kundua, P., & Guin, C. (2003). One-pot synthesis of dihydropyrimidinones catalysed by lithium bromide: an improved procedure for the Biginelli reaction. *Tetrahedron Letters, 44*, 2757–2758. https://doi.org/10.1016/S0040-4039(02)02859-9

14 Baruah, P. P., Gadhwal, S., Prajapati, D., & Sandhu, J. S. (2002). The Biginelli Condensation: A Novel and Efficient Regioselective Synthesis of Dihydropyrimidin-2(1H)-ones Using Lithium Bromide. *Chemistry. Letters, 31*, 1038–1039. https://doi.org/10.1246/cl.2002.1038

15 Saini, A., Kumar, S., & Sandhu, J. S. (2007). Gallium (III) halides catalyzed, microwave enhanced, synthesis of 3,4-dihydropyrimidin-2-(1H)-ones under solvent free condition. *Indian Journal of Chemistry, 46B*, 1886–1889.

16 Suzuki, I., Suzumura, Y., & Takeda, K. (2006). Metal triflimide as a Lewis acid catalyst for Biginelli reaction in water. *Teterahedron Letters, 47*, 7861–7864. https://doi.org/10.1016/j.tetlet.2006.09.019

17 Bose, A. K., Manhas, M. S., Pednekar, S., Ganguly, S. N., Dang, H., He, W., & Mandadi, A. (2005). Large scale Biginelli reaction via water-based biphasic media: a green chemistry strategy. *Tetrahedron Letters, 46*, 1901–1903. https://doi.org/10.1016/j.tetlet.2005.01.087

18 Polshettiwar, V., & Varma, R. S. (2007). Biginelli reaction in aqueous medium: a greener and sustainable approach to substituted 3,4-dihydropyrimidin-2(1H)-ones. *Tetrahedron Letters, 48*, 7343–7346. https://doi.org/10.1016/j.tetlet.2007.08.031

19 Paraskar, A. S., Dewkar, G. K., & Sudalai, A. (2003). $Cu(OTf)_2$: a redusable catalyst for high-yield synthesis of 3,4-dihydropyrimidin-2(1H)-ones. *Tetrahedron Letters, 44*, 3305–3308. https://doi.org/10.1016/S0040-4039(03)00619-1

20 Reddy, C. V., Mahesh, M., Raju, P. V. K., Babu, T. R., & Reddy, V. V. N. (2002). Zirconium (IV) chloride catalyzed one-pot synthesis of 3,4-dihydropyrimidi-2(1H)-ones. *Tetrahedron Letters, 43*, 2657–2659. https://doi.org/10.1016/S0040-4039(02)00280-0

21 Lu, J. & Ma, H. R. (2000). Iron (III)-Catalyzed Synthesis of Dihydropyrimidinones, Improved conditions for the Biginelli Reaction. *Synlett, 1*, 63–64. https://doi.org/10.1055/s-2000-6469

22 Surya, K. De, & Gibbs, R. A. (2005). Ruthenium(III) chloride-catalyzed one pot synthesis of 3,4-dihydropyrimidin-2-(1H)-ones under solvent free conditions. *Synthesis, 11*, 1748–1750. https://doi.org/10.1055/s-2005-869899

23 Khodaei, M. M., Khosropour, A. R., & Jowkar, M. (2005). $Bi(NO_3)_3{\cdot}5H_2O$ – TBAF as an Efficient Reagent for in situ Oxidation: Dihydropyrimidinone formation from Benzyl Halides. *Synthesis, 8*, 1301–1304. https://doi.org/10.1055/s-2005-861876

24 Han, X., Xu, F., Luo, Y., & Shen, Q. (2005). An Efficient One-pot synthesis of Dihydropyrimidiononones by a Samarium Diiodide Catalyzed Biginelli reaction under Solvent free Conditions. *European Journal of Organic Chemistry, 8*, 1500–1503. https://doi.org/10.1002/ejoc.200400753

25 Zamani, F. & Izadi, E. (2013). Synthesis and characterization of sulfonated-phenylacetic acid coated Fe_3O_4 nanoparticles as a novel acid magnetic catalyst for the Biginelli reaction. Catalysis Communications, 42, 104–108. https://doi.org/10.1016/j.catcom.2013.08.006

26 Nasr-Esfahani, M., Hoseini, S. J. & Mohammadi, F. (2011). Fe_3O_4 Nanoparticles as an Efficient and Mangentically Recoverable Catalyst for the Synthesis of 3,4-dihydropyrimidin-2(1H)-ones under solvent free conditions. *Chinese Journal of Catalysis, 32*, 1484–1489. https://doi.org/10.1016/S1872-2067(10)60263-X

27 Girija, D., Naik, H. S. B., Kumar, B. V., Sudhamani, C. N., & Harish, K. N. (2019). Fe_3O_4 Nanoparticle supported Ni(II) Complexes: A Mangentically recoverable Catalyst for Biginelli reaction. *Arabian Journal of Chemistry, 12*, 420–428. https://doi.org/10.1016/j.arabjc.2014.08.008

28 Safari, J. & Zarnegar, Z. (2013). Biginelli reaction on Fe_3O_4–MWNT nanocomposite: excellent reactivity and facile recyclability of the catalyst combined with ultrasound irradiation. *RSC Advances, 3*, 17962–17967. https://doi.org/10.1039/C3RA43014F

29 Mistry, S. R., Joshi, R. S., Sahoo, S. K., & Maheria, K. C. (2011). Synthesis of Dihydropyrimidinones Using Large Pore Zeolites. *Catalysis Letters, 141*, 1541–1547. https://doi.org/10.1007/s10562-011-0639-6

30 Rani, V. R., Srinivas, N., Kishan, M. R., Kulkarni, S. J., & Raghavan, K. V. (2001). Zeolite-catalyzed cyclocondensation reaction for the selective synthesis of 3,4-dihydropyrimidin-2(1H)-ones. *Green Chemistry, 3*, 305–306. https://doi.org/10.1039/B107612B

31 Kang, L., Jin, D., & Cai, Y. (2013). Silica-supported ionic liquid Si[SbSipim][PF6]: An efficient catalyst for the synthesis of 3,4-dihydropyrimidine-2-(1H)-ones. *Synthetic Communications, 43*, 1896–1901. https://doi.org/10.1080/00397911.2012.678462

32 Pourjavadi, A., Salimi, H., Barzegar, S., & Eftekharisis, B. (2007). A Novel Polymeric catalyst for One-Pot synthesis of 3,4-dihydropyrimidin-2-(1H)-ones via Biginelli Reaction. *Acta Chimica Slovenica, 54*, 140–143.

33 Li, J. T., Han, J. F., Yang, J. H., & Li, T. S. (2003). An efficient synthesis of 3,4-dihydropyrimidin-2-ones catalyzed by NH_2SO_3H under ultrasound irradiation. *Ultrasonics Sonochemistry, 10*, 119–122. https://doi.org/10.1016/S1350-4177(03)00092-0

34 Yadav, J. S., Reddy, B. V. S., Reddy, K. B., Raj, K. S., & Prasad, A. R. (2001). Ultrasound- accelerated synthesis of 3,4-dihydropyrimidin-2(1H)-ones with ceric ammonium nitrate. *Journal of the Chemical Society, Perkin Transactions 1*, 1939–1941. https://doi.org/10.1039/B102565C

35 Cheng, J. & Qi, D. Y. (2007). ChemInform Abstract: An Efficient and Solvent-Free One-Pot Synthesis of Dihydropyrimidinones under Microwave Irradiation. *Chinese Chemical Letters, 18*, 647–650. https://doi.org/10.1016/j.cclet.2007.04.002

36 Felluga, F., Benedetti, F., Berti, F., Drioli, S., & Regini, G. (2018). Efficient Biginelli Synthesis of 2-Aminodihydropyrimidines under Microwave Irradiation. *Synlett, 29*, 986–992. http://doi.org./10.1055/s-0036-1591900

37 Misra, A. K., Agnihotri, G., & Madhusudan, S. K. (2001). Microwave induced eco-friendly solvent-free Biginelli reaction catalyzed by calcium chloride. *Indian Journal of Chemistry, 43B*, 2018–2020.

38 Hazarkhani, H. & Karimi, B. (2004). N-Bromosuccinimide as an Almost Neutral Catalyst for Efficient Synthesis of Dihydropyrimidinones Under Microwave Irradiation. *Synthesis, 8*, 1239–1242. https://doi.org/10.1055/s-2004-822348

39 Mohamed, M. O., Alshammari, A. G. & Lemine, O. M. (2016). Green High-Yielding one-pot approach to Biginelli Reaction under catalyst-free and solvent free Ball Milling conditions. *Applied Sciences, 6*, 431–437. https://doi.org/10.3390/app6120431

40 Carlone, A., Cabrera, S., Marigo, M. & Jorgensen, K. A. (2007). A new approach for an organocatalytic multicomponent domino asymmetric reaction. *Angewandte Chemie International Edition, 46*, 1101–1104. https://doi.org/10.1002/anie.200604479

41 Xie, H. Zu, Li., Li, H., Wang, J. & Jiang, W. J. (2007). Organocatalytic Enantioselective cascade Michael-Alkylation reactions: Synthesis of chiral Cyclopropanes and Investigation of Unexpected organocatalyzed Stereoselective Ring opeing of cyclopropanes. *Journal of the American Chemical Society, 129*, 10886–10894. https://doi.org/10.1021/ja073262a

42 Martin, N. J. A., Ozores, L. & List, B. (2007). Organocatalytic Asymmetric transfer Hydrogenation of nitroolefins. *Journal of the American Chemical Society, 129*, 8976–8977. https://doi.org/10.1021/ja074045c

43 Li, G., Liang, Y. & Antilla, J.C. (2007). A vaulted Biaryl Phosphoric acid-catalyzed reduction of α-Imino Esters: The Highly Enantioselective preparation of α-amino esters. *Journal of the American Chemical Society, 129*, 5830–5831. https://doi.org/10.1021/ja070519w

44 Gopula, V. B. (2021) Mandelic acid: organocatalyst for efficient synthesis of secondary amines from aldehydes and primary amines. *Journal of Advanced Scientific Research, 12(03)*, 292-296. https://doi.org/10.55218/JASR.202112341

45 Louis S. Hegedus (2009). Organocatalysis in Organic Synthesis. *Journal of the American Chemical Society, 131*, 17995–17997. https://doi.org/10.1021/ja908581u

46 List, B. (2007). Introduction: Organocatalysis. *Chemical Reviews, 107*, 5413–5415. https://doi.org/10.1021/cr078412e

47 Kumar, A. & Maurya, R. M. (2007). An efficient baker's yeast catalyzed synthesis of 3,4-dihydropyrimidin-2-(1H)-ones. *Tetrahydron Letters, 48*, 4569–4571. https://doi.org/10.1016/j.tetlet.2007.04.130

48 Suzuki, I., Iwata, Y. & Takeda, K. (2008). Biginelli Reactions catalyzed by hydrazine type organocatalyst. *Tetrahydron Letters, 49*, 3238–3241. https://doi.org/10.1016/j.tetlet.2008.03.080

49 Sangshetti, J. N., Shinde, D. B. & Kokare, N. D. (2008). Oxalic acid as a versatile catalyst for one pot facile synthesis of 3,4-dihydropyrimidin-2-(1H)-ones and their thione analogues. *Journal of Heterocyclic Chemisty, 45*, 1191–1193. https://doi.org/10.1002/jhet.5570450440

50 Mohamadpour, F., Maghsoodlou, M. T., Heydari, R. & Lashkari, M. (2016). Oxalic acid dehydrate catalyzed synthesis of 3,4-dihydropyrimidin-2-(1H)-one derivatives under thermal and solvent free conditions. *Iranian Journal of Catalysis, 6*(3), 127–131.

51 Ramu, E., Kotra, V., Bansal, N., Varala, R. & Adapa, S. R. (2008). Green approach for the efficient synthesis of Biginelli compounds promoted by citric acid under solvent free conditions. *Rasayan Journal of Chemistry, 1*, 188–190.

52 Tu, S., Fang, F., Miao, C., Jiang, H., Feng, Y., Shi, D. & Wang, X. (2003). One-pot synthesis of 3,4-dihydropyrimidin-2(1H)-ones using boric acid as catalyst. *Tetrahedron Letters, 44*, 6153–6155. https://doi.org/10.1016/S0040-4039(03)01466-7

53 Debache, A., Boumoud, B., Amimour, M., Belfaitah, A., Rhouatia, S. & Carboni, B. (2006). Phenylboronic acid as a mild and efficient catalyst for Biginelli Reaction. *Tetrahedron Letters, 47*, 5697–5699. https://doi.org/10.1016/j.tetlet.2006.06.015

54 Mabry, J. & Ganem, B. (2006). Studies on the Biginelli reaction: a mild and selective route to 3,4-dihydropyrimidin-2(1H)-ones via enamine intermediates. *Tetrahedron Letters, 47*, 55–56. https://doi.org/10.1016/j.tetlet.2005.10.124

55 Saini, S. A., Kumar, D. & Sandhu, J. S. (2009). Multicomponent eco-friendly synthesis of 3,4-dihydropyrimidine-2-(1H)-ones using an organocatalyst Lactic acid. *Green Chemistry Letters and Reviews, 1*, 29–33. https://doi.org/10.1080/17518250902973833

56 Tale, R. H., Shinde, S. V., Gopula, V. B. & Wankhede, D. S. (2016). Methylboronic acid: A Mild, Green and recyclable Organocatalyst for Transformation of β-keto esters. *Journal of Chemical and Pharmaceutical Research, 8*(10), 169–175.

57 Ma, Y., Qian, C., Wang, L & Yang, M. (2000). Lanthanide triflate catalyzed Biginelli reaction. one-pot synthesis of dihydropyrimidinones under solvent-free conditions. *Journal of Organic Chemistry, 65*(12), 3864–3868. https://doi.org/10.1021/jo9919052

58 Shaabani, A., Bazgir, A. & Teimouri, F. (2003). Ammonium chloride-catalyzed one-pot synthesis of 3,4-dihydropyrimidin-2-(1H)-ones under solvent-free conditions. *Tetrahedron Letters, 44*(4), 857–859. https://doi.org/10.1016/S0040-4039(02)02612-6

Information about authors*

Gopula, Venkatesh Balkishan (*corresponding author)* — Assistant Professor, Department of Chemistry, Anandibai Raorane Arts, Commerce and Science College, Vaibhavwadi, Dist. Sindhudurg, Maharashtra, 416810, India; e-mail: gopulavenkatesh@gmail.com; https://orcid.org/0000-0002-6193-5921;

Pathan, Mohsin Khan Moin Khan — Sr. Executive, Dept. of Analytical Method Development Lab (R&D), Jamjoom Pharmaceutical, Jeddah, 21442, Saudi Arabia; e-mail: mohsin0506@gmail.com; https://orcid.org/0000-0001-9307-3732

*The author's name is presented in the order: *Last Name, First and Middle Names*

How to Cite: Turdybekov, K.M., Rakhimova, B.B., Makhmutova, A.S., Gatilov, Yu.V., & Adekenov, S.M. (2023) Isolation and Spatial Structure of 5,7-Dihydroxy-6,3′,4′-Trimethoxyflavone. *Eurasian Journal of Chemistry, 109(1), 13-19.* https://doi.org/10.31489/2959-0663/1-23-1

Article

Received: 11 November 2022 | Revised: 26 January 2023 | Accepted: 02 February 2023 | Published online: 06 March 2023

UDC 547.972+548.737

https://doi.org/10.31489/2959-0663/1-23-1

Koblandy M. Turdybekov[1*], Bibilul B. Rakhimova[2], Almagul S. Makhmutova[2], Yurii V. Gatilov[3], Sergazy M. Adekenov[4]

[1]*Karagandy University of the name of Academician E.A. Buketov, Kazakhstan;*
[2]*Karaganda Medical University, Kazakhstan;*
[3]*N.N. Vorozhtsov Novosibirsk Institute of Organic Chemistry, Russia;*
[4]*JSC "International Research and Production Holding "Phytochemistry", Karaganda, Kazakhstan*
*(*Corresponding author`s e-mail: xray-phyto@yandex.kz)*

Isolation and Spatial Structure of 5,7-Dihydroxy-6,3′,4′-Trimethoxyflavone

The article presents the results of a chemical study of semi-dry wormwood (*Artemisia semiarida*), an endemic plant of Kazakhstan. The amount of extractive substances was obtained by extraction with chloroform from air-dried crushed above-ground part of the plant collected in the vegetative phase. The compound was isolated using a column chromatography method. Silica gel of the KSK brand was used with the ratio of the sum of substances – carrier = 1:10. When the column was eluted with a 13:7 petroleum ether – ethyl acetate mixture, a yellow crystalline substance of the composition $C_{18}H_{16}O_7$ with m.p. 234–237° C was obtained (recrystallization from ethyl acetate). The structure of the obtained compound (5,7-dihydroxy-6,3′,4′-trimethoxyflavone or eupatilin) was established by analysis of IR and NMR spectra. The spatial structure of eupatilin was determined by X-ray diffraction. In the crystal structure of 5,7-dihydroxy-6,3′,4′-trimethoxyflavone the rotation of the phenyl ring relative to the main framework (chromene ring) was found to be only 4.1°. Four conformers with different rotations of the phenyl ring (the torsional angles of O1C2C1′C2′ are 30°, 140°, 210° and 320°, respectively) and small energy barriers (about 8.4 kJ/mol) can be realized in the free state of the molecule.

Keywords: NMR spectroscopy, IR spectroscopy, X-ray analysis, quantum chemistry, *Artemisia semiarida*, endemic, 5,7-dihydroxy-6,3′,4′-trimethoxyflavone, eupatilin, phenolic compounds.

Introduction

Natural phenolic compounds in the form of flavonoids are one of the potential sources of herbal medicines. Flavonoids represent the most numerous class of natural phenolic compounds and due to their structural diversity exhibit high and versatile biological activity with low toxicity [1–3]. The wide range of biological activity of flavonoids is due to the presence in their structure of aromatic and double bonds, keto- and hydroxyl groups in different positions [1–3]. In this regard, in Kazakhstan we continue works on the search for natural biologically active phenolic compounds isolated from plant raw materials, including endemics. In continuation of these works on isolation of polyphenolic compounds from plant raw materials, the chemical composition of semi-dry wormwood (*Artemisia semiarida* (Krasch. & Lavrenko) Filatova), an endemic species of the genus wormwood (*Artemisia* L.) was studied. The aim of this work is to study the stereochemistry of 5,7-dihydroxy-6,3',4'-trimethoxyflavone (eupatilin), a widespread phenolic compound.

Experimental

The melting point was determined on a Boetius heating table. The IR spectrum was recorded on an Avatar 360 instrument (Thermo Nicolet) in KBr tablets. NMR spectra were obtained on a Bruker DRX-300 spectrometer. The X-ray diffraction experiment was carried out on a Bruker APEX-II CCD diffractometer. Column chromatography was carried out on KSK silica gel using mixtures of petroleum ether with ethyl acetate with an increasing (from 0 to 100 %) content of the latter as an eluent. Thin layer chromatography (TLC) was performed using Sorbfil plates, imaging with a 1 % aqueous solution of $KMnO_4$ and a 3 % aqueous solution of $FeCl_3$. The herb of *Artemisia semiarida* was collected in flowering period in May 2009 at Betpakdala desert, Zhanaarka district, Karaganda region and air-dried for 2 weeks.

Isolation of 5,7-dihydroxy-6,3′,4′-trimethoxyflavone (eupatilin) (**1**). Ground plant material (1.6 kg) was extracted with boiled chloroform three times (2 h) with plant : solvent ratio of 1:10. The obtained extracts were combined and filtered through a cellulose filter. The solvent was evaporated in vacuo to obtain a vis-

cous green chloroform extract (105 g) and treated three times with an ethanol : water mixture (2:1) at 70–75 °C (extract : mixture ratio 3:1 *w*/*v*).

The precipitated ballast substances were decanted and the solution was filtered off. The filtrate was extracted with chloroform (4 × 0.5 L) and the chloroform extracts were combined and evaporated to dryness. The dry residue (65 g, yield 4.06 % of air-dry plant) was separated by open-air column chromatography on silica (1235 g, 0.5 ml fraction, KSK, manufacturer LTD QihgdaoHiland Trading CO (China)) using petroleum ether : ethyl acetate (13:7) as an eluent to yield a yellow crystalline substance with m.p. 234–237 °C (ethyl acetate). Molecular formula is $C_{18}H_{16}O_7$; R_f is 2.25 (TLC, silica, petroleum ether : ethyl acetate 1:1).

IR spectrum (KBr, *v*, cm^{-1}): 3069 (OH group), 2949, 2839, 1654 (C=O), 1624, 1600, 1588 (C=C), 1505, 1466, 1440, 1428, 1412, 1376, 1334, 1305, 1269, 1215, 1175, 1149, 1109, 1093, 1044, 1023, 991, 945, 893, 837, 814, 770, 684, 633, 614, 593, 574, 518, 482, 434.

^{1}H NMR spectrum (300 MHz, $CDCl_3/CD_3OD$, δ, ppm, J/Hz): 6.70 (1H, s, H3), 6.67 (1H, s, H8), 7.05 (1H, d, J=2.0, H2′), 7.07 (1H, d, J=2.0, H5′), 7.22 (1H, dd, J=8.0. 2.0, H6′), 3.57 (3H, s, CH_3-C6), 3.63 (3H, s, CH_3-C3′), 3.61 (3H, s, CH_3-C6′).

Quantum chemistry calculations were performed using the MOPAC version 9.0 software package. The PM6 method was used to optimize the metric data of the molecule [4].

X-ray diffraction study of compound **1**. Determination of unit cell parameters and intensity of 12324 diffracted reflections (2689 independent, R_{int} 0.049) were measured on a Bruker Kappa APEXII CCD diffractometer (MoK_α, graphite monochromator, ω-scan, $1.74° \le \theta \le 25.85°$) at 200 K. Monoclinic crystals, space group P21/n, a = 12.9763(9), b = 8.7508(5), c = 15.3679(11) Å, β = 113.998(2)°, V = 1594.4(2) $Å^3$, Z = 4 ($C_{18}H_{16}O_7$), calculated density d = 1.434 g/cm^3, absorption coefficient μ = 0.112 mm^{-1}. The experimental array of reflections was corrected for absorption. The absorptions were counted using SAINT [5] and SADABS [6] programs (multi-scan method, $T_{min.}$ 0.9161, $T_{max.}$ 0.9780).

The structure was deciphered by direct phase determination. The coordinates of non-hydrogen atoms were refined using the anisotropic approximation of thermal vibrations by the full-matrix least-squares method. The positions of hydrogen atoms, with the exception of hydroxyl ones, were calculated geometrically and refined in the isotropic approximation of thermal vibrations (rider model). The H atoms of the hydroxyl groups were revealed from the difference synthesis, and their positions were refined in the isotropic approximation. The structure was deciphered and the coordinates were refined using the SHELXS software package [7] and the SHELXL-2018/3 software [8]. A total of 2040 independent reflections with $I \ge 2\sigma(I)$ were used in the calculations; the number of refined parameters was 230.

The divergence coefficients were $R_1 = 0.0538$, $_wR_2 = 0.1521$ (for reflections with $I \ge 2\sigma(I)$), $R_1 = 0.0772$, $_wR_2 = 0.1756$ (for all reflections), GooF = 1.243. Maximum and minimum residual density were Δρ = 0.623 and –0.457 e/$Å^3$. The coordinates of atoms in the crystal are presented in Table 1.

Table 1

Coordinates of atoms in fractions of the cell (×10^4, H×10^3) and equivalent thermal parameters ($Å^2$, ×10^3) in the structure 1

Atom	*x*	*y*	*z*	$U_{eq.}$
1	2	3	4	5
O1	6481(1)	9115(2)	867(1)	28(1)
O2	4082(2)	6161(2)	937(1)	34(1)
O3	4873(2)	6504(2)	2770(1)	34(1)
O4	6558(2)	7810(2)	4399(1)	35(1)
O5	7949(2)	9973(2)	4153(1)	34(1)
O1′	5028(2)	8108(2)	–3352(1)	35(1)
O2′	6641(2)	9943(2)	–3128(1)	37(1)
C2	5766(2)	8426(3)	54(2)	23(1)
C3	4957(2)	7448(3)	63(2)	27(1)
C4	4834(2)	7068(3)	915(2)	25(1)
C4a	5625(2)	7784(3)	1776(2)	23(1)
C5	5639(2)	7486(3)	2684(2)	26(1)
C6	6437(2)	8162(3)	3489(2)	25(1)
C7	7200(2)	9219(3)	3392(2)	27(1)

Continuation of Table 1

Atom	*x*	*y*	*z*	$U_{eq.}$
1	2	3	4	5
C8	7203(2)	9540(3)	2511(2)	28(1)
C8a	6423(2)	8801(3)	1718(2)	24(1)
C9	5678(3)	8313(4)	4656(2)	60(1)
C1′	5991(2)	8868(3)	–769(2)	23(1)
C2′	5358(2)	8246(3)	–1676(2)	24(1)
C3′	5579(2)	8646(3)	–2447(2)	25(1)
C4′	6458(2)	9690(3)	–2334(2)	26(1)
C5′	7062(2)	10324(3)	–1446(2)	30(1)
C6′	6832(2)	9920(3)	–671(2)	28(1)
C7′	4068(2)	7151(3)	–3546(2)	36(1)
C8′	7454(3)	11082(3)	–3070(2)	46(1)
H3	445(3)	613(4)	220(3)	52(1)
H5	808(3)	949(4)	469(3)	51(1)

Results and Discussions

A yellow substance with $C_{18}H_{16}O_7$ molecular formula (**1**) was isolated from the extract of the aerial part of *Artemisia semiarida* after separation of the chloroform extract by column chromatography on silica eluted with petroleum ether : ethyl acetate (13:7) [9].

In the IR spectrum (KBr, ν, cm^{-1}) (1), there were observed absorption bands, corresponding to the hydroxyl groups OH at 3069 and 3002 cm^{-1}, the carbonyl group C=O at 1654 cm^{-1}, double C=C-bonds of aromatic rings at 1588 and 1505 cm^{-1} conjugated with the C=O group, methoxy groups OCH_3 at 1376 cm^{-1} (bending vibrations), C–O–C bonds at 1094 cm^{-1}. The intensity of the absorption bands at wavelengths of 838, 771, and 685 cm^{-1} indicated the presence of substituents at the C3′ and C4 atoms of the phenyl ring.

In the ^{1}H NMR spectrum of **1**, the methoxyl group protons were observed as singlets at δ_H3.57 (C6′-OCH_3), 3.61 ppm. (C4′-OCH_3) and 3.63 ppm. (C3′-OCH_3). The protons H3 and H8 protons of chromene skeleton appeared as singlets at δ_H6.70 and 6.67 and the protons of the phenyl ring were represented by the spin system AMX at δ_H 7.05 (J=2.0 Hz, H2′), 7.07 (J=2.0 Hz, H5′), and 7.22 (J=8.0, 2.0 Hz, H6).

According to IR and NMR spectroscopy, substance **1** was identified as 5,7-dihydroxy-6,3',4'-trimethoxyflavone (eupatilin). Eupatilin previously isolated from *Eupatorium semiserratum* DC (*Asteraceae*) [10] has anti-inflammatory and antioxidant activity (Fig. 1).

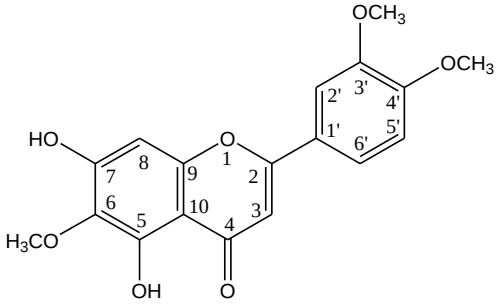

Figure 1. Structure of 5,7-dihydroxy-6,3',4'-trimethoxyflavone (eupatilin) **(1)**

In continuation of the stereochemistry study of phenolic compounds, an X-ray diffraction investigation of 5,7,3′-trihydroxy-6,3′,4′-trimethoxyflavone was carried out. Previously, the spatial structure of molecule **1** was carried out by other authors [11]. In our work, we obtained more accurate data on the metric of the elementary lattice and the crystal structure of the molecule, which will be submitted into the Cambridge Crystallographic Data Center.

The general view of the molecule **1** is shown in Figure 2.

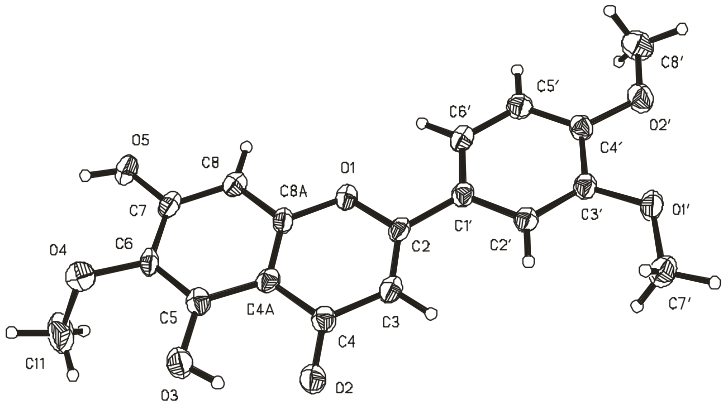

Figure 2. Crystal structural of 5,7-dihydroxy-6,3′,4′-trimethoxyflavone (eupatilin) **(1)**
(thermal vibration ellipsoids shown with a probability of 50 %)

From the data obtained, it follows that the bond lengths (Table 2) and bond angles (Table 3) in compound **1** are close to normal ones [12].

Table 2

Bond lengths (d, Å) in the structure 1

Bond	d	Bond	d
O1-C2	1.358(3)	C4a-C5	1.412(4)
O1-C8a	1.368(3)	C4a-C8a	1.395(3)
O2-C4	1.269(3)	C5-C6	1.382(4)
O3-C5	1.360(3)	C6-C7	1.406(4)
O4-C6	1.377(3)	C7-C8	1.384(4)
O4-C9	1.422(3)	C8-C8a	1.388(4)
O5-C7	1.350(3)	C1′-C2	1.462(4)
O1′-C3′	1.363(3)	C1′-C2′	1.407(4)
O1′-C7′	1.429(3)	C1′-C6′	1.388(3)
O2′-C4′	1.354(3)	C2′-C3′	1.373(4)
O2′-C8′	1.427(3)	C3′-C4′	1.416(3)
C2-C3	1.358(3)	C4′-C5′	1.383(4)
C3-C4	1.422(4)	C5′-C6′	1.385(4)
C4-C4a	1.446(3)		

Table 3

Valent angles (ω, deg.) in the structure 1

Angle	ω	Angle	ω
1	2	3	4
C2-O1-C8a	120.5(2)	O5-C7-C6	121.4(2)
C6-O4-C9	116.2(2)	O5-C7-C8	117.4(2)
C3′-O1′-C7′	117.8(2)	C8-C7-C6	121.2(2)
C4′-O2′-C8′	117.0(2)	C7-C8-C8a)	118.3(2)
C3-C2-O1	120.8(2)	O1-C8a-C4a	121.3(2)
O1-C2-C1′	112.1(2)	O1-C8a-C8	116.2(2)
C3-C2-C1′	127.1(2)	C8-C8a-C4a	122.4(2)
C2-C3-C4	122.2(2)	C2′-C1′-C2	120.8(2)
O2-C4-C3	123.1(2)	C6′-C1′-C2	120.5(2)
O2-C4-C4a	120.9(2)	C6′-C1′-C2′	118.7(2)
C3-C4-C4a	116.0(2)	C1′-C2′-C3′	120.9(2)
C5-C4a-C4	122.9(2)	O1′-C3′-C2′	125.9(2)
C8a-C4a-C4	119.1(2)	O1′-C3′-C4′	114.2(2)
C8a-C4a-C5	118.0(2)	C2′-C3′-C4′	119.9(2)

Continuation of Table 3

Angle	ω	Angle	ω
1	2	3	4
O3-C5-C4a	119.7(2)	O2′-C4′-C5′	125.9(2)
O3-C5-C6	119.7(2)	O2′-C4′-C7′	115.0(2)
C6-C5-C4a	120.6(2)	C5′-C4′-C3′	119.0(2)
O4-C6-C5	123.2(2)	C4′-C5′-C6′	120.8(2)
O4-C6-C7	117.4(2)	C5′-C6′-C1′	120.7(2)
C5-C6-C7	119.4(2)		

Flavones compared to other flavonoids have the lowest conformational mobility due to the presence of a large number of double and aromatic bonds as well as substituents in the main skeleton. Thus, in structure **1**, the chromene skeleton is flat with an accuracy of ±0.017 Å, and the oxygen atoms of the OH groups are almost in the plane of the main skeleton. The deviation of O3 and O5 atoms from the middle plane is 0.008 and 0.037 Å, respectively. An exception is the O4 atom of the methoxy group with the deviation of –186 Å. The phenyl ring is flat within ±0.007 Å with the deviation of O1' and O2' atoms by 0.009 and –0.078 Å, respectively. The methoxy groups in the phenyl ring are slightly outside of its middle plane (torsion angles C2′C3′O1′C7' 6.1° and C5′C4′O2′C8′ –6.8°). The angle of rotation of the chromene skeleton and the phenyl ring is insignificant and amounts to –4.1° as well as in most flavones like 6,8-dimethyl-5,4'-dihydroxy-7-methoxyflavone [13], 5-hydroxy-6,7,4'-trimethoxyflavone [14] and 5,6,7-trihydroxyflavone [15].

In the crystal, the molecules are linked by an intramolecular hydrogen bond O3-H....O2 (x, y, z) (distances O3-H 0.89 Å, O3…. O2 2.59 Å, H3…. O2 1.80 Å, angle O3-H…. O2 147°) and intermolecular hydrogen bonds O5-H…. O2 (0.5+x, 1.5-y, 0.5+z) (distances O3-H 0.88 Å, O5….O2 2.72 Å, H5….O2 2.91 Å, angle O5-H….O2 151°), forming flat ribbons along direction [1 0 1] (Fig. 3).

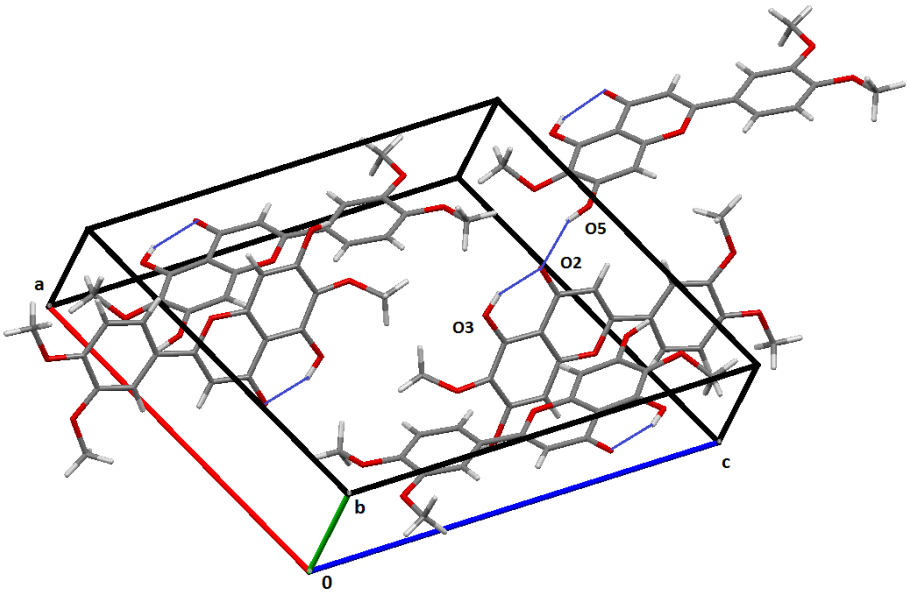

Figure 3. Crystal packing of molecules **1**

As is known, in the crystalline state, molecules of organic compounds can take a conformational state, which is not the most energetically favorable, if based on the close packing principle, its change is beneficial [16]. Based on this principle, quantum-chemical calculations were carried out to determine the various possible conformers of compound **1** using the semi-empirical PM6 method [4]. The conformers were determined by rotating the phenyl ring about the C2-C1' bond and establishing the possible orientation of the methoxy groups relative to the chromene skeleton.

From the calculations obtained, it was found that four conformers could be realized for molecule **1** at various rotations of the phenyl ring along the C2-C1′ bond with the values of the torsion angle O1C2C1′C2′ 30°, 140°, 210° and 320°, respectively. The energy barriers between them were insignificant and were about 8.4 kJ/mol. Similar rotations of the phenyl ring relative to the chromene skeleton were observed in

6-hydroxy-1′,2′,3′-trimethoxyflavone (τ (O1C2C1′C2′) = 161.3°) [17], 5,4'-dihydroxy-6,7-dimethoxyflavone (τ (O1C2C1′C2′) = 337.8°) [18] and 5,6,7,4′-tetramethoxyflavone (τ (O1C2C1′C2′) = 18.3°) [19].

Favorable orientations of the methoxy group in the chromene skeleton of molecule **1** fall on the position of the methoxy group at the torsion angle τ(C5C6O4C11) equal to 70° and 270°.

Conclusions

Artemisia semiarida, an endemic plant of Kazakhstan, was studied and 5,7-dihydroxy-6,3′,4′-trimethoxyflavone (eupatilin) was isolated and identified using IR and NMR data. Result of X-ray diffraction studies showed that the chromene skeleton is flat with an accuracy of ±0.014 Å. The phenyl ring is slightly unfolded relative to the chromene one, the dihedral angle between them is 4.1°. For free molecules of 5,7-dihydroxy-6,3′,4′-trimethoxyflavone, four conformers with the values of the torsion angle O1C2C1'C2' 30°, 140°, 210° and 320°, respectively, can be realized. The energy barriers between them are insignificant and are about 8.4 kJ/mol value. The smallest value of enthalpy during rotation along the C6-O4 bond falls on the position of the methoxyl group at the torsion angle τ(C5C6O4C11) equal to 70° and 270°.

References

1 Landete, J. M. (2012). Updated knowledge about polyphenols: Functions, bioavailability, metabolism, and health. *Crit. Rev. Food Sci. Nutr*., *52*(10), 936–948. https://doi.org/10.1080/10408398.2010.513779

2 Bubols, G. B., da Rocha, V. D., Medina-Remon, A. Gilsane von Poser, Lamuela-Raventos, & R. M., Eifler-Lima V. L. et.al. (2013). The antioxidant activity of coumarins and flavonoids. *Mini-Rev. Med. Chem. 13*, 318–334. https://doi.org/10.2174/138955713804999775

3 Lago J. H. G., Toledo-Arruda A. C., Mernak M., Barrosa R. H., Martins M. A., & Tibério I. F. L. et.al. (2014). Structure-activity association of flavonoids in lung diseases. *Molecules*, *19*, 3570–3595. https://doi.org/10.3390/molecules19033570

4 Stewart J. J. P. (2007). Optimization of parameters for semiempirical methods V: modification of NDDO approximations and application to 70 elements. *J. Mol. Modeling*, 13, 1173–1213. https://doi.org/10.1007/s00894-007-0233-4

5 Bruker (2015). SAINT. Bruker AXS Inc., Madison, Wisconsin, USA.

6 Bruker (2015). SADABS. Bruker AXS Inc., Madison, Wisconsin, USA.

7 Sheldrick, G. M. (2008). Crystal structure solution with SHELXS. *Acta Crystaollogr., Sect. A*, *64*, 112–122. https://doi.org/10.1107/S0108767307043930

8 Sheldrick, G. M. (2015). Crystal structure refinement with SHELXL. *Acta Crystaollogr., Sect. C*, *71*, 3–8. https://doi.org/10.1107/S2053229614024218

9 Turdybekov, K. M., Rakhimova, B. B., Makhmutova, A. S., Smailova, Zh. R., Nurkenov, O. A., & Adekenov, S. M. (2014). Stereochemistry of methoxylated flavonoids from *Artemisia semiarida*. *Chem. Nat. Comp.*, *50*(1), 135–136. https://doi.org/10.1007/s10600-014-0889-9

10 Kupchan, S. M., Sigel, C. W., Hemingway, R. J., Knox, J. R., & Udayamurthy, M. S. (1969). Tumor inhibitors — XXXIII. Cytotoxic flavones from *Eupatorium* species. *Tetrahedron*, *25*(8), 1603–1615. https://doi.org/10.1016/s0040-4020(01)82733-2

11 Suleimenov, E. M., Smagulova, F. M., Morozova, O. V., Raldugin, V. A., Bagryanskaya, I. Yu., Gatilov, Yu. V., Yamovoi V. I., & Adekenov, S. M. (2005). Sesquiterpene Lactones and Flavonoids from Artemisia albida. *Chemistry of Natural Compounds*, *41*, 689–691. https://doi.org/10.1007/s10600-006-0013-x

12 Allen, F. H., Kennard, O., Watson, D. G., Brammer, L., Orpen, A. G., & Taylor R. (1987). Tables of bond lengths determined by x-ray and neutron diffraction. *J. Chem. Soc. Perkin Trans. 2*, S1-S19. https://doi.org/10.1039/p298700000s1

13 Pagola, S., Tracanna, M. I., Amani, S. M., Gonzáles, A. M., Raschi, A. B., & Romano, E. et.al. (2008). Sideroxylin from Miconiaioneura: Monohydrate crystal structure from high resolution X-ray powder diffraction. *Nat. Prod. Commun.*, *3*, 759–764. https://doi.org/10.1177/1934578x0800300516

14 Ali M. S., Ali S., Anjum S., & Ahmad W. (2006). 5-Hy-droxy-4′,6,7-tri-meth-oxy-flavone. *Acta Crystallogr., Sect.E: Struct.Rep.Online,62*, o1107-o1109. https://doi.org/10.1107/S1600536806005617

15 Rossi, M, Meyer, R, Constantinou, P, Caruso, F, Castelbuono, D, & O'Brien, M et.al. (2001). Molecular structure and activity toward DNA of baicalein, a flavone constituent of the Asian herbal medicine "Sho-saiko-to". *J. Nat. Prod.*, *64*, 26–31. https://doi.org/10.1021/np000068s

16 Kitaigorodskii, A. I. (1971). *Molekulyarnye kristally [Molecular crystals]*. Moscow: Nauka [in Russian].

17 Habsaoui, A., Gaydou, E. M., & Wallet, J.-C. Cristal structure of 6-hydroxy-2',3',4'-trimethoxyflavone. (1999). *Z. Kristallogr. — New Cryst. Struct., 214*, 465–466. https://doi.org/10.1515/ncrs-1999-0433

18 Chou, N. H.-H., Parvez, M., Ali, M. S., Ahmed, S., & Ahmed, W. (2002). Cirsimaritin. *Acta Crystallogr., Sect. E: Struct. Rep. Online*. *58*, o285–o287. https://doi.org/10.1107/S1600536802002660

19 Shoja, M., Bisso, S., Kabbani, R., & Athanasopoulos, D. (1999). Cristal structure of 6-hydroxy-2'-methoxyflavone. *Z. Kristallogr. — New Cryst. Struct., 214*, 237–238. https://doi.org/10.1515/ncrs-1999-0244

Information about authors*

Turdybekov, Koblandy Muboryakovich *(correspondent author)* — Doctor of chemical sciences, Professor, Karagandy University of the name of academician E.A. Buketov, Universitetskaya street, 28, 100024, Karaganda, Kazakhstan; e-mail: xray-phyto@yandex.kz; https://orcid.org/0000-0001-9625-0060;

Rakhimova, Bibilul Bagdatovna — Candidate of chemical sciences, Associate Professor, Karaganda Medical University, Gogol str., 40, 100008, Karaganda, Kazakhstan; e-mail: bibigul_rahimova@mail.ru; https://orcid.org/0000-0003-2662-536X;

Makhmutova, Almagul Satybaldievna — Candidate of chemical sciences, Associate Professor, Karaganda Medical University, Gogol str., 40, 100008, Karaganda, Kazakhstan; e-mail: almagul_312@mail.ru; https://orcid.org/0000-0002-0194-8739;

Gatilov, Yurii Vasilevich — Doctor of chemical sciences, Leading researcher, N.N. Vorozhtsov Institute of Organic Chemistry of Siberian Branch of Russian Academy of Sciences, Novosibirsk, Lavrentiev Avenue, 9, 630090, Russia; e-mail: gatilov@nioch.ncs.ru; https://orcid.org/0000-0002-4128-7293;

Adekenov, Sergazy Mynzhasarovich — Doctor of Chemical Sciences, Professor, CEO, JSC "International Research and Production Holding "Phytochemistry", Gazaliev str. 4, 100009, Karaganda, Kazakhstan, e-mail: arglabin@phyto.kz; https://orcid.org/0000-0001-7588-6174

*The author's name is presented in the order: *Last Name, First and Middle Names*

How to Cite: Surve, N.S., Thomas, A.B., Bhole, R.P., & Patil, C.Y. (2023) Flash Chromatography and Semi-Preparative HPLC: Review on the Applications and Recent Advancements over the Last Decade. *Eurasian Journal of Chemistry, 109(1), 20-30.* https://doi.org/10.31489/2959-0663/1-23-9

PHYSICAL AND ANALYTICAL CHEMISTRY

Review

Received: 21 November 2022 | Revised: 23 December 2022 | Accepted: 26 January 2023 | Published online: 06 March 2023

UDC 543.544.5

https://doi.org/10.31489/2959-0663/1-23-9

Namita S. Surve, Asha B. Thomas*, Ritesh P. Bhole, Chyandrajyoti Y. Patil

Department of Pharmaceutical Quality Assurance, Dr. D.Y. Patil Institute of Pharmaceutical Sciences and Research, Pimpri, Pune, MS, India (Affiliated with the Savitribai Phule Pune University, Pune)
*(*Corresponding author'se-mail: asha.thomas@dypvp.edu.in)*

Flash Chromatography and Semi-Preparative HPLC: Review on the Applications and Recent Advancements over the Last Decade

Flash chromatography and Semi-Preparative High Performance Liquid Chromatography have showed themselves as promising separation tools. These techniques assist in the process of isolation, fractionation and purification of chemical, biological and pharmaceutical substances. The present article describes the recent advancements made in flash chromatography and semi-preparative HPLC techniques in the last decade with specific focus on natural products. This article highlights the basics, instrumentation, current advancements made to facilitate the separation, advantages and applications of these two techniques. Flash chromatography is a versatile tool for the rapid but efficient separation and purification of analytes in relatively pure form. Nowadays, there are even functionalized silica pre-packed cartridges with different silica weights and particle sizes that are available to use. Flash separation using dual columns can be used to enhance separation of complex mixtures and can be applied to numerous classes of compounds. The semi-preparative techniques, despite their high cost, can be helpful in high purity separation and production of reference standards for the pharmaceutical industry. This comprehensive review presents a brief analysis of all the recent research employing these two techniques for varied applications. This review will help chromatography specialists to make the decision of applying these two techniques in order to accelerate their research and development journey.

Keywords: Flash chromatography, Semi-preparative HPLC, Isolation, Fractionation, Purification, Recent advancements, Evolution, Applications.

Contents

List of abbreviations

MIP: Molecular Imprinting Polymers
SPE: Solid phase extraction
FA: Formic acid

GLA-ME: Gamma-linolenic acid methyl ester
FG and F2G: Mono- and diferuloyl glycerol,
TF1: Theaflavin
TF2A: Theaflavin-3-gallate
TF2B: Theaflavin-3'-gallate
TF3: Theaflavin-3,3'-digallate
RP-HPLC: Reverse phase — High Performance Liquid Chromatography
HSCCC: High speed counter current chromatography
EA: Ethyl acetate
YMC: Octadecylsilane semi-preparative column
YMC ODS-AQ: Semi-preparative column
LDH: Lactate dehydrogenate
ALA: α-linolenic acid
LA, 18:2n6: Linoleic
BHP: Biohydrogenation products
RA: Rumenic acid,
VA: Vaccenic acid

Review plan

Inclusion and Exclusion criteria: The present review focuses on some of the recent advancements in flash chromatography and semi-preparative HPLC over the last decade and also highlights various applications and advantages of these two chromatographic methods. The data reported in recent research publications is summarized to make better understanding of the applications and improvements made in these two chromatographic techniques.

Various web search engines, including Google Scholar, PubChem, Science Direct Database, and others, were used to collect data from researches in which both flash and semi-preparative HPLC are applied. The data was gathered through papers published the last decade, from 2011 to 2021. The key words used in search of the data included: liquid chromatography, flash chromatography, semi-preparative HPLC, evolution, applications, recent advancements, purification, fractionation. Few manufacturer application notes are also summarized here. Collected data was further sorted on the basis of specific inclusion-exclusion criteria. In this present review, we summarized research papers based on flash chromatography and semi-preparative HPLC after 2010. The articles published before 2010 are excluded from our review.

Introduction

In the pharmaceutical industry, all manufactured products need to be of highest quality to ensure least risk to the patients. To confirm that the pharmaceutical products meet the required standards, researchers, manufacturers and developers across the globe apply numerous analytical tools and techniques during the development process, for the qualitative or quantitative estimations and for elucidation of structures of components in complex mixtures. Chromatography has a vital position in global research for its wide field of applications. The last few decades presented tremendous technological advancements in chromatographic instrumentation and techniques. Among these, the techniques of flash chromatography and semi-preparative HPLC continue to grow, providing solutions to many analytical problems across varied research scopes. The present review attempts to focus on some of the recent advancements in flash chromatography and semi-preparative HPLC over the last decade and also highlights various applications and advantages of these two chromatographic methods.

Flash chromatography

It is a modified version of column chromatography first proposed in 1978 by W.C. Still in order to purify desired products during chemical synthesis [1]. Due to its several advantages, including low cost, lesser time consumption and high yield, it was later used in natural products extraction [2, 3], sample enrichment, and purifying [4, 5] procedures. This technique is analogous to the traditional column chromatography, however with positive pressure being applied to drive the solvent through the column [6]. As this chromatographic technique operates at lower pressures compared to HPLC, it is also referred to as low or medium pressure chromatography. It is now the most widely used approach for macroscale purifications in academic, research and development laboratories [7]. Flash chromatography generally is an air-driven fusion of medium-

pressure and short-column chromatography which has been successfully used for quick separations. It can be applied to both reverse and normal phase separation [8]. Some of the recent advancements in flash chromatography include the optimization of numerous operating parameters such as flow rate, mass of sample load, and separation time using the binary gradient, binary solvent gradient slope, silica and modified silica based stationary phases in order to isolate and purify milligram to few hundredth of gram amounts of analytes in a relatively purified form [9]. The chromatogram obtained from a flash chromatographic run is represented in Fig. 1.

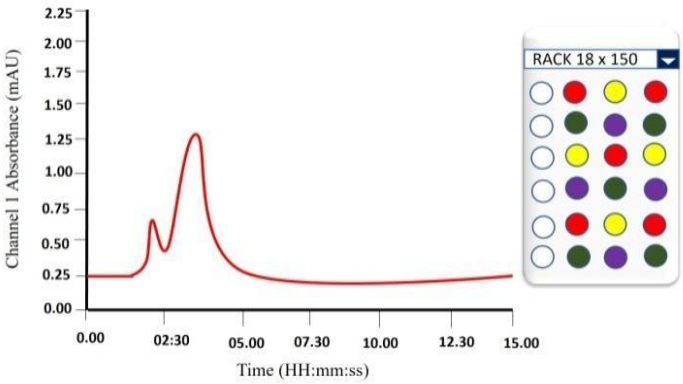

Figure 1. Flash chromatogram with fraction collection

Current reports using flash chromatographic separations

Selman *et al.* has reported the development of functionalized silica materials which allow the purification of fullerenes [10]. Nowadays flash purification systems are equipped with pre-packed cartridges with different silica weights and particle sizes, that are commercially available to assist versatile separation processes [11]. Duckworth *et al.* (2017) utilized dual-column flash chromatography approach (i.e. reverse phase absorption and size exclusion) to purify pyoverdine from *Pseudomonas putida* GB1 [12]. In modern flash chromatography systems, the solvent is pumped through the cartridges which can also be bought pre-packed. Preliminary purification and concentration of organic compounds [13], separation and purification of bioactive compounds [14] are the two major applications of flash chromatography. Today, a wide range of industrial flash chromatographic equipment is available, each featuring manually packed columns or pre-packed cartridges, high-efficiency solvent pumps, automatic fraction collectors and microcomputer-controlled detectors [15]. Reversed phase flash chromatography has been used to purify oregonin from aqueous solution of spray-dried alder extract [16]. With the benefits of the improved instrumentation, nowadays flash separation offers high loading capacity, increased speed of separation and ease of use, thereby making it viable for large-scale separations.

There is also a report on the use of Molecular Imprinting Polymers (MIPs) for flash separation techniques. In this study, Xue *et al*., 2013 extracted pure shikimic acid from Chinese star anise by simple flash column chromatography using MIPs [21, 22] as the adsorbent produced by dispersion polymerization technique [23, 24]. MIPs were packed onto HPLC or Solid phase extraction (SPE) micro-columns [7] in order to extract active ingredients from herbal plants. The extraction on an industrial scale, however, failed due to the poor mechanical stability of MIP in the columns, complexity and discontinuity in SPE micro-columns. By combining molecular imprinting technology and flash chromatography, Xue *et al*., 2014 developed a highly selective flash chromatography method for separation of shikimic acid. Researchers used columns with MIP-containing micropore filters, pre-equilibrated with acetic acid: water (5:95 %v/v) before loading the sample. They loaded non-purified ethyl acetate extract onto the MIP-flash column with elution at 1.7 ml/min with EtOH: water (40:60 %v/v), that leaded to the successful separation of shikimic acid enriched fraction [25]. The fractions obtained were then evaporated to dryness using a rotary evaporator. The study reported that the MIP-flash column provided better capability and reusability than the HPLC columns packed with MIPs. This method allows the large-scale isolation of highly purified active compounds from any herbal plant; is easy, repeatable, and cost-effective.

In another study, Hossain *et al*., 2018 used the flash chromatography technique to separate polyphenols from pure red onion extract. The 80 % methanolic extract of powdered red onion was loaded on a Telos C18

reverse flash column and separated using water (A) : 0.5 % FA (formic acid) in ACN(B) as the mobile phase at 40 ml/min flow rate. Polyphenols were isolated using a sequential gradient of 0–100 % B over 35 minutes, with over 70 fractions recovered at a time scale of 0.5min/fraction. This study established the utility of flash chromatographic fractionation for the effective separation of polyphenols [26].

Ma Xiaoqin *et al*., 2016, has developed the flash chromatography method with large spherical MIPs used as stationary phase for the extraction of highly purified solanesol from tobacco leaves. MIP activated flash cartridges were loaded with methanolic extract of tobacco leaves and eluted at different flow rates (2, 4, 6 and 8 ml/min). Next, the un-absorbed solanesol was removed by leaching the column with MeOH at 2 ml/min flow rate for 20 min. Finally, the adsorbed solanesol was extracted with acetic acid/methanol mixtures in different ratios (3/7, 2/8, 1/9, 0/10 v/v) at specific flow rates for 1 h, and the highly purified solanesol was obtained [27]. The reusability of these MIP-flash columns was tested by repetitive loading (n = 5) on the same column under the optimal flash chromatographic condition. It was observed that these columns are reversible during five rounds of regeneration, with a standard deviation of 4 % for five separate adsorption rate assessments, indicating that the MIP-flash column has excellent reusability capacity [27].

In other research, Jubie *et al*., 2015 utilized flash chromatography system to isolate gamma-linolenic acid methyl ester (GLA-ME) from *Spirulina platensis*, a commercially well-known blue-green micro algae [28] rich in phenolic acids, tocopherol and GLA [29, 30]. Using a high-performance flash chromatography approach (Isolera system), omega-6 PUFA i.e., GLA was isolated as its methyl ester (GLA-ME), which acts as a molecular target for lung cancer treatment. GLA-ME was isolated by loading the vacuum dried enhanced GLA fraction (0.5 g) in a 50 g KPSilBiotage SNAP cartridge, using 60 % hexane and 40 % acetone as the mobile phase at a constant flow rate (50 ml/min). A total of 105 fractions, each of 22 ml, were collected at 254 nm, then each fraction was proceeded to TLC for additional analysis. GLA-ME was found to be present in fractions 6-17. This high-performance flash chromatography method improved the productivity of GLA-ME extraction from *Spirulina platensis* [31].

Compton *et al*., 2020 developed and optimized a flash chromatography method using silica stationary phase with a binary gradient of acetone and hexane as the mobile phase to isolate and purify naturally occurring phenylpropenoids i.e., mono- and diferuloyl glycerol, (FG and F2G respectively) which provide protection form UV radiations and oxidation in plants. Flash chromatography system (Teledyne, CombiflashRF200) was used to purify the crude precipitate and Redisep column was used for the following separation. The method was optimized with consideration to the size of used Redisep column, flow rate of solvent, solvent gradient program and volume of the sample load. For purification of FG and F2G, the 3.0 g crude precipitate dissolved in acetone was loaded onto the Redisep column (12 g) using syringe injection, which was then aspirated to dryness for 1 hour before being pumped to the the Redisep separation load column (120 g) at 57 ml/min flow rate. Separation was performed in "liquid load" mode with 0-100 % acetone in hexane gradient. The fractions that included target peaks were combined and evaporated to dryness to obtain purified FG (yellow, oily liquid) and F2G (white solid) [32].

This solid sample loading provided great consistency with no pumping issues and leakages, assisting in rapid purification and obtaining low concentrations of FG and F2G.

RediSepRf Gold® C18Aq columns are reported to be useful for removal of salts and buffers from solvents that are commonly used to purify chemicals. The ability of these columns to adsorb chemicals under highly aqueous conditions without phase collapse makes them excellent for desalting samples. This approach was used to desalt brilliant blue using a methanol water gradient [33].

The application of CombiFlash® Rf-200 columns to purify C60 fullerene from soot is also reported. As most solvents make it difficult to purify fullerenes, the isolation of C60 fullerene was accomplished by dissolving 25 mg sample of soot in carbon disulphide loaded on a CombiFlash® Rf 200 column using a 2-propanol/toluene mixture with ultraviolet detector at 310 nm [34].

A very practical and successful method for the purification of primary amines from a complex mixture was achieved using a ledyne C-18 IscoRediSep reversed phase column with water/ACN as the mobile phase [35]. A large number of the manufacturers of flash chromatographic systems are providing several advancements in their instrumentation including multiple column ports, automated injections with multiple stationary phase chemistries and solvent systems, multiple channel detections using UV, fluorescence and mass guided separation in order to provide more effective and accurate fractionations and increase the purity of the fractions collected through these separations. Robust method transfer from TLC to flash separation through various computer controlled softwares are also being applied today [36].

Semi-preparative HPLC

Since its introduction several decades ago, HPLC continues to remain as one of the most versatile tools in chemical analysis. Semi-preparative HPLC, which evolved in the early 1970's, is now being used for numeral applications including the isolation and purification of compounds from natural product extracts [17], purification of drugs and their by-products during manufacturing process and impurity analysis. The capability to scale-up from analytical operations is one of the key benefits of semi-preparative separation. In the 1970s, the first preparative HPLC system was created to enhance separation power. Semi-preparative HPLC falls under the small scale preparative HPLC and is being used for the separation of small quantities of sample [19]. Using the optimized HPLC parameters (flow rate, mobile phase, stationary phase, maximum amount of sample load, separation temperature), analysis specialists can improve preparative operations thereby saving time and resources [20]. Semi-preparative HPLC allows the separation of high purity compounds [18] which can be used as reference standards in pharmaceutical industries. A typical semi-preparative high performance liquid chromatographic result graph is depicted in Fig. 2.

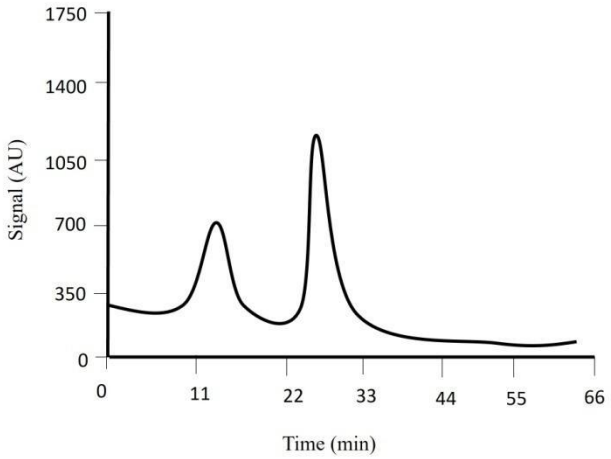

Figure 2. Chromatogram showing isolation of compounds in semi-preparative HPLC

Scale-up process of Analytical HPLC to Semi-preparative HPLC

In the scale-up process, analytical runs are initially performed to establish the separation efficiency, which includes determination and optimization of the appropriate mobile phase, flow rate, stationary phase, separation temperature, and other HPLC parameters. Using the optimized HPLC parameters, this method can be effectively scaled up from analytical to semi-preparative and preparative analysis [37].

The major steps involved in semi-preparative HPLC scale-up and optimization include the modification of the analytical approach in terms of resolution, overcharging on the analytical column and extension of the column size to semi-preparative and preparative scale. The prime parameters that need to be scaled up are the flow rate of separation and the column loading.

The equations that are used to scale up the flow rate (1) and volume (2) are:

$$V_1/V_2 = r_1^2/r_2^2, \quad (1)$$

where V_1 is the flow rate column 1; V_2 is the flow rate column 2.

$$X_1/(\pi \times r_1^2) = X_2/(\pi \times r_2^2) \times 1/C_L, \quad (2)$$

where r_1 is the radius of column 1; X_1 is the max. volume column 1; r_2 is the radius of column 2; X_2 is the max. Volume column 2; C_L is the ratio lengths of columns = 1; Column 1 is the Analytical Column; Column 2 is the Preparative Column.

Current reports using Semi-preparative HPLC separations

In this study, Xu *et al*. (2010) applied the semi-preparative HPLC to isolate and purify four major theaflavins found in black tea, including theaflavin (TF1), theaflavin-3-gallate (TF2A), theaflavin-3'-gallate (TF2B), and theaflavin-3,3'-digallate (TF3). Black tea is at about 80 % of global tea output and has several therapeutic effects, including antioxidant properties [38–40], inhibition of carcinogenesis [41], suppression of lipid peroxidation [42] and protection against cardiovascular diseases [43] due to the action of these four

primary theaflavins [44]. In this study, 35 g of the black tea extract TF50 was loaded on a Mitsubishi SP-207 resin filled column (highly porous modified adsorbent material). Progressive elution with a gradient of 20 %, 30 %, 40 %, 50 %, and 70 % aq. EtOH at a flow rate of 33 ml/min, generated an 80 % pure mixture of these theaflavins (TF80). Further separation on a C18 preparative column with ACN / dist. water / GAA (26:73.5:0.5, v/v/v) as mobile phase at 5 ml/ min flow rate resulted in isolation of the pure theaflavins. Compared to the traditional isolation processes that lasted several hours, this semi-preparative HPLC method required only 45 minutes enabling effective separation of the theaflavins [45].

In another study, Basar *et al*. (2014) developed and validated a simple semi-preparative-RP-HPLC/ PDA method of isolation and quantification of glycyrrhizin from nine distinct samples of *Glycyrrhiza glabra* root collected from different geographical regions. The isolation and quantification were proceeded on reversed phase semi-preparative column with octadecylsilane guard column using binary gradient elution with 30–100 % solvent B [0.1 % v/v trifluoroacetic acid in MeOH] in solvent A [0.1 % v/v trifluoroacetic acid in water] at 3.00 mL/min flow rate at 25–28 °C for 30 min. Prior to loading, the residue obtained from the extracts of each sample was re-dissolved in methanol and filtered. For the analysis, 100 µl sample was injected into the system and the runs were monitored at 254 nm. The study report also demonstrated the validation of the method using nine different samples of *Glycyrrhiza glabra* roots. This method allowed the efficient and quick isolation and quantification of glycyrrhizin with high accuracy and low cost [46].

High speed counter current chromatography (HSCCC) is a continuous liquid-liquid partition chromatography method that works by isolating substances between two immiscible liquid phases. It has numerous benefits, including irreversible adsorption, minimal potential of sample denaturation, complete sample recovery, and relatively low cost [47, 48]. In this study, for the semi-preparative isolation of 10 isomers of caffeoylquinic acid derivatives obtained from the roots of Burdock (*Arctiumlappa* L.), Zheng *et al*. (2018) developed and applied semi-preparative HPLC in combination with HSCCC. These 10 isomers were isolated from the ethyl acetate (EA) extract of Burdock roots which was further fractionated using macroporous resin chromatography yielding three fractions (Fraction 1–3) from the elution of 40 % MeOH. Fractions were collected and purified by HSCCC using EA-petroleum ether-MeOH-water as a solvent system at different ratios as shown in [49]. This revealed that Fraction 1 mainly contains compounds A–C, Fraction 2 mainly contains compound D, and Fraction 3 mainly contains compounds E–J. So, After the separation of derivatives by HSCCC, these collected fractions (i.e., blend of the derivatives) were further proceeded for the purification and identification by YMC octadecylsilane semi-preparative column with mobile phase ACN – 0.1 % FA in water (25:75, v/v) and MeOH – 0.1 % FA in water (25:75, v/v) at 3.0 mL/min flow-rate, observed at 280 nm. This research showed that combination of semi-preparative HPLC and HSCCC is a highly effective method for isolation of ten bioactive caffeoylquinic acid derivatives from natural products [49].

Using semi-preparative HPLC system, Li Aifeng *et al*. (2014) extracted seven known flavonoids (mainly quercetin, apigenin, diosmetin, luteolin and their glycosides**)** from the dried *T. kirilowii Maxim* peel, which is broadly used in traditional Chinese medication as a cure to a cardiovascular, cerebrovascular, and respiratory diseases [50]. The EA fraction of dried peel of *T. kirilowii Maxim* was concentrated by elution through a glass column wet-packed with polyamide resins with a gradient elution program consisting of aqueous ethanol 10 % – 100 % EtOH. Fractions, eluted with 70 % and 90 % EtOH, yielded two subfractions (I and II), which were injected into the semi-preparative column (YMC ODS-AQ) for further isolation of seven flavonoids (I to VII) using isocratic elution mode with MeOH-water as mobile phase in different ratios [for subfraction-I (46:54, v/v) and subfraction-II (66:34, v/v)] at a flow rate of 3.5 ml/min. The column eluent was checked with the UV detector set to 350 nm and manually collected according to the chromatograms. The study suggests the suitability of this procedure for the large-scale isolation of flavonoids from plant extracts [50].

In this study, Zhao Xu *et al*. (2020) applied semi-preparative HPLC to isolate high-purity anthocyanin monomers from grape pomace [51]. To extract anthocyanin from grape pomace, ultrasonification (59 kHz) with acidified methanol (500 ml methanol solution containing 2 % formic acid) was conducted for 10 min. Obtained concentrated crude extract was purified by Amberlite XAD-7HP resin (28 mm×400 mm) column until the resin was saturated. High-purity anthocyanin monomers were isolated from the purified crude extract using semi-preparative HPLC system with gradient elution using ACN/ water/FA (6/92/2, v/v/v) (A) and ACN/water /FA (54/44/2, v/v/v) (B) as the solvent system. Purified fractions of anthocyanin were collected by the automatic fraction collector. This study is the first time report of the effective separation of anthocyanin monomers using a single-step semi-preparative HPLC technique [51].

When a patient suffers from ischemic stroke, the level of LDH in their blood increases quickly, which leads to organ damage. Exploration of LDH inhibitors derived from medicinal plants could be a promising approach for invention of therapeutic drugs for those suffering from ischemic stroke [52, 53]. Isoflavonoids, which have been mainly used to treat ischemic stroke, are powerful LDH inhibitors [54, 55]. So here, in this study, Senlin Li *et al*. (2016) employed ultrafiltration HPLC coupled with PDA detection, and ESI-MS to screen and identify sixisoflavonoids-I to VI (i.e., LDH inhibitors Tectoridin. Iristectorin A, Iridin, Tectorigenin, Irigenin and Irisflorentin) which are the primary active compound of *Belamcandaechinensis* [56]. Further semi-preparative HPLC was performed with the primal optimization of its conditions, including composition of solvent system, flow rate, and injection volume, to separate and isolate these d LDH inhibitors from the extract of *B. chinensis* rhizome. As per this study report, the optimized solvent system contained solvent A (0.5 % acetic acid in water) and solvent B (ACN), with gradient elution times of 0–3 minutes for 10 to 20 % B; 3–6 minutes for 20 to 23 % B; 6–9 minutes for 23 to % B; 9–15 minutes for 30 to 50 50 % B; and 15–20 minutes for 50 % B. The optimal separation was achieved using 10 ml/min flow rate and 1.0 ml injection volume. This method proposed the isolation of the LDH inhibitors (% purity>92 %) by applying ultrafiltration-LC-MS in combination with Semi-preparative HPLC, that proved to be of low-cost and high-efficiency, indicating its significant potential for commercial applications [57].

The traditional process for identification of natural active compounds includes purification followed by one-to-one screening, which takes longer time, affects the stability and sensitivity of the method [58]. Zhang *et al*. (2018) developed a method for the rigorous screening, preparation, and evaluation of antioxidant potential of natural products [59] by utilizing semi-preparative HPLC with two step separation approach followed by on-line HPLC-radical scavenging detection. Rigol semi-prep-HPLC system was applied to separate and purify seven representative antioxidants from *Magnolia officinalis* using a two-step separation procedure that included both gradient and isocratic elution. The separation of compounds was achieved under specific conditions, for compounds 1–4: injection volume (200 μl), 3.0 ml/min flow rate, detection wavelength of 275 nm with mobile phase solvent A (0.2 % CH_3COOH in water, v/v) and solvent B (MeOH) in gradient elution mode. Compounds 5–7 were obtained at flow rate (3.0 ml/min), injection volume 300 μL at 275 nm with mobile phase composed of solvent A (0.2 % CH_3COOH in water, v/v) and B (MeOH) in isocratic elution mode [58].

Turner *et al*. (2014) used Silver ion solid-phase extraction (Ag^+-SPE) and semi-preparative Ag^+-HPLC to isolate and collect pure isomers, including several t-monoenes (t12, t13, t14, t15, and t16-18:1) as well as non-conjugated dienes (i.e. t10, c15, t11, t15-, and t11, c15-18:2) unique to α-linolenic acid ALA [57]. Linoleic (LA, 18:2n6) and α-linolenic acid (ALA, 18:3n3) [60] are two polyunsaturated fatty acids (PUFAs) found in bovine feed that are metabolized by rumen microbes, leading to generation of various biohydrogenation products (BHP) that can be found in milk and meat. Biological functions of LA-BHP, which include conjugated linoleic acid [cis (c) 9, trans (t) 11-18:2 (Rumenicacid, RA) and t10, c12-18:2], as well as trans fatty acid isomers [t9, t10, and t11-18:1 (Vaccenic acid, VA)], have been investigated, but the influence of many BHP specific to ALA still has not been thoroughly researched, taking into consideration that most ALA-BHP are not available in the marketplace. In this reported study, a semi-preparative silver ion (Ag^+) HPLC approach was developed for the purification and collection of ALA-BHP. Researchers used Ag^+-solid phase extraction approach to fractionate the sample and collected the t-18:1, 18:2, and 18:3 fractions. Collected fraction were further isolated using semi-preparative Ag^+-HPLC, and the t-18:1 isomer, 18:2 isomer, and 18:3 isomers were obtained [57].

Conclusions

This review summarizes the effective application of flash chromatography and semi-preparative HPLC for the fractionation, isolation and purification process. Enlisted research papers specifically discuss their applications in the area of natural compounds. The flash chromatography with its ease of use, varied stationary phase chemistries, multiple columns and detectors, automated fraction collectors represents a very viable tool for fractionation and purification. Semi-preparative separation can assist in obtaining highly purified compounds which expands its applicability in diverse scopes. This review will help chromatography specialists to make decision of applying these two techniques to improve their research and development studies.

Acknowledgments

The authors would like to thank the management and principal of DPU, Pharmacy for providing the necessary support and facilities to undertake this work. The authors would like to express their sincere grati-

tude to DST for the Flash chromatographic facility established through the FIST Program at the institute (Order dated 12th Dec 2019 from the Government of India, Department of Science and Technology, R and D-Infrastructure Division) which allowed us to write this review.

References

1 Still, W. C., Kahn, M. & Mitra, A. (1978). Rapid chromatographic technique for preparative separations with moderate resolution. *The Journal of Organic Chemistry*, *43*(14), 2923–2925. https://doi.org/10.1021/jo00408a041

2 Chen, C., Chen, T., Liu, Y., Zou, D., You, J., Li, Y. et al. (2015). Rapid screening, identification, separation, and purification of four bioactive compounds from Swertia mussotii Franch. *Separation Science and Technology*, *50*(4), 604–610. https://doi.org/10.1080/01496395.2014.957316

3 Wang, X. Y., Li, J. F., Jian, Y. M., Wu, Z., Fang, M. J., Qiu, Y. K. et al. (2015). On-line comprehensive two-dimensional normal-phase liquid chromatography× reversed-phase liquid chromatography for preparative isolation of Peucedanum praeruptorum. *Journal of Chromatography A*, *1387*, 60–68. https://doi.org/10.1016/j.chroma.2015.02.003

4 Keck-Wilhelm, A., Kratz, E., Mildau, G., Ilse, M., Schlee, C., Lachenmeier, D. W. et al. (2015). Chemical analysis and risk assessment of prohibited colouring agents in face paint with special regard to CI 15585 (D & CR ed No. 9, P pigment R ed 53: 1). *International Journal of Cosmetic Science*, *37*(2), 187–195. https://doi.org/10.1111/ics.12181

5 Liang, Z., Li, B., Liang, Y., Su, Y. & Ito, Y. (2015). Separation and purification of two minor compounds from Radix isatidis by integrative MPLC and HSCCC with preparative HPLC. *Journal of liquid chromatography & related technologies*, *38*(5), 647–653. https://doi.org/10.1080/10826076.2014.936606

6 Dar, A. A., Raina, A. & Kumar, A. (2022). Development, method validation and simultaneous quantification of eleven bioactive natural products from high altitude medicinal plant by high performance liquid chromatography. *Biomedical Chromatography*, e5408. https://doi.org/10.1002/bmc.5408

7 Xie, Z., Xu, X., Xie, C., Liang, Z., Yang, M., Huang, J., Yang, D. et al. (2014). Preparative isolation of tetrandrine and fangchinoline from Radix Stephania tetrandra using reversed-phase flash chromatography. *Journal of Liquid Chromatography & Related Technologies*, *37*(3), 343–352. https://doi.org/10.1080/10826076.2012.745139

8 Weber, P., Hamburger, M., Schafroth, N. & Potterat, O. (2011). Flash chromatography on cartridges for the separation of plant extracts: rules for the selection of chromatographic conditions and comparison with medium pressure liquid chromatography. *Fitoterapia*, *82*(2), 155–161. https://doi.org/10.1016/j.fitote.2010.08.013

9 Compton, D. L., Appell, M., Kenar, J. A. & Evans, K. O. (2020). Enzymatic synthesis and flash chromatography separation of 1,3-Diferuloyl-sn-glycerol and 1-feruloyl-sn-glycerol. *Methods and protocols*, *3*(1), 8. https://doi.org/10.3390/mps3010008

10 Selmani, S., Shen, M. Y. & Schipper, D. J. (2017). Iptycene-functionalized silica gel for the purification of fullerenes using flash chromatography. *RSC advances*, *7*(31), 19026–19029. https://doi.org/10.1039/C7RA01575E

11 Kasprowiak, A., Cazier-Dennin, F. & Danjou, P. E. (2020). Flash Chromatography System: A Practical Tool for Demonstrating the Influence of Column Characteristics on Chromatographic Resolution. *Journal of Chemical Education*, *97*(4), 1145–1150. https://doi.org/10.1021/acs.jchemed.9b00929

12 Duckworth, O. W., Markarian, D. S., Parker, D. L., & Harrington, J. M. (2017). A two-column flash chromatography approach to pyoverdin production from Pseudomonas putida GB1. *Journal of microbiological methods*, *135*, 11-13. https://doi.org/10.1016/j.mimet.2017.01.019

13 Xue, M., Wang, Y., Meng, Z., Zhang, W., Wu, Y. & Jiang, S. et al. (2013). Extraction of shikimic acid from Chinese star anise using flash column chromatography on a molecularly-imprinted polymer column. *Journal of Liquid Chromatography & Related Technologies*, *36*(19), 2677–2686. https://doi.org/10.1080/10826076.2012.725690

14 Madhu, S. K., Shaukath, A. K. & Vijayan, V. A. (2010). Efficacy of bioactive compounds from Curcuma aromatica against mosquito larvae. *Acta tropica*, *113*(1), 7–11. https://doi.org/10.1016/j.actatropica.2009.08.023

15 Naumiec, G. R., Del Padre, A. N., Hooper, M. M., St. Germaine, A. & DeBoef, B. (2013). A Modern Apparatus for Performing Flash Chromatography: An Experiment for the Organic Laboratory. *Journal of chemical education*, *90*(3), 376–378. https://doi.org/10.1021/ed300360f

16 Lea, C. S., Simhadri, C., Bradbury, S. G., Wulff, J. E. & Constabel, C. P. (2021). Efficient purification of the diarylheptanoid oregonin from red alder (Alnus rubra) leaves and bark combining aqueous extraction, spray drying and flash-chromatography. *Phytochemical Analysis*, *32*(4), 554–561. https://doi.org/10.1002/pca.3005

17 Huber, U. (2006). Solutions for preparative HPLC–Application Compendium. *Agilent Technologies Application.*

18 Jadhav, B. G., Jadhav, A. M., Shirode, A. R. & Kadam, V. J. (2014). A Comprehensive Review for the Learners and Users: Preparative High Performance Liquid Chromatography. *International Journal of Chemical and Pharmaceutical Analysis*, *1*, 121–129.

19 Warren, W. J. & Vella, G. (1995). Principles and methods for the analysis and purification of synthetic deoxyribonucleotides by high-performance liquid chromatography. *Molecular biotechnology*, *4*(2), 179–199. https://doi.org/10.1007/BF02921611

20 Lee, P. (2008). Development of a semi-preparative C_{30} HPLC column for carotenoids separation. https://doi.org/10.31979/etd.w7eg-73z9

21 Pan, G., Shen, J., Ma, Y., He, Y., Bao, Y., Li, R. & Dang, J. (2019). Preparative separation of isoquinoline alkaloids from Corydalis impatiens using a middle-pressure chromatogram isolated gel column coupled with two-dimensional liquid chromatography. *Journal of Separation Science*, *42*(20), 3182–3190. https://doi.org/10.1002/jssc.201900252

22 Xue, M., Wang, Y., Meng, Z., Zhang, W., Wu, Y. & Jiang, S. et al. (2013). Extraction of shikimic acid from Chinese star anise using flash column chromatography on a molecularly-imprinted polymer column. *Journal of Liquid Chromatography & Related Technologies*, *36*(19), 2677–2686. https://doi.org/10.1080/10826076.2012.725690

23 Ye, L. & Mosbach, K. (2001). Molecularly imprinted microspheres as antibody binding mimics. *Reactive and Functional Polymers*, *48*(1–3), 149–157. https://doi.org/10.1016/S1381-5148(01)00050-5

24 Ye, L., Cormack, P. A. & Mosbach, K. (2001). Molecular imprinting on microgel spheres. *Analytica Chimica Acta*, *435*(1), 187–196. https://doi.org/10.1016/S0003-2670(00)01248-4

25 Candeias, N. R., Assoah, B. & Simeonov, S. P. (2018). Production and synthetic modifications of shikimic acid. *Chemical Reviews*, *118*(20), 10458–10550. https://doi.org/10.1021/acs.chemrev.8b00350

26 Hossain, M. B., Lebelle, J., Birsan, R. & Rai, D. K. (2018). Enrichment and assessment of the contributions of the major polyphenols to the total antioxidant activity of onion extracts: A fractionation by flash chromatography approach. *Antioxidants*, *7*(12), 175. https://doi.org/10.3390/antiox7120175

27 Ma, X., Meng, Z., Qiu, L., Chen, J., Guo, Y., Yi, D. & Xue, M. et al. (2016). Solanesol extraction from tobacco leaves by Flash chromatography based on molecularly imprinted polymers. *Journal of Chromatography B*, *1020*, 1–5. https://doi.org/10.1016/j.jchromb.2016.03.007

28 Jubie, S., Ramesh, P. N., Dhanabal, P., Kalirajan, R., Murugananthan, N., Antony, A. S. et al. (2015). Synthesis, antidepressant and antimicrobial activities of some novel stearic acid analogues. *European journal of medicinal chemistry*, *54*, 931–935. https://doi.org/10.1016/j.ejmech.2012.06.025

29 Makori, A. J., Abuom, P. O., Kapiyo, R., Anyona, D. N. & Dida, G. O. (2017). Effects of water physico-chemical parameters on tilapia (Oreochromis niloticus) growth in earthen ponds in Teso North Sub-County, Busia County. *Fisheries and Aquatic Sciences*, *20*(1), 1-10. https://doi.org/10.1186/s41240-017-0075-7

30 Sajilata, M. G., Singhal, R. S. & Kamat, M. Y. (2008). Fractionation of lipids and purification of γ-linolenic acid (GLA) from Spirulina platensis. *Food Chemistry*, *109*(3), 580–586. https://doi.org/10.1016/j.foodchem.2008.01.005

31 Qiu, P. L., Liu, S. Y., Bradshaw, M., Rooney-Latham, S., Takamatsu, S., Bulgakov, T. S., Braun, U. et al. (2020). Multilocus phylogeny and taxonomy of an unresolved, heterogeneous species complex within the genus Golovinomyces (Ascomycota, Erysiphales), including G. ambrosiae, G. circumfusus and G. spadiceus. *BMC microbiology*, *20*(1), 1–16. https://doi.org/10.1186/s12866-020-01731-9

32 Compton, D. L., & Appell, M. (2020). Rapid Raman spectroscopic determination of 1-feruloyl-sn-glycerol and 1,3-diferuloyl-sn-glycerol. *Spectrochimica acta. Part A, Molecular and biomolecular spectroscopy*, *229*, 118020. https://doi.org/10.1016/j.saa.2019.118020

33 Takano, Y., Kashiyama, Y., Ogawa, N. O., Chikaraishi, Y. & Ohkouchi, N. et al. (2010). Isolation and desalting with cation-exchange chromatography for compound-specific nitrogen isotope analysis of amino acids: application to biogeochemical samples. *Rapid Communications in Mass Spectrometry*, *24*(16), 2317–2323. https://doi.org/10.1002/rcm.4651

34 Ravelo-Pérez, L. M., Herrera-Herrera, A. V., Hernández-Borges, J. & Rodríguez-Delgado, M. Á. (2010). Carbon nanotubes: solid-phase extraction. *Journal of Chromatography A*, *1217*(16), 2618–2641. https://doi.org/10.1016/j.chroma.2009.10.083

35 Staub, A., Guillarme, D., Schappler, J., Veuthey, J. L. & Rudaz, S. (2011). Intact protein analysis in the biopharmaceutical field. *Journal of pharmaceutical and biomedical analysis*, *55*(4), 810–822. https://doi.org/10.1016/j.jpba.2011.01.031

36 Huber, U. & Majors, R. E. (2007). Principles in preparative HPLC. *Agilent Technologies Inc., Germany*, *2*, 60–71.

37 Łuczaj, W. & Skrzydlewska, E. (2005). Antioxidative properties of black tea. *Preventive medicine*, *40*(6), 910–918. https://doi.org/10.1016/j.ypmed.2004.10.014

38 Yang, Z., Jie, G., Dong, F., Xu, Y., Watanabe, N. & Tu, Y. (2008). Radical-scavenging abilities and antioxidant properties of theaflavins and their gallate esters in H2O2-mediated oxidative damage system in the HPF-1 cells. *Toxicology in Vitro*, *22*(5), 1250–1256. https://doi.org/10.1016/j.tiv.2008.04.007

39 Yang, Z., Tu, Y., Xia, H., Jie, G., Chen, X. & He, P. (2007). Suppression of free-radicals and protection against H_2O_2-induced oxidative damage in HPF-1 cell by oxidized phenolic compounds present in black tea. *Food chemistry*, *105*(4), 1349–1356. https://doi.org/10.1016/j.foodchem.2007.05.006

40 Tu, Y. Y., Tang, A. B. & Watanabe, N. (2004). The theaflavin monomers inhibit the cancer cells growth in vitro. *Acta Biochimica et Biophysica Sinica*, *36*(7), 508–512. https://doi.org/10.1093/abbs/36.7.508

41 Leung, L. K., Su, Y., Chen, R., Zhang, Z., Huang, Y., Chen, Z. Y. et al. (2001). Theaflavins in black tea and catechins in green tea are equally effective antioxidants. *The Journal of nutrition*, *131*(9), 2248–2251. https://doi.org/10.1093/jn/131.9.2248

42 Gardner, E. J., Ruxton, C. H. S. & Leeds, A. R. (2007). Black tea–helpful or harmful? A review of the evidence. *European journal of clinical nutrition*, *61*(1), 3-18. https://doi.org/10.1038/sj.ejcn.1602489

43 Balentine, D. A. (1992). Manufacturing and chemistry of tea. *Phenolic Compounds in Food and Their Effects on Health I*, Chapter 8, 102-117 https://doi.org/10.1021/bk-1992-0506.ch008

44 Xu, Y., Jin, Y., Wu, Y. & Tu, Y. (2010). Isolation and purification of four individual theaflavins using semi-preparative high performance liquid chromatography. *Journal of liquid chromatography & related technologies*, *33*(20), 1791–1801. https://doi.org/10.1080/10826076.2010.526865

45 Ito, Y. (2005). Golden rules and pitfalls in selecting optimum conditions for high-speed counter-current chromatography. *Journal of Chromatography A*, *1065*(2), 145–168. https://doi.org/10.1016/j.chroma.2004.12.044

46 Basar, N., Talukdar, A. D., Nahar, L., Stafford, A., Kushiev, H., Kan, A., Sarker, S. D. et al. (2014). A Simple semi-preparative reversed-phase HPLC/PDA method for separation and quantification of glycyrrhizin in nine samples of Glycyrrhiza glabra root collected from different geographical origins. *Phytochemical analysis*, *25*(5), 399–404. https://doi.org/10.1002/pca.2507

47 Skalicka-Woźniak, K. & Garrard, I. (2015). A comprehensive classification of solvent systems used for natural product purifications in countercurrent and centrifugal partition chromatography. *Natural product reports*, *32*(11), 1556–1561. https://doi.org/10.1039/C5NP00061K

48 Li, A., Sun, A., Liu, R., Zhang, Y. & Cui, J. (2014). An efficient preparative procedure for main flavonoids from the peel of Trichosanthes kirilowii Maxim. using polyamide resin followed by semi-preparative high performance liquid chromatography. *Journal of Chromatography B*, *965*, 150–157. https://doi.org/10.1016/j.jchromb.2014.06.003

49 Zheng, Z., Wang, X., Liu, P., Li, M., Dong, H. & Qiao, X. et al. (2018). Semi-preparative separation of 10 caffeoylquinic acid derivatives using high speed counter-current chromatography combined with semi-preparative HPLC from the roots of burdock (Arctium lappa L.). *Molecules*, *23*(2), 429. https://doi.org/10.3390/molecules23020429

50 Li, A., Sun, A., Liu, R., Zhang, Y., & Cui, J. (2014). An efficient preparative procedure for main flavonoids from the peel of Trichosanthes kirilowii Maxim. using polyamide resin followed by semi-preparative high performance liquid chromatography. *Journal of chromatography. B, Analytical technologies in the biomedical and life sciences*, *965*, 150–157. https://doi.org/10.1016/j.jchromb.2014.06.003

51 Zhao, X., Zhang, S. S., Zhang, X. K., He, F. & Duan, C. Q. et al. (2020). An effective method for the semi-preparative isolation of high-purity anthocyanin monomers from grape pomace. *Food chemistry*, *310*, 125830. https://doi.org/10.1016/j.foodchem.2019.125830

52 Kolappan, S., Shen, D. L., Mosi, R., Sun, J., McEachern, E. J., Vocadlo, D. J., Craig, L. et al. (2015). Structures of lactate dehydrogenase A (LDHA) in apo, ternary and inhibitor-bound forms. *Acta Crystallographica Section D: Biological Crystallography*, *71*(2), 185–195. https://doi.org/10.1107/S1399004714024791

53 Lin, S. H., Huang, K. J., Weng, C. F. & Shiuan, D. (2015). Exploration of natural product ingredients as inhibitors of human HMG-CoA reductase through structure-based virtual screening. *Drug design, development and therapy*, *9*, 3313. https://doi.org/10.2147/DDDT.S84641

54 Chen, Y., Yu, H., Wu, H., Pan, Y., Wang, K., Liu, L., Zhang, C. et al.(2015). Tracing novel haemostatic compounds from heating products of total flavonoids in Flos Sophorae by spectrum–effect relationships and column chromatography. *Journal of Separation Science*, *38*(10), 1691–1699. https://doi.org/10.1002/jssc.201500100

55 Woźniak, D. & Matkowski, A. (2015). Belamcandae chinensis rhizoma — a review of phytochemistry and bioactivity. *Fitoterapia*, *107*, 1–14. https://doi.org/10.1016/j.fitote.2015.08.015

56 Li, S., Li, S., Tang, Y., Liu, C., Chen, L. & Zhang, Y. (2016). Ultrafiltration-LC–MS combined with semi-preparative HPLC for the simultaneous screening and isolation of lactate dehydrogenase inhibitors from Belamcanda chinensis. *Journal of separation science*, *39*(23), 4533–4543. https://doi.org/10.1002/jssc.201600703

57 Turner, T. D., Meadus, W. J., Mapiye, C., Vahmani, P., Lopez-Campos, O., Duff, P., Dugan, M. E. R. & et al. (2015). Isolation of α-linolenic acid biohydrogenation products by combined silver ion solid phase extraction and semi-preparative high performance liquid chromatography. *Journal of Chromatography B*, *980*, 34–40. https://doi.org/10.1016/j.jchromb.2014.11.038

58 Naczk, M. & Shahidi, F. (2004). Extraction and analysis of phenolics in food. *Journal of chromatography A*, *1054*(1–2), 95–111. https://doi.org/10.1016/j.chroma.2004.08.059

59 Zhang, M., Cheng, S., Liang, Y., Mu, Y., Yan, H., Liu, Q., Zhao, H. et al. (2018). Rapid purification of antioxidants from Magnolia officinalis by semi-prep-HPLC with a two-step separation strategy guided by on-line HPLC-radical scavenging detection. *Journal of Chromatography B*, *1100*, 140–147. https://doi.org/10.1016/j.jchromb.2018.09.030

60 EDEN Mother-Child Cohort Study Group Bernard Jonathan Y. jonathan. bernard@ inserm. fr De Agostini Maria Forhan Anne de Lauzon-Guillain Blandine Charles Marie-Aline Heude Barbara. (2013). The dietary n6:n3 fatty acid ratio during pregnancy is inversely associated with child neurodevelopment in the EDEN mother-child cohort. *The Journal of nutrition*, *143*(9), 1481–1488. https://doi.org/10.1016/j.jpeds.2012.11.090

Information about authors*

Surve, Namita S. — Post graduate research scholar, Department of Pharmaceutical Quality Assurance, Dr. D.Y. Patil Institute of Pharmaceutical Sciences and Research, Pimpri, Pune-411018, MS, India (Affiliated to Savitribai Phule Pune University, Pune); e-mail: namitasurve04@gmail.com, https://orcid.org/0000-0003-4960-2785

Thomas, Asha B. *(corresponding author)* — Professor and Head, Department of Pharmaceutical Quality Assurance, Dr. D.Y. Patil Institute of Pharmaceutical Sciences and Research, Pimpri, Pune-411018, MS, India (Affiliated with the Savitribai Phule Pune University, Pune); e-mail: asha.thomas@dypvp.edu.in, https://orcid.org/0000-0003-1058-8779;

Bhole, Ritesh Prakash — Associate Professor, Department of Pharmaceutical Quality Assurance, Dr. D.Y. Patil Institute of Pharmaceutical Sciences and Research, Pimpri, Pune-411018, MS, India (Affiliated with the Savitribai Phule Pune University, Pune); e-mail: ritesh.bhole@dypvp.edu.in, https://orcid.org/0000-0003-4088-7470;

Patil, Chyandrajyoti Y. — Post graduate research scholar, Department of Pharmaceutical Quality Assurance, Dr. D.Y. Patil Institute of Pharmaceutical Sciences and Research, Pimpri, Pune-411018, MS, India (Affiliated to Savitribai Phule Pune University, Pune); e-mail: patilchandrajyoti@gmail.com, https://orcid.org/0000-0002-6030-1353

*The author's name is presented in the order: *Last Name, First and Middle Names*

How to Cite: Nagababu, U., Sujatha, D., Jyothi, U., Manikyala Rao Vissa, & Srinivasa Kumar, B. (2023) Validated Stability Indicating HPLC Method for the Quantification of Process Related Impurities of Ubrogepant in Pharmaceutical Formulations. *Eurasian Journal of Chemistry, 109(1), 31-40.* https://doi.org/10.31489/2959-0663/1-23-7

Article

Received: 07 October 2022 | Revised: 23 January 2023 |
Accepted: 16 February 2023 | Published online: 06 March 2023

UDC 543.06

https://doi.org/10.31489/2959-0663/1-23-7

Uppu Nagababu[1]*, D. Sujatha[2], Uppalapati Jyothi[3], Manikyala Rao Vissa[4], B. Srinivasa Kumar[5]

[1]*Department of Engineering Chemistry, S.R.K.R. Engineering College, Chinna Amiram, Bhimavaram, India;*
[2]*Department of Chemistry, GVSM Government Degree College, Ulavapadu, SPSR Nellore, India;*
[3]*Department of Chemistry, Anil Neerukonda Institute of Technology & Sciences, Sangivalasa, Visakhapatnam, India;*
[4]*Department of Civil Engineering, Swarnandhra College of Engineering and Technology, Seetharampuram, India;*
[5]*Department of Engineering Mathematics, College of Engineering, Koneru Lakshmaiah Education Foundation, Vaddeswaram, Guntur; India*
*(*Corresponding author's e-mail: nagababu.nss@gmail.com)*

Validated Stability Indicating HPLC Method for the Quantification of Process Related Impurities of Ubrogepant in Pharmaceutical Formulations

Ubrogepant is a medical drug prescribed for the treatment of migraine in adults. Literature analysis has shown, that no suitable analytical method has been published to date for the quantification of impurities of Ubrogepant. Therefore, this study aims to develop a simple and sensitive stability indicating HPLC method for quantifying Ubrogepant and its impurities 1 and 2. The optimized and best separation was achieved using ProntoSIL ODS C18 (250×4.6 mm; 5 µ id) column as stationary phase, phosphate buffer (pH 4.5) and methanol in 65:35 (v/v) at 1.0 mL/min as mobile phase and 246 nm as detector wavelength. The method reports 0.015 µg/mL and 0.05 µg/mL as limit of detection *(*LOD*)* and limit of quantitation (LOQ) for both impurities. This proves that the method has sufficient levels of sensitivity to detect impurities. The method passes all validation parameters as recommended, confirming that the method is valid. The method can show very less % degradation in various stress tests such as acid, base, peroxide, thermal and UV light conditions, and can efficiently resolve different compounds generation during stress exposure, as well as its known impurities prove the stability indicating nature of the method. Based on the experimental findings, it was shown that the method is significantly useful for the routine analysis of Ubrogepant and its impurities 1 and 2.

Keywords: Ubrogepant, HPLC impurity analysis, impurity A, impurity B, Method Development, Method Validation, Formulation analysis, Stress studies.

Introduction

Ubrogepant is the first approved Calcitonin gene-related peptide antagonist prescribed for the immediate treatment of migraine in adults [1]. It was not indicated for the preventive treatment of migraine [2]. Dry mouth, tiredness and nausea are the possible side effects occurred while using the Ubrogepant [3]. It has the molecular formula of $C_{29}H_{26}F_3N_5O_3$ with molecular mass of 549.55 g/mol and IUPAC name of *(6S)-N-[(3S,5S,6R)-6-Methyl-2-oxo-5-phenyl-1-(2,2,2-trifluoroethyl)-3-piperidinyl]-2'-oxo-1',2',5,7-tetrahydrospiro-[cyclopenta[b]pyridine-6,3'-pyrrolo[2,3-b]pyridine]-3-carboxamide*. Molecular structure of Ubrogepant is depicted in Figure 1.

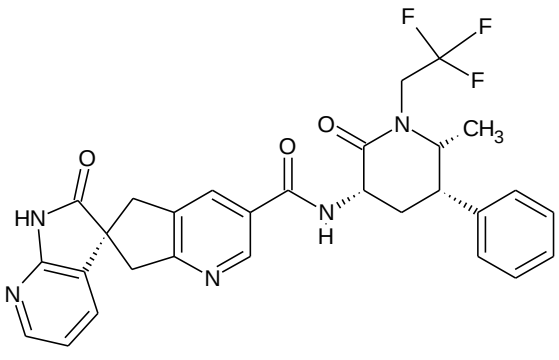

Figure 1. Molecular structure of Ubrogepant

Impurities in a pharmaceutical product are the unwanted chemical compound / substance that remain along with active pharmaceutical ingredients (APIs). These were arise from source as starting material or may be during the synthesis of API like reagents, solvents, catalysts, intermediates and reaction by-products. The ultimate safety of a drug product depends on the quantity of various impurities present on it, and therefore the need to identify, quantify and control impurities plays an important role in drug development. High performance liquid chromatography (HPLC) is a versatile analytical tool that has the ability to identify and quantify a wide range of pharmaceutical impurities.

The extensive review of the available analytical methods for the evaluating of Ubrogepant confirms that there is no analytical method reported / published on open access for the separation and quantification of impurities of Ubrogepant. Therefore, the present study aimed to develop a simple and economical HPLC method for the separation and simultaneous quantification of Ubrogepant impurities. Based on the availability, the impurity 1 (4-Nitro benzoate salt of amine intermediate) with IUPAC name *(3R,5R,6S)-3-amino-6-methyl-5-phenyl-1-(2,2,2-trifluoroethyl)piperidin-2-one, 4-nitrobenzoic acid* and impurity 2 (acid intermediate) with IUPAC name *2'-Oxo-1',2',5,7-tetrahydrospiro[cyclopenta[b]pyridine-6,3'-pyrrolo[2,3-b]pyridine]-3-carboxylic acid* were selected for the study. The molecular structure of impurities is shown in Figure 2.

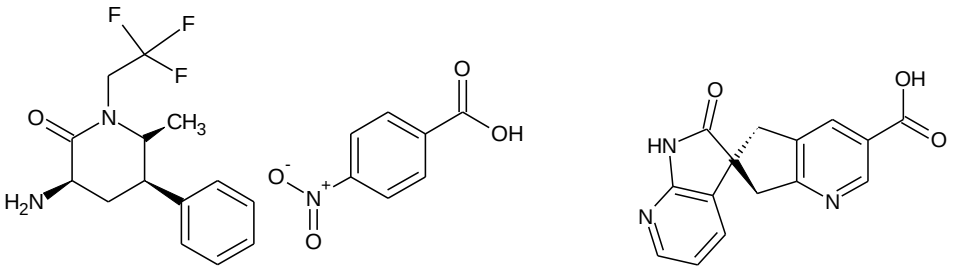

Impurity 1
(4-Nitro benzoate salt of amine intermediate)

Impurity 2
(Acid intermediate)

Figure 2. Molecular structure of Ubrogepant impurities under study

The synthesis mechanism given by Chi *et al*. (2018) in patent owned by Merck Sharp & Dohme Corp., Rahway, NJ, USA [4], confirms that possible route of formation of impurities in the final product. The impurity 1 was the intermediate product whereas the impurity 2 was used as intermediate reactant in the synthesis of Ubrogepant. The unreacted and leftover of these compounds will remain in the final product of Ubrogepant. Therefore, there is a need to quantify these impurities in the Ubrogepant final product in order to obtain high quality and pure APi of Ubrogepant.

Experimental

Chemicals and reagents:

The 98.26 % pure Ubrogepant API with its two studied impurities, and its 100 mg tablet form under the brand Ubrelvy® were purchased from Allergan India Private Ltd, Bangalore. The ultra-pure (Milli-Q®) water and other HPLC grade solvents used in the study were purchased from Merck chemicals, Mumbai. The analytical reagent grade chemicals used in the study such as hydrogen peroxide, sodium hydroxide, hydrochloric acid and buffer chemicals were also purchased from Merck chemicals, Mumbai.

Instrumental conditions:

The study was carried out on an Agilent (USA) 1100HPLC instrument, which includes a G1311 Aquaternary pump for delivery of solvents, a 0.1–1500 µL volume injectable auto-sampler with thermostat and UV detector (G 1314 A). Various configurations of stationary phases were used for the method development studies and the column eluents were integrated using Agilent chem-station software.

Sample preparation:

Standard solution: An accurately weighed 50 mg of Ubrogepant, impurity 1 and 2 were dissolved separately in a 50 mL clean and dry volumetric flask. Then, 25 mL of methanol were added separately to each flask, and the flasks were sonicated for 2 min to completely dissolve the analytes in the solvent. Then the content was filtered through 0.2 µ membrane filter in a separate clean and dry flask and the final volume was made up to the mark with the same solvent. The standard Ubrogepant, impurity 1 and 2 solution at a concentration of 1000 µg/mL was obtained separately. The combined standard solutions were prepared by accurate-

ly mixing equal volumes of individual known standard stock solutions in a separate flask and were used to develop and validate the method.

Sample solution: Ubrelvy® 100 mg tablets were made in to a fine and uniform powder using a clean and dry mortar and pestle. The tablet powder, weighed so that the powder sample contained 10 mg of Ubrogepant equivalent, was taken into a dry 100 mL volumetric flask. Then diluent (50 mL) was added and sonicated at room temperature for 10 min. Then the content was filtered through a 0.2 µm membrane filter and the solution was brought to the mark with the same diluent. The standard formulation solution at a concentration of 1000 µg/mL was obtained and was further diluted to the required concentration using the same diluents, and the selected concentration solution was used for the quantification of Ubrogepant and its impurities in the formulation sample.

Method development:

The systematic method development strategies were applied to develop a method for the analysis of Ubrogepant and its impurities. While developing the analytical method, the maximum absorbing wavelength for the detection of analytes was assessed using spectrophotometer. The iso-absorption wavelength of impurities 1, 2 and Ubrogepant was determined using a spectrophotometer, and the iso-absorption wavelength was fixed as the detection wavelength during the development of HPLC method. During the initial method development steps, the mobile phase flow rate was fixed as 1.0 mL/min, and after the completion of the development the flow was further optimized in the range of 0.5 mL/min to 1.5 mL/min. The analytes in the study were polar in nature, also non-polar columns were used as stationary phases in the method development. The high non-polar c18 columns of various brands and configurations were studied as stationary phase in the development study. The solvent ratios and its pH was finalized by change in various ratios of the mobile phase with different pH ranges was studied.

In all the method development studied conditions, the standard solution was injected at a concentration of 100 µg/mL and the chromatographic response was recorded. The peak area response, peak intensity, peak shape, and the system suitability were summarized in all the studied conditions. The method conditions providing the best system suitability with high peak intensity and significant absence of noise were considered as suitable conditions for the separation and analysis of Ubrogepant and its impurities [5–11]. These developed method conditions were further studied for method validation study.

Method Validation:

The Ubrogepant standard solution spiked with 0.1 % of both the impurities was analyzed by the optimized method, and the chromatographic response of the obtained chromatograms was summarized to evaluate the system suitability. The Ubrogepant standard solution without impurities, blank (only solvent), placebo solution prepared with commonly used formulation excipients, was analyzed in the developed method to evaluate method specificity.

A series of dilution of Ubrogepant standard solution spiked with 0.1 % of both the impurities was prepared in various concentration levels. The prepared dilutions were analyzed in the developed method and the peak area response of standard and both the impurities were tabulated separately. The calibration curve was plotted for Ubrogepant and its impurities separately by taking the peak area response of analyte in y-axis and its concentration on x-axis. The correlation coefficient and the regression equation of standard Ubrogepant and its impurities were obtained from its corresponding calibration curves.

The method accuracy was evaluated by conducting the spiked recovery study and was performed at 50 %, 100 % and 150 % spiked levels. The spiked level solution of Ubrogepant containing 0.1 % of Ubrogepant solution was spiked to a 100 % formulation solution and the recovery solution was analyzed in the optimized method. The peak area response of the recovery solution was compared with the calibration curve results in the same level and the % recovery of each analysis results and in each spiked level the % relative standard deviation (% RSD) was calculated. The % recovery of 98-102 and %RSD of < 2 was considered as acceptable.

The reproducibility of the method was evaluated in terms of precision and was carried as intraday and interday precision. At the same time, the standard Ubrogepant solution containing 0.1 % of studied impurities was spiked, and the spiked solution was evaluated six times in one day for intraday precision and 6 times in three consecutive days for interday precision. The peak area response of standard and both impurities was tabulated and the %RSD of the peak area response was calculated. The %RSD of less than 2 in both the precision studies for all the analytes was considered as the method was precise and repeatable.

The efficiency of the developed method that remains unaffected when there is a small change in the established method conditions as well as the change in analyte was assessed in ruggedness and robustness

study. In ruggedness, the solution at precision level was prepared and analyzed by three different analysts and the peak area values were tabulated and %RSD of < 2 was acceptable. In robustness study, both positive and negative minor variations in the established method conditions made intentionally and the standard solution at precision level was analyzed in each changed condition. The % change in peak area of each analyte in each changed condition was determined and a value of < 2 was acceptable.

The smallest analyte concentration that can detect and quantify in the established method was considered as limit of detection and quantification respectively. This information of the method confirms its sensitivity. The signal (s) to noise (n) ratio method was adopted for the evaluation of sensitivity.

The stability indicating nature of the method was assessed by performing stress degradation studies. Stress studies such as acid, base, peroxide, thermal and UV light degradation was performed for the standard drug. An accurately weighed 50 mg of standard Ubrogepant was mixed separately with 50 mL of hydrochloric acid (0.1 N), sodium hydroxide (0.1 N) and hydrogen peroxide (3 %) in acid, base and peroxide degradation studies respectively. The solutions were incubated for 24 h in dark, neutralized and then bring it to standard concentration prior to the analysis. The standard Ubrogepant was exposed to 60 ^{0}C for 24 h in an air oven and UV light at 254 nm for 24 h in thermal and UV light degradation studies, respectively. Both these standard drugs after stress exposure were diluted to standard concentration before analysis. All the stress exposed Ubrogepant dilute solutions were evaluated by the established method, and the chromatograms observed in each analysis were used to confirm the acceptability of the method. The resultant chromatograms provides the number of stress degradation compounds generated as a results of stress exposure, and the method applicability for the separation of stress degradation compounds was assessed. The peak area in each stress study was used for calculating the % degradation of Ubrogepant by comparing with unstressed peak area response of Ubrogepant in the developed method [4–10].

The developed method was applied for the separation, detection and quantification of Ubrogepant and its impurities in formulation. The formulation sample solution prepared from 100 mg tablets of Ubrogepant (Ubrelvy®) was assessed in the developed method. The peak area response was used to calculate the % content in the sample by comparison with the corresponding standard calibration curve results.

Results and Discussions

The wavelength overlay scan spectrum of the individual wavelength scans of Ubrogepant and its impurities confirms that 246 nm is the appropriate wavelength for the detection of analytes. Therefore, 246 nm was initially confirmed as a suitable wavelength and was fixed as detector wavelength in the method development study.

Initially, Kromasil C18 (250×4.6 mm, 5 μm) column was selected as stationary phase, pH 5.2 sodium acetate buffer and methanol in equal volumes were selected as mobile phase. The chromatogram identified in this condition (Fig. 3A) does not show a clear separation of the analytes. A single asymmetric split peak was detected on the chromatogram, confirming that the used column could not separate the analytes and therefore was not suitable for further study.

The column was replaced with Phenomenex Luna C18 (250×4.6 mm, 5 μm) and the same mobile phase was continued in sample 2. In this case, the peaks correspond to Ubrogepant and its impurities were identified, but no clear separation of analytes was observed. Baseline on the chromatogram was unstable and retention time of identified compounds was very high (Fig. 3B). The peak symmetry was also observed to be asymmetric, and hence the conditions were not suitable for the separation of analytes.

The method development was continued with the same column with change in buffer. In this case, pH 5.5 phosphate buffer and acetonitrile in the ratio of 75:25 (v/v) were used as mobile phase. The obtained chromatogram in this case (Fig. 3C) doesn't show a peak for Ubrogepant, whereas the peaks for both impurities were detected and well resolved. This proved that the column in the study could not separate the analytes, and therefore further study was proposed with change in the column as well as the mobile phase composition.

Further method development was continued with ProntoSIL ODS C18 (250×4.6 mm; 5 μm) column as stationary phase, and pH 4.5 phosphate buffer and methanol in 20:80 (v/v) were selected as mobile phase. The chromatogram observed under these conditions (Fig. 3D) shows clear separation of the peaks corresponding to Ubrogepant and its impurities. The baseline throughout the run time was noticed to be little fluctuated and the identified peaks were slightly broad with high tail factors. The peak area response corresponding to impurity 2 was smaller compared with the other analytes in the study. Therefore, the conditions were not suitable for the analysis. Figure 3 represents the chromatograms observed in the method development study.

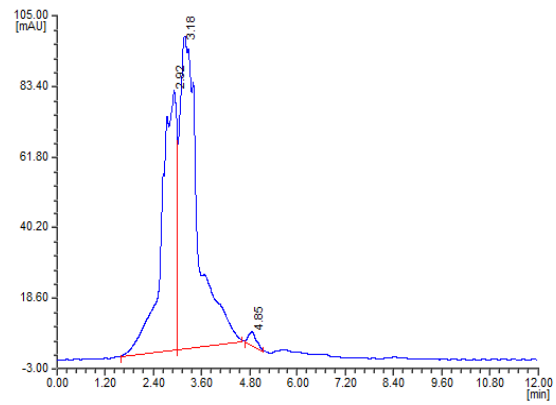

Fig. 3A

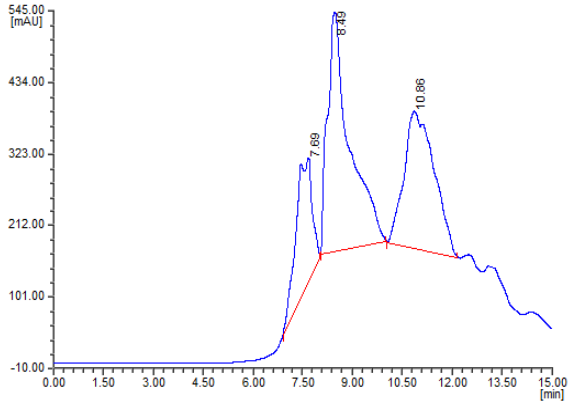

Fig. 3B

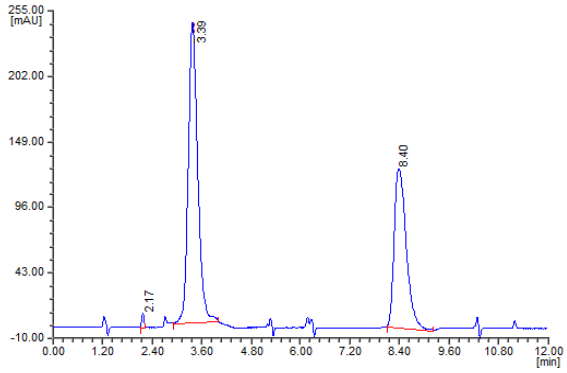

Fig. 3C

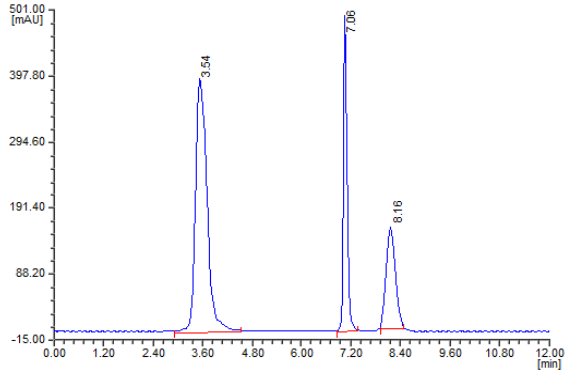

Fig. 3D

Fig. 3A & 3B: No clear separation of analytes was observed in this trail condition;
Fig. 3C: Ubrogepant peak was not identified and the peaks corresponding the impurities were detected in this trail;
Fig. 3D: Peaks corresponds to standard and impurities were identified but it doesn't pass system suitability and base line fluctuations identified throughout the run time

Figure 3. Chromatograms observed during method development

The method development study was continued with increase and decrease in the composition of buffer in the mobile phase, flow rate of mobile phase and detector wavelength for achieving the best chromatographic separation with acceptable system suitability. The separation was achieved on the ProntoSIL ODS C18 (250×4.6 mm; 5 µm) as stationary phase, pH 4.5 phosphate buffer and methanol in 65:35 (v/v) as mobile phase at 1.0 mL/min and UV detection at 246 nm. Under these optimized chromatographic conditions, a clear separation of Ubrogepant and its impurities was achieved without additional detection of impurities or other co-eluting compounds. The analytes were identified at a retention time of 7.05 min, 3.54 min and 8.14 min respectively for Ubrogepant, impurity 1 and 2, whereas the blank chromatogram does not show any chromatographic detection throughout the run time. This confirms the specificity of the established method for the detection of Ubrogepant and its impurities in the study. The chromatogram of the blank and standard observed under the developed method condition is shown in Figures 4A and 4B, respectively.

The signal-to-noise (S/N) approach was adopted for the evaluation of LOD and LOQ of method optimized for analyzing Ubrogepant with its impurities 1 and 2. The LOD was determined as 1.5 µg/mL and 0.015 µg/mL respectively for Ubrogepant and impurities. Based on LOD, the LOQ was calculated as 5 µg/mL and 0.05 µg/mL respectively for Ubrogepant and impurities. This confirms that the method can effectively detect the impurities down to a very low concentration of 0.015 µg/mL and can quantify down to 0.05 µg/mL. The sensitivity levels of analytes were taken into account when preparing the standard dilution of Ubrogepant and impurities. The standard calibration curve solutions of Ubrogepant containing 0.1 % of each impurity was prepared and analyzed by the optimized method. The high correlated calibration curve was obtained in the analyte range of 50–300 µg/mL and 0.05–0.30 µg/mL for Ubrogepant and both the impurities, respectively. The regression equation was derived as $y = 2896.9x + 570.22$ ($R^2 = 0.9999$), $y = 315628x + 4223.9$ ($R^2 = 0.9993$) and $y = 288800x + 3864.8$ ($R^2 = 0.9993$) respectively for Ubrogepant, impurity 1 and 2. The peak area results identified in the linearity study are presented in Table 1.

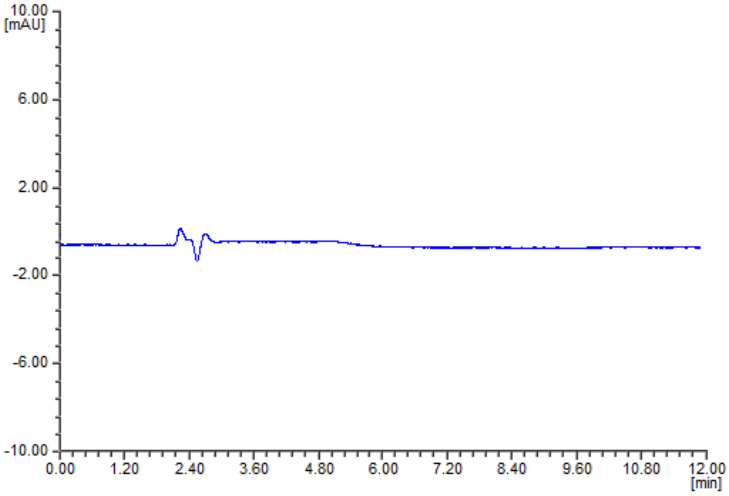

Fig. 4A (Blank chromatogram)

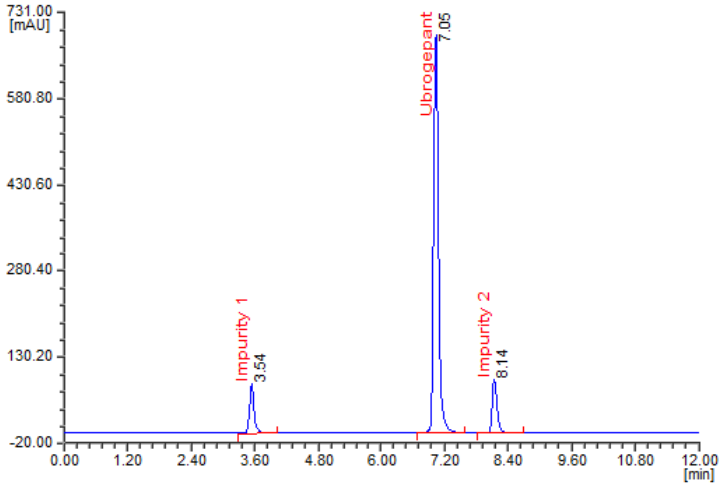

Fig. 4B (Standard chromatogram)

Figure 4. System suitability chromatograms of Ubrogepant and its impurities in the developed method

Table 1

Linearity results

S. No	Ubrogepant		Impurity 1		Impurity 2	
	Concentration in µg/mL	Peak Area	Concentration in µg/mL	Peak Area	Concentration in µg/mL	Peak Area
1	50	145159.1	0.05	19683.7	0.05	18010.6
2	100	290576.2	0.10	35683.1	0.10	32650.0
3	150	436957.4	0.15	51352.9	0.15	46987.9
4	200	575874.5	0.20	68961.5	0.20	63099.8
5	250	727493.1	0.25	82574.6	0.25	75555.8
6	300	869157.8	0.30	98496.9	0.30	90124.7

A 100 µg/mL Ubrogepant standard solution spiked with 0.1 % impurities was assessed in an optimized system suitability method. The system suitability parameters of the chromatographic results were summarized and the method system suitability was assessed. As shown in Table 2, the developed method passes the system suitability, which confirms the suitability of the developed method.

Table 2

System suitability results

S No	Parameter	Results achieved for		
		Ubrogepant	Impurity 1	Impurity 2
1	Concentration prepared	100µg/mL	0.10 µg/mL	0.10 µg/mL
2	Retention Time	7.05 min	3.54 min	8.14 min
3	Theo plate	7961	5127	9068
4	Tail Factor	1.07	0.95	0.98
5	Resolution	16.9	–	6.4

The 100 % solution of Ubrogepant containing 0.1 % of both impurities was evaluated in the precision and ruggedness study. The peak area response of each analyte was summarized in each study. The % RSD was calculated as 0.44, 0.96 and 1.07 for intraday precision, 0.59, 0.88 and 1.44 for interday precision and 0.62, 1.08 and 1.52 for ruggedness for Ubrogepant, impurity 1 and 2 respectively. The %RSD was achieved at acceptable levels for all the analytes in each study, proving the precision and ruggedness of the method.

The effect of the variations in the developed method conditions on the chromatographic response was assessed in robustness study. In robustness study, the composition of mobile phase was altered as 60:40 (MP 1) and 70:30 (MP 2) of buffer and methanol. The pH of buffer was altered as 4.4 (pH 1) and 4.6 (pH 2) as well as the detector wavelength was changed as 241 nm (WL 1) and 251 nm (WL 2) (Table 3).

Table 3

Robustness results

S No	Compound	Change	Peak Area	% Change	Plate Count	Tail factor	Resolution
1	Ubrogepant	MP 1	288484.1	99.28	7968	1.07	16.8
2		MP 2	287554.2	98.96	7847	1.09	16.5
3		pH 1	286944.0	98.75	7625	1.08	16.7
4		pH 2	288571.2	99.31	7691	1.07	16.8
5		WL 1	287815.7	99.05	7719	1.07	16.9
6		WL 2	288338.8	99.23	7835	1.08	16.8
7	Impurity 1	MP 1	35069.4	98.28	5230	0.96	–
8		MP 2	35194.2	98.63	5154	0.95	–
9		pH 1	35251.3	98.79	5196	0.95	–
10		pH 2	35533.2	99.58	5085	0.96	–
11		WL 1	35436.9	99.31	5176	0.96	–
12		WL 2	35358.4	99.09	5144	0.95	–
13	Impurity 2	MP 1	32539.0	99.66	9162	0.98	6.5
14		MP 2	32153.8	98.48	9418	0.99	6.4
15		pH 1	32235.4	98.73	9685	0.98	6.4
16		pH 2	32222.3	98.69	9472	0.98	6.5
17		WL 1	32016.6	98.06	9825	0.98	6.6
18		WL 2	32274.6	98.85	9326	0.99	6.5

The method accuracy was evaluated in a spiked recovery study and the experiment was performed at 50 %, 100 % and 150 % spiked levels. The solutions were evaluated by the optimized method and the peak area response was compared with the standard calibration results at the same level. The % recovery for each injection and the % RSD in each spiked level was calculated. The % recovery was observed to be at acceptable levels of 98–102 % and the % RSD was less than 2 for each spiked level (Table 4), confirming the method accuracy.

Table 4

Recovery results

S. No.	Compound	Recovery Level	Concentration in µg/mL			Amount found* Mean ± SD	% recovered* Mean ± SD	% RSD of Recovery
			Target	Spiked	Final			
1	Ubrogepant	50 %	100	50	150	148.77±0.716	99.18±0.478	0.48
2		100 %	100	100	200	198.12±1.140	99.06±0.570	0.58
3		150 %	100	150	250	246.05±0.737	98.42±0.295	0.30
4	Impurity 1	50 %	0.10	0.05	0.15	0.148±0.0002	98.44±0.11	0.12
5		100 %	0.10	0.10	0.20	0.199±0.0004	99.56±0.18	0.18
6		150 %	0.10	0.15	0.25	0.247±0.0009	98.70±0.35	0.35
7	Impurity 2	50 %	0.10	0.05	0.15	0.147±0.0003	98.24±0.20	0.20
8		100 %	0.10	0.10	0.20	0.199±0.0007	99.37±0.33	0.33
9		150 %	0.10	0.15	0.25	0.249±0.0006	99.50±0.22	0.22

Note: *n = 3

The method was evaluated for its applicability for the separation and analysis of various compounds generated due to stress degradation of Ubrogepant. The Ubrogepant standard drug was exposed to various stress conditions and then the stressed sample was evaluated by the developed method. The resultant chromatograms (Fig. 5) and their results were analyzed to evaluate their applicability for the separation of stress degradants. In acid degradation study, three additional compounds were identified at 5.1 min, 5.9 min and 9.1 min with % assay of 91.85 and % degradation of 8.15. In base degradation study, the % degradation was observed to be 7.32 % with three addition degradation products retained at 1.1 min, 9.1 min and 9.6 min. In peroxide degradation study, less % degradation of 3.8 min with two degradation compounds retained at 2.4 min and 9.6 min. In thermal and UV light degradation study one and four degradation compounds were identified with a % degradation of 4.15 % and 6.63 %. In all stress conditions, the standard Ubrogepant was detected along with the two impurities in the study. It was noticed that the % degradation is less than 10 under all stress conditions, and the method can effectively resolve the known studied impurities along with the stress degradants, effectively proving that the method is stable.

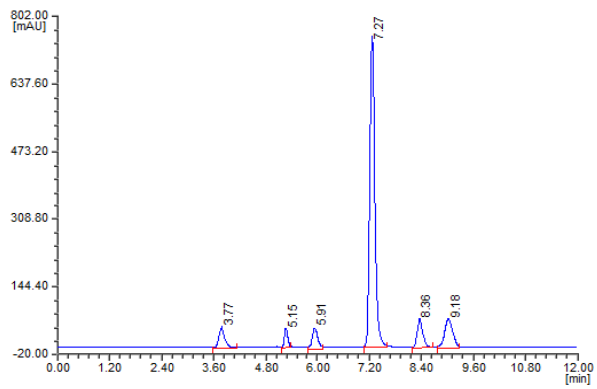

Acid Degradation

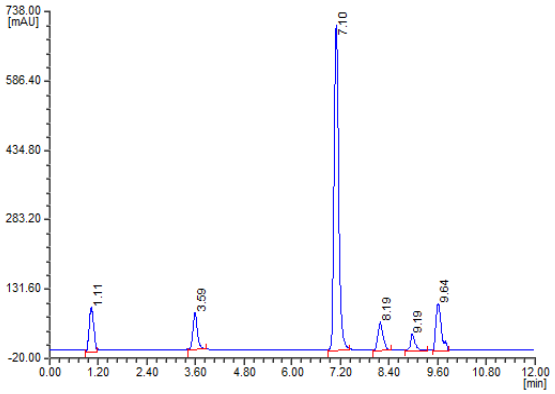

Base Degradation

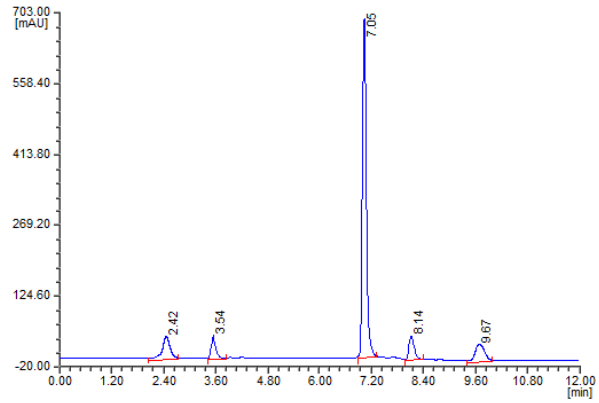

Peroxide Degradation

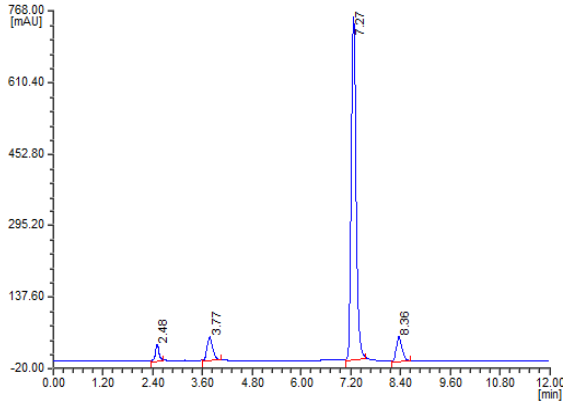

Thermal Degradation

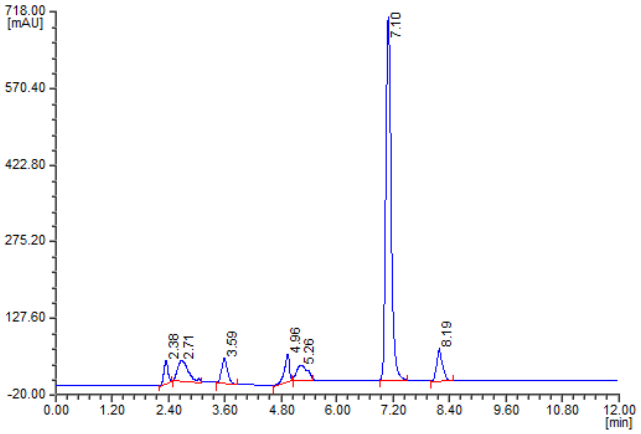

Figure 5. Forced degradation chromatograms

The analytical method optimized in the study was applied for its applicability to the estimation of Ubrogepant and its impurities. The formulation solution prepared with 100 mg of Ubrelvy® was used for the formulation assay study. The resultant chromatogram (Fig. 6) shows clear identification and resolution of both impurities in the study along with standard Ubrogepant. The % assay was observed to be 98.75 % for Ubrogepant, 0.09 % for impurity 1 and 0.07 % for impurity 2. The impurities were observed to be under the permissible levels and there is no detection of additional compounds, additional impurities as well as the formulation excipients on the chromatogram. This confirms that the method was significantly used for the evaluation of studied impurities and Ubrogepant in dosage forms.

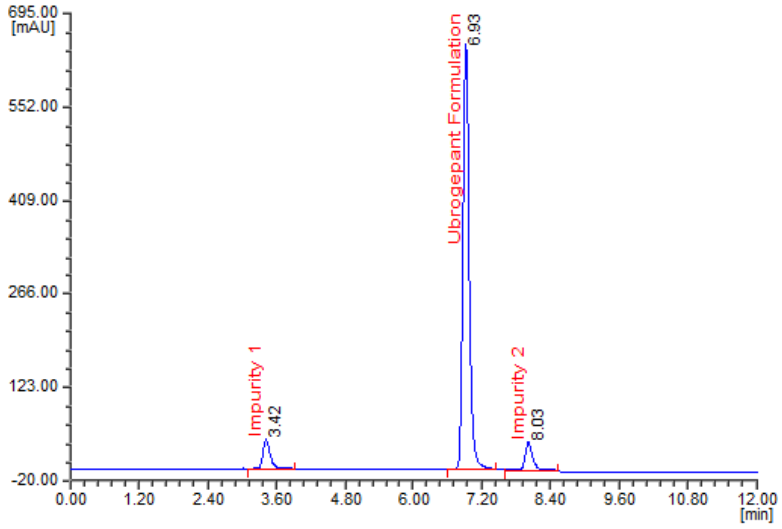

Figure 6. Formulation chromatogram

Conclusions

A simple and novel stability indicating analytical RP-HPLC method was optimized for separation and quantification of two potential impurities, i.e. impurity 1 and 2 of Ubrogepant. The method reports a very sensitive calibration range of 0.05 µg/mL to 0.30 µg/mL, which was achieved for impurity A and B. This confirms that the method can detect impurities at very low levels. Other validation parameters such as specificity, system suitability, accuracy/recovery, repeatability and reproducibility results were under the acceptable level. The method can efficiently resolve, detect and quantify unknown stress degradation products and known impurities of Ubrogepant. Based on the obtained validation results and method application studies, it can be concluded that the method can be effectively utilized for the analysis of Ubrogepant and its impurities in stress samples, bulk drug as well as in formulations.

References

1 Dos Santos, J. B. R., & Da Silva, M. R. R. (2022). Small molecule CGRP receptor antagonists for the preventive treatment of migraine: A review. *Eur J Pharmacol*, 922, 174902. https://doi.org/10.1016/j.ejphar.2022.17490

2 Dodick, D. W., Lipton, R. B., Ailani J., Lu, K., Finnegan, M., Trugman, J. M., & Szegedi, A., (2019). Ubrogepant for the Treatment of Migraine. *The New England Journal of Medicine*, 381, 2230–2241. https://doi.org/10.1056/NEJMoa1813049

3 Moore, E., Fraley, M. E., Bell, I. M., Burgey, C. S., White R. B., Li C. C. et al. (2020). Characterization of Ubrogepant: A Potent and Selective Antagonist of the Human Calcitonin Gene–Related Peptide Receptor. *J Pharmacol Exp Ther*, 373(1), 160–166. https://doi.org/10.1124/jpet.119.261065

4 Chi C. L., David M., Gene M., Kyle F., Rebecca W., Mark F., Leonardo A., Tiffani V., & John L. (2018). *United States Patent No., US 2018 / 0092899 A1*, Merck Sharp & Dohme Corp., Rahway, NJ, USA.

5 Mallu, U. R., Anna, V. R., & Kasimala, B. B. (2019). Rapid Stability Indicating HPLC Method for the Analysis of Leflunomide and Its Related Impurities in Bulk Drug and Formulations. *Turk J Pharm Sci*, 16(4), 457–465. https://doi.org/10.4274 %2Ftjps.galenos.2018.34635

6 Prasad, S. S., Krishna Mohan, G. V., & Naga Babu, A. (2019). Development of simple and robust RP-HPLC method for determination of everolimus and its impurities in oral solid dosage form. *Asian J Chem*, 31(5), 1002–1008. https://doi.org/10.14233/ajchem.2019.21723

7 Palacharla, S. K., & Krishna Mohan, G. V. (2019). HPLC method for determination of aspirin, rosuvastatin, ezetimibe and clopidogrel in combination drug products. *Asian J Chem*, 31(10), 2275–2283. https://doi.org/10.14233/ajchem.2019.22050

8 Palacharla, S. K., Krishna Mohan, G. V., & Naga Babu, A. (2019). RP-HPLC estimation of bumetanide and its impurities in oral solid dosage form. *Asian J Chem*, 31(10), 2275–2283. https://doi.org/10.14233/ajchem.2019.22069

9 Bikshal, B. K., Venkateswara, R. A., & Useni, R. M. (2018). Stability-indicating reversed-phase HPLC method for the separation and estimation of related impurities of cilnidipine in pharmaceutical formulations. *Indian drugs*, 55(12), 41–49. https://doi.org/10.53879/id.55.12.11185

10 Girija, K. S., Kasimala, B. B., & Anna, V. R. (2021). A New High-Performance Liquid Chromatography Method for the Separation and Simultaneous Quantification of Eptifibatide and Its Impurities in Pharmaceutical Injection Formulation. *International Journal of Applied Pharmaceutics*, 13(2), 165–172. https://doi.org/10.22159/ijap.2021v13i2.39895

11 Bikshal, B. K., Useni, R. M., Venkateswara, R. A., & Maheshwara R. L. (2018). Intended high-performance liquid chromatography procedure for the quantification of norfloxacin and its potential impurities in active pharmaceutical ingredient and tablet dosage forms. *Thai Journal of Pharmaceutical Sciences*, 42(1), 27–36.

Information about the authors*

Nagababu, Uppu *(corresponding author)* — Assistant Professor, Department of Engineering Chemistry, S. R. K.R. Engineering College, Chinna Amiram, A.P., India-534204; e-mail: nagababu.nss@gmail.com; https://orcid.org/0000-0002-3328-9280;

Sujatha, D. — Lecturer in Chemistry, Department of Chemistry, GVSM Government Degree College, Ulavapadu, SPSR Nellore, A.P., India — 523292; e-mail: dr.dsujatha@gmail.com; https://orcid.org/0000-0002-8562-9144;

Jyothi, Uppalapati — Assistant Professor; Department of Chemistry, Anil Neerukonda Institute of Technology & Sciences, Sangivalasa, Visakhapatnam A.P., India — 531162; e-mail: jyothi.uppalapati10@gmail.com; https://orcid.org/0000-0002-0828-8198;

Manikyala Rao, Vissa — Department of Civil Engineering, Swarnandhra College of Engineering and Technology, Seetharampuram, AP, India — 534280, A.P, India; e-mail: vissamanikyalarao@gmail.com; manikyalaraonss.21@gmail.com; https://orcid.org/0000-0003-0005-3201

Srinivasa Kumar, B. — Associate Professor, Department Of Engineering Mathematics, College of Engineering, Koneru Lakshmaiah Education Foundation, Vaddeswaram, Guntur, A.P., India — 522502; e-mail: sk.bhavirisetti@gmail.com; https://orcid.org/0000-0001-6237-4313

*The author's name is presented in the order: *Last Name, First and Middle Names*

How to Cite: Saiko, D.S., Titov, S.A., Saranov, I.A., Andreev, D.G., & Lobacheva, N.N. (2023) Moisture Transfer During its Evaporation from Sugar Solutions. *Eurasian Journal of Chemistry, 109(1), 41-50.* https://doi.org/10.31489/2959-0663/1-23-4

Article

Received: 22 August 2022 | Revised: 12 January 2023 |
Accepted: 07 February 2023 | Published online: 06 March 2023

UDC 536.60.547.455.663.6

https://doi.org/10.31489/2959-0663/1-23-4

Dmitry S. Saiko[1], Sergey A. Titov[2], Igor A. Saranov[2],
Danila G. Andreev[2], Natalja N. Lobacheva[2]

[1]*Federal State Budget Educational Institution of Higher Education "Voronezh State Technical University", Voronezh, Russian Federation;*
[2]*Federal State Budget Educational Institution of Higher Education «Voronezh State University of Engineering Technologies», Voronezh, Russian Federation*
*(*Corresponding author's e-mail: mr.saranov@mail.ru)*

Moisture Transfer During its Evaporation from Sugar Solutions

In this work, studies were carried out on the water evaporation from concentrated solutions of such sugars as sucrose, fructose, glucose, galactose, to determine the evaporation mechanisms. Differential scanning calorimetry (DSC) method in the temperature range from –70° C to +200° C, as well as the combined thermogravimetric analysis with differential scanning calorimetry under isothermal conditions at temperatures of 30°, 45°, 60 °C were used. The analysis of the DSC curves of sucrose solutions at low temperatures shows that in sugar solutions with a concentration of 65 %, water does not produce melting peaks. Therefore, it can be considered bound in the first hydration shells of sucrose. Isothermal thermogravimetric measurements give close to linear dependences of mass loss on time, and their slope being determined by temperature. At higher concentrations of sucrose solutions DSC curves for disaccharides are shifted relative to the curves for monosaccharides. This may be due to the lower permeability of the film surface for water. The evaporation model based on the vacancy mechanism of water molecules movement in concentrated sugar solutions was proposed. According to this model, the region enriched with vacancies of water molecules gradually penetrates deep into the sample. In this case, the number of water molecules in each layer of the region sets at a certain level. The given model constructions are applicable to the initial stages of water evaporation from concentrated sugar solutions.

Keywords: moisture, bond, sugar solutions, mathematical model, process, evaporation, thermal analysis, differential scanning calorimetry, differential thermal analysis, concentration, glass transition.

Introduction

The study of phase transitions, such as evaporation, and in particular water evaporation from various materials is one of the important problems of physical chemistry. It can be considered as moisture transfer from the liquid to the gas phase. This process is both of great theoretical and practical value.

The processes of moisture transfer and, in particular, evaporation, play an important role, for example, in food production. However, unlike many other cases of moisture transfer, for example, water evaporation from natural reservoirs, in food technology moisture is often transferred in systems containing not only free, but also the so-called bound water, that is, water present in the hydration shells of food material molecules. For example, the productivity of membrane technological processes, accompanied by the formation of polarization layers at the membrane boundary, depends directly on their rheological characteristics (viscosity, ultimate shear stress), which, in turn, depend on these particles hydration. Drying of food systems is greatly slowed down at a certain stage of dehydration, which is caused by some peculiarities of moisture transfer in materials containing bound water.

In recent years, bound water was actively studied by modern physical methods, such as X-ray microtomography, analysis of the microbalance of quartz crystals with a deposited material that binds water [1], absorption spectroscopy of electromagnetic radiation in the terahertz range [2], proton nuclear magnetic resonance [3], T -2 magnetic resonance relaxometry [4], etc.

Differential scanning calorimetry DSC [5] and differential thermal analysis DTA in combination with thermogravimetry are of special importance among the physical methods that can be effectively used for bound water characteristics measuring [6].

Isothermal DSC methods are of particular interest for the analysis of the bound water state [7]. They make it possible to choose the temperature which does not cause any structural transformations of the sample.

DSC is a very informative method for studying physical characteristics of intermolecular bonds in various materials. Thermal effects associated with phase transitions and chemical reactions depending on temperature are studied within the framework of this method. Information about the composition and thermophysical properties of food systems can be obtained with the help of DSC curve (heat flux versus temperature). Some researchers used DSC and DTA methods to study water binding in various food materials and additives, for example, in beef [8] and starch-gelatin food films [9]. Oxygen-functionalized porous activated bio-carbons with a large surface area obtained from grape seeds with the DSC method were studied in [10].

These bio-carbons are aimed to absorb CO_2 from the atmosphere. Samples with the largest surface area, pore volume, and the maximum number of surface oxygen functional groups showed the largest endothermic peak in terms of area according to DSC data, as well as the largest weight loss in the range of 80–100 °C.

The authors of [11] studied the sludge remaining after wastewater filtration by DTA and DSC methods. It was found out that the average binding power of water with the dry matter of sludge at a sufficiently high moisture content (above 50 %) ranges from 38 to 68 kJ/kg, depending on the type of sludge, and increases almost 10 times in the moisture range of 0–50 %.

Some modern thermal analysis instruments allow simultaneous thermal analysis (STA), i.e. combine the DSC or DTA method with the thermogravimetry (TG) method. Attempts to quantify bound water in food systems by this method were made earlier. Thus, in [12], thermogravimetry (TG) data were processed by the method of nonisothermal kinetics. It consisted of determining the logarithm dependence of the transformation degree α on temperature with thermogravimetric curves. The slope tangent of this graph, up to a constant factor, is equal to the amount of energy spent on the sample dehydration. The type of water binding with the material studied is determined by the range of dehydration powers. Therefore, this method can be used to characterize the distribution of water in a sample according to binding forms. However, an enormous spread in the values of kinetic parameters is considered to be one of the disadvantages of the non-isothermal approach [13].

However, there are no works using DSC and DTA methods that would clearly describe the mechanism of moisture transfer in systems with bound water.

The purpose of this work is to study a particular case of moisture transfer (evaporation) in systems with bound water, namely in concentrated solutions of food sugars such as sucrose, glucose, fructose, lactose, galactose.

Experimental

Samples of sugar solutions were produced in the laboratory at FSBEI HE VSUET (Federal State Budget Educational Institution of Higher Education “Voronezh State University of Engineering Technologies”).

DSC analysis at low temperatures and simultaneous thermal analysis (hereinafter STA) (DSC+TG) were performed on a STA 449 F3 Jupiter® simultaneous thermal analysis apparatus from NETZSCH (Germany). Calibration of the E-sensor by temperature and enthalpy taken from calibration substances (C10H16, C12H10, In, Bi, Zn) was previously carried out. Samples of raw materials weighing 15–22 mg were taken for analysis and placed in aluminum crucibles.

Differential scanning calorimetry (DSC) in the temperature range from –70° to +20° C, heating rate of 5 deg/min was used in the DSC method of analysis. The system was cooled with liquid nitrogen at a rate of 5 deg/min. The measurements were taken in a helium atmosphere (purge gas flow rate 10 ml/min, shield gas flow rate 10 ml/min). Temperature measurement accuracy was ±0.3° C.

Isothermal conditions at temperatures of 30°, 45°, 60° C were used in TG measurements. Measurements were carried out in the high-purity nitrogen atmosphere (purge gas flow rate 50 ml/min, shielding gas flow rate 10 ml/min).

Isothermal conditions at temperatures of 30°, 45°, 60° C were used for STA (TG+DSC) measurements. The measurements were taken in high-purity nitrogen atmosphere (purge gas flow rate 50 ml/min, shielding gas flow rate 10 ml/min).

Statistical processing of the experimental results was carried out as follows.

The experiment standard error was determined by the formula:

$$S.E. = \sqrt{\frac{\sum_{s=1}^{m}\sum_{i=1}^{n} y_{is}^{2}}{\left(n_y - 1\right)\left(n_y\right)}},$$

where *s* is the number of array; *i* is the number of point in the array; *m* is the array number for point *y* on the chart; *n* is the number of points in each array; y_{is} is the data value of array *s* and *i*-th point; n_y is the total number of data values in all arrays.

Results and Discussion

Studies by differential scanning calorimetry method at low temperature were carried out to determine the concentration of sugar solutions at which all water molecules are bound in the first hydrate shells.

The results of differential scanning calorimetry of a 45 % sucrose solution are shown in Figure 1.

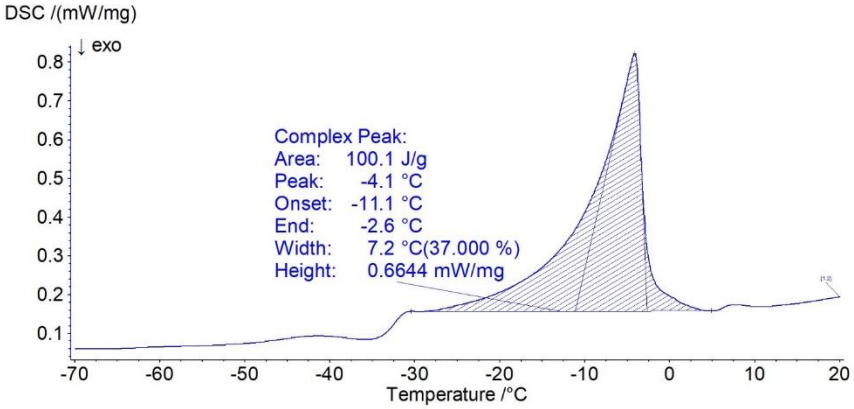

Figure 1. Thermogram of a 45 % mass concentration of sucrose solution melting DSC, mW/mg·10^2

As can be seen in Figure 1, the frozen sucrose solution melts in the temperature range of –35...0 °C, and the largest area of the melting peak falls in the range of –7°...–3 °C. Comparing the peak melting area for the sigmoidal baseline (100.1 J/g of solution) with the corresponding pure water surface area (334.3 J/g), we come to conclusion that it is only 0.30 of this value.

Taking into account the water content in a 45 % sugar solution and comparing the peak areas, we obtain approximately 55 % of the water frozen and then melted in this solution. The rest part is non-frozen and considered to be bound water.

The DSC curve for a 65 % sugar solution (Fig. 2) shows the presence of two exo- and endothermic peaks of approximately the same area. These areas are very small compared to the peaks corresponding to ice melting. This dependence is characteristic of the glass transition of a sugar solution [14] and is not directly related to water melting. Therefore, we can conclude that all water is in a bound state in a 65 % solution.

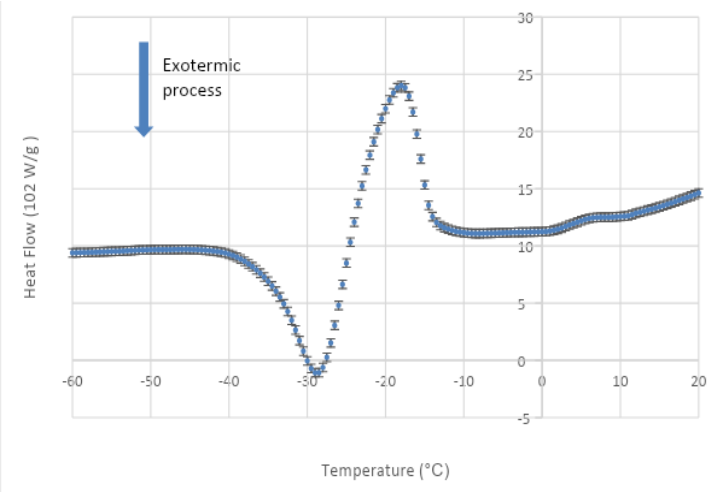

Figure 2. Thermogram of a 65 % mass concentration of sucrose solution melting

If we count the number of water molecules bound with hydroxyl groups per one sucrose molecule, their mass assessment will give about 35 % of the entire solution mass, i.e. all water in the 65 % sugar solution is hydrogen bonded to sucrose.

TG measurements in isothermal mode were also carried out. To do this, a container with a sugar solution was placed in the measuring cell of the calorimeter, which was openly placed in a nitrogen atmosphere and thermostated at a temperature of $T_1 = 29$ °C. The sample mass relative to the initial mass was recorded as a function of time (the value of TG in Fig. 3).

Figure 3 shows that the sample temperature sets at a level close to 29 °C in approximately 12 minutes after the experiment start.

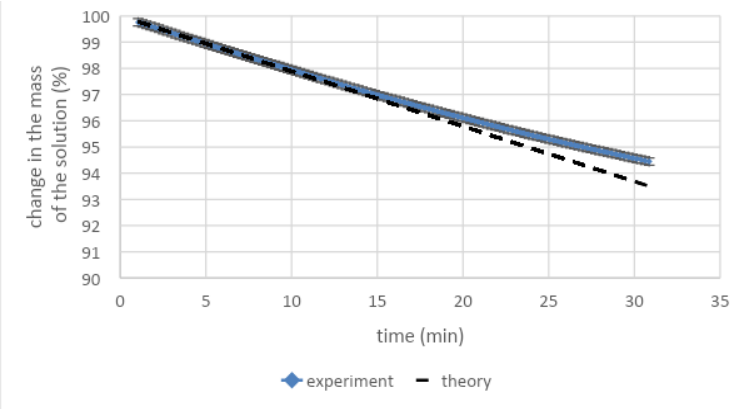

Figure 3. TG measurements in the isothermal mode of a sucrose solution with a mass concentration of 65 % at 30 °C

In practice, water evaporation usually occurs from systems containing both bound and free water. Therefore, we took isotherms of water evaporation from solutions of various sugars with a concentration of 20 % at a raised temperature. Under such conditions, water from the crucible is almost completely evaporated during the experiment, i.e., the solution concentration increases with time due to evaporation.

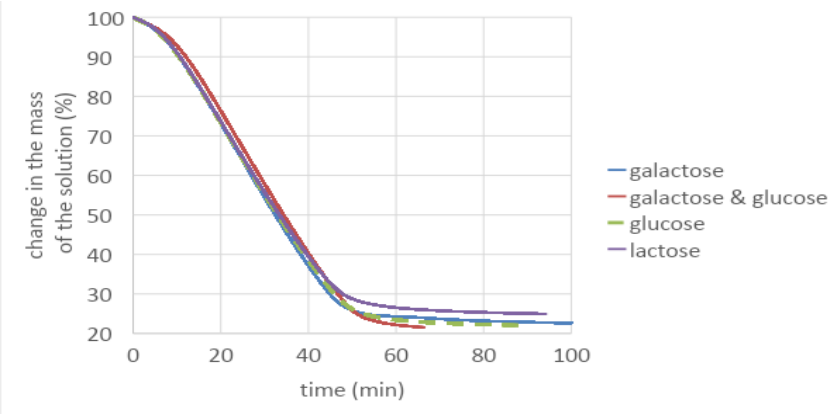

Figure 4. Results of simultaneous thermal analysis (TG + DSC) of measurements of sugar solutions with a mass concentration of 18 % at a temperature of 60 ºC

Figure 4 shows that the curves slope remains constant both over time and for different sugars up to a sugar concentration of 60-70 %. However, the slope of m versus t graph turns out to be smaller than that one for distilled water under the same conditions (Fig. 5). The reason for this phenomenon requires further research. However, a monolayer sugar film is possible to be formed on the surface of solutions with a weak concentration, preventing partially the evaporation of water. The level at which the mass stabilizes at an evaporation time of more than 50 minutes is different for all solutions. It is the highest for lactose solution. This means that a certain amount of water still remains in it after the end of active evaporation.

Great differences between sugars appear at 62–67 % solutions concentration. This is especially evident in the DSC curves. The amount of heat used to evaporate moisture decreases rapidly at a certain concentra-

tion due to a sharp drop in the evaporation rate. The DSC curve for lactose disaccharide runs more to the left than for a mixture of lactose and galactose monosaccharides. A similar pattern is observed for sucrose and its hydrolysis products — glucose and fructose (Fig. 5).

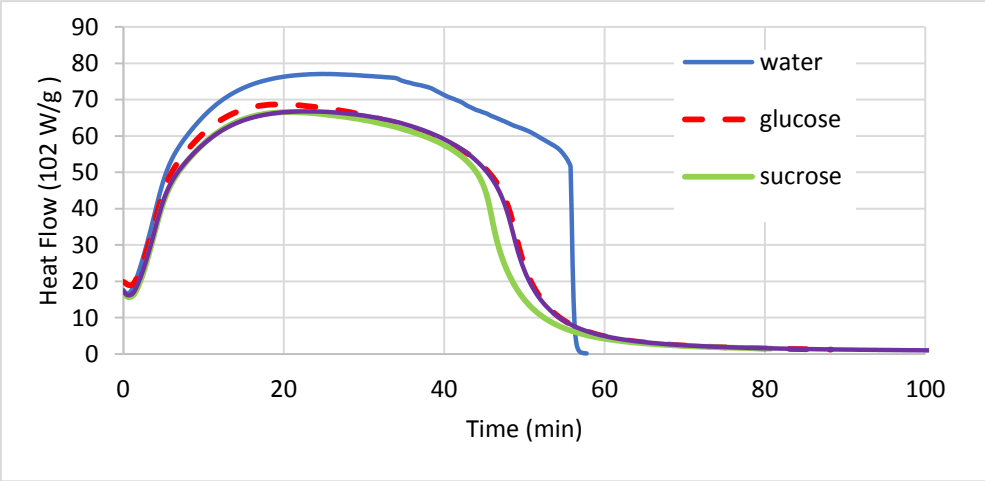

Figure 5. DSC curves of 20 % mass concentration of sugar solutions and distilled water at 60 °C

This means that unlike monosaccharides a dense, weakly permeable film begins to form on disaccharide solutions surface at a lower concentration. In other words, disaccharides films are less permeable to water at the same concentration.

Let us present some model ideas about the evaporation process from such solutions.

Let there be a solution where all water molecules are bound in sugar molecules first hydrate shells, i.e., they are attached to the hydroxyl groups of the sugar molecule by a hydrogen bond. Since water molecules are much smaller than sugar molecules, let us imagine the sugar molecules as immobile, and the water molecules moving relative to them and then moving into the gas phase in the process of evaporation. Water molecules movement can be as follows in such a system. If a water molecule leaves the solution due to evaporation, a vacancy forms in the hydrate shell of the sugar molecule. It is filled with a water molecule from the hydrate shell of the same or neighboring sugar molecule, leaving a vacancy filled by the next water molecule, and so on. That is, the sucrose molecules hydroxyl groups, to which water molecules can be attached by hydrogen bonds, can be represented as a positions grid that can or cannot be filled with water molecules.

Let us consider the solution volume, imagining the evaporation mechanism as shown in Figure 6. There are fixed positions, marked with light circles, in which molecules can reside (dark circles).

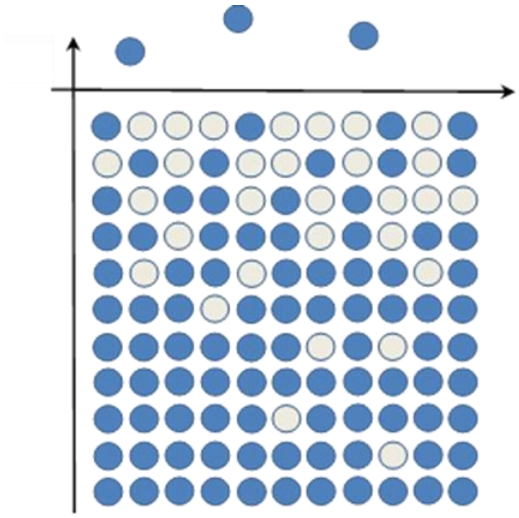

Figure 6. Graphical representation of the mechanism of evaporation from sugar solutions

As an initial approximation, we accept that a molecule transition in some characteristic time is possible only horizontally and vertically to an unoccupied place. Let N_0 be the total number of seats in one layer, N_i be the number of occupied seats in the layer with number i. Let there be three probabilistic parameters:

– probability r of the molecule exit from the first layer into the gas;

– probability p of a molecule transition from one layer to another, and the motion direction along the z axis does not matter;

– probability s of a molecule transition within one layer.

Let us consider changes kinetics in the population of layer i in one "cycle" of time. We will take the directions as shown in Figure 7.

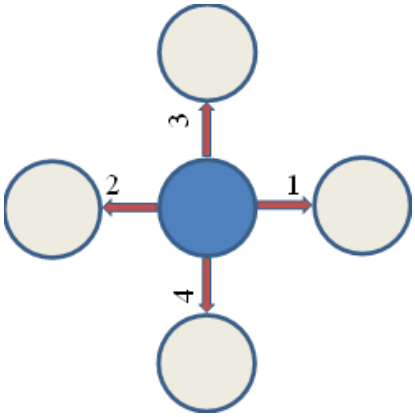

Figure 7. Graphical representation of the directions of the layer i population for one time "cycle"

The probabilities that the positions indicated in the figure will be free are, respectively, for positions 1 and 3: $1-\frac{N_i-1}{N_0}\approx 1-\frac{N_i}{N_0}$; for position 2: $1-\frac{N_{i\ -1}}{N_0}$; for position 4: $1-\frac{N_{i+1}}{N_0}$.

Let us take into account the probabilities of molecular migrating accepted in the model. Then, with a one-step movement, we get:

$$\Delta N_i = N_0 p \cdot \left(\frac{N_{i-1}}{N_0}\left(1-\frac{N_i}{N_0}\right)+\frac{N_{i+1}}{N_0}\left(1-\frac{N_i}{N_0}\right)-\frac{N_i}{N_0}\left(1-\frac{N_{i-1}}{N_0}\right)-\frac{N_i}{N_0}\left(1-\frac{N_{i+1}}{N_0}\right)\right). \quad (1)$$

Let us take into account the probabilities of molecular migrating accepted in the model. Then, with a one-step movement, we get:

$$\Delta N_1 = N_0 p \cdot \left(\frac{N_2}{N_0}\left(1-\frac{N_1}{N_0}\right)-\frac{N_1}{N_0}\left(1-\frac{N_2}{N_0}\right)\right)-N_0 r \cdot \frac{N_1}{N_0}. \quad (2)$$

After simplification, we obtain the system of equations

$$\begin{aligned} \Delta N_i &= p\left(N_{i-1}+N_{i+1}-2N_i\right); \\ \Delta N_1 &= p\cdot\left(N_2-N_1\right)-rN_1. \end{aligned} \quad (3)$$

After introducing the notation $\nu_i = \frac{N_i}{N_0}$, these equations can be written as differential equations

$$\left\{ \frac{d\nu_i}{dt} = -p\left(2\nu_i-\nu_{i-1}-\nu_{i+1}\right);\ \frac{d\nu_1}{dt} = -p\left(\nu_1-\nu_2\right)-r\nu_1;\ \nu_\infty(t)=1. \right. \quad (4)$$

It is easy to write the system of equations for three layers together with the initial and boundary conditions in an explicit form:

$$\left\{ \frac{d}{dt}\nu_1(t) = -p\left(\nu_1(t)-\nu_2(t)\right)-r\nu_1(t),\ \frac{d}{dt}\nu_2(t) = -p\left(\nu_2(t)-\nu_1(t)\right)-\nu_3(t)),\ \nu_1(0)=1,\ \nu_2(0)=1,\ \nu_3(0)=1 \right\}. \quad (5)$$

The third layer is assumed to be always filled. We can write the solution in the form:

$$\nu_1(t) = \frac{p + r \cdot e^{-\frac{1}{2}(3p+r)t}\left(2ch(tq) + \frac{2p-r}{q} sh(tq)\right)}{p+2r}; \quad (6)$$

$$\nu_2(t) = \frac{p + r \cdot e^{-\frac{1}{2}(3p+r)t}\left(ch(tq) + \frac{3p+r}{2q} sh(tq)\right)}{p+2r}, \quad (7)$$

where the q parameter is:

$$q = \frac{1}{2}\sqrt{5p^2 - 2pr + r^2}.$$

Graphs for arbitrarily chosen values of the parameters $p = 0.03$, $r = 0.1$ are shown in Figure 8.

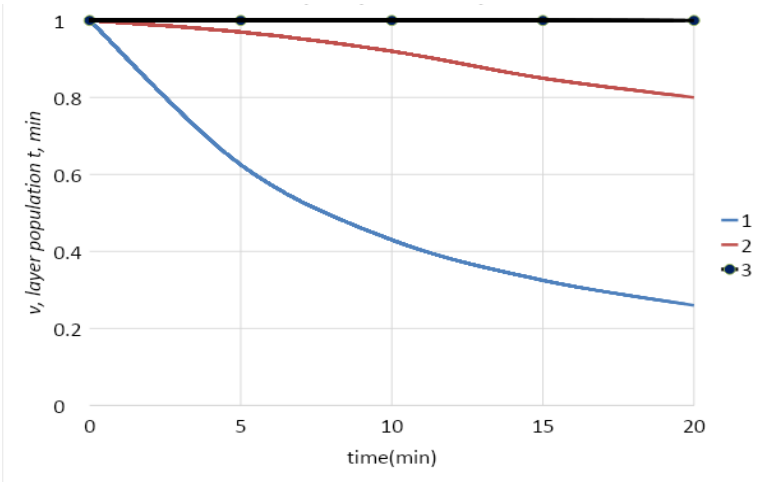

Figure 8. Graphs of the dependence of layers 1, 2 and 3 population on time (s)

Figure 8 shows that the number of molecules in the first layer tends to a certain stationary value in the interval of 0–20 minutes. That is, in some time after the process start, we can assume that $\frac{\partial \nu_1}{\partial t} = 0$.

At the same time, the number of water molecules in the second layer decreases in this time interval, while in the third layer it remains at the maximum level. This means that the front of the area depleted of water molecules penetrates gradually deep into the sample, the number of water molecules in each layer of this area setting at a certain level.

The probability r included in system (5) can be expressed in terms of the binding power of water with a sucrose molecule in a layer of sucrose solution adjoining air with the Boltzmann distribution:

$$r = e^{-\frac{U_1}{kT}}. \quad (8)$$

In this case, a water molecule bound to a sucrose molecule is represented as a particle in a potential well with depth U_1, where U_2 is the binding power of a water molecule with a sucrose molecule

The probability p can be expressed in a similar way:

$$p = e^{-\frac{U_2}{kT}}. \quad (9)$$

Here U_2 is the binding power of a water molecule with a sucrose molecule in the solution second layer. Let us introduce the value θ as the ratio of the number of molecules leaving the layer to the total number of molecules in the layer:

$$\theta = \frac{\Delta N}{N_0}, \quad (10)$$

where ΔN is the number of molecules leaving the layer in some time τ_0, equal to the particle oscillation period in the potential well.

Expressing θ in terms of water mass Δm leaving the layer in time τ_0 and the water molecule mass $m_{мв}$, we obtain:

$$\theta = \frac{\Delta m}{m_{мв} N_0}. \quad (11)$$

On the other hand, it is obvious that:

$$\theta = \nu_1 r. \quad (12)$$

Taking into account expressions (10)–(12), for the stationary case, the solution of the system of equations (5) is as follows:

$$\left(\frac{1}{\tau_0 \theta} - e^{\frac{u_1}{kT}} \right) e^{-\frac{u_2}{kT}} = 2. \quad (13)$$

If the evaporation process is carried out at temperatures T_1 and T_2, then the following equations will take place in the first and the second cases, respectively:

$$\frac{1}{\tau_{01}\theta_1} - e^{\frac{u_1}{kT_1}} = 2e^{\frac{-u_2}{kT_1}}; \quad (14)$$

$$\frac{1}{\tau_{02}\theta_2} - e^{\frac{u_1}{kT_2}} = 2e^{\frac{u_2}{kT_2}}.$$

Here θ_1 and θ_2 are the values determined by formula (11) by the mass loss of the sample at temperatures T_1 and T_2, respectively. Having determined their values from the experiment and taking into account (11), we can find the binding powers u_1 and u_2, and then the values r and p respectively with formulas (14).

The value Δm included in equation (11) can be determined from the slope of the experimental graph $m(t)$ during 12–15 minutes from the start of the experiment.

Substituting the obtained values Δm_1 for a temperature of 29 °C and Δm_2 for a temperature of 45 °C into formula (11), and solving the system of equations (14), we obtained the following values of the binding power of water with a sucrose molecule in the layer, adjacent to air U_1 = 2875 J/g and in the second layer U_2 = 3520 J/g.

In this case, the characteristic period of thermal vibrations of a water molecule near a sucrose molecule was $\tau_0 = 0{,}32 \cdot 10^{-8}$ c.

The theoretical graph $m(t)$, built with the found values, is shown in Figure 8.

It is linear, while the slope of the experimental graph decreases with time. This means that the above considerations can be applied to the initial stages of the evaporation process. Apparently, at a sufficiently large depletion area width, stationary diffusion of water molecules occurs through the depletion area. However, it is necessary to choose the vacancy mechanism for the movement of water molecules in solution as a basis for diffusion describing process. To build a theoretical graph of m versus t, for example, for sucrose solutions, it is necessary to know the specific values of p and r for solutions of a certain concentration.

The binding powers values obtained here are approximate, since it is not known exactly which part of the curve Δm versus t corresponds to the stationary filling of the upper layer. However, it is obvious that $E_{св}$ in the sample depth is much larger than that one on the surface.

One water molecule falls on one OH- group of the disaccharide molecule at concentrations of 62–67 %. This means that if at lower concentrations there is free water, which is not bound to hydroxyl groups, in the surface film, then in this case, on the contrary, vacancies of water molecules appear in hydrate shells of sugar molecules. At the same time the mechanism of water diffusion through the surface film changes greatly.

The water molecule evaporates, forming a vacancy in the hydrate shell of the sugar molecule. A molecule of water occupies the vacated seat from the hydrate shell of the neighboring sugar molecule. Then another water molecule gets there, and thus the diffusion flow of water from the depth to the surface of the solution goes. Since disaccharide molecules are larger than monosaccharide molecules, in the first case,

the water molecule moves mainly from one OH-group to another within one molecule. And only after a few jumps they move on to another. And in the second case, the number of jumps from one molecule to another is greater. It is possible that the stereometry of the molecules in the film is such that the latter transition is more probable. Then the diffusion coefficient of water in monosaccharides films will be higher than in the case of disaccharides, which is observed experimentally.

Conclusions

Thus, the results of the work show that the parameters of bound water transfer can be determined from dehydration isotherms not only at the boundary with the gas phase, but also in the bulk of the water-binding material. The vacancy mechanism of moisture movement in high concentration sugar solutions was proposed and mathematically substantiated in the work. The surface film with an increased concentration of sugar in the case of disaccharides solutions is less permeable to water than to monosaccharides.

Acknowledgments

The authors appreciate the Center for Collective Use “Test Center” on the basis of the FSBEI HE VSUET (Federal State Budget Educational Institution of Higher Education “Voronezh State University of Engineering Technologies”) for organizing and supporting research with its own material base and the assistance of Specialists.

References

1 Rudolph, G., Hermansson, A., Jönsson, A. S., & Lipnizki, F. (2021). In situ real-time investigations on adsorptive membrane fouling by thermomechanical pulping process water with quartz crystal microbalance with dissipation monitoring (QCM-D). *Separation and Purification Technology*, 254, 117578. https://doi.org/10.1016/j.seppur.2020.117578

2 Liang, W., Zuo, J., Zhou, Q., & Zhang, C. (2022). Quantitative determination of glycerol concentration in aqueous glycerol solutions by metamaterial-based terahertz spectroscopy. *Spectrochimica Acta Part A: Molecular and Biomolecular Spectroscopy*, 270, 120812. https://doi.org/10.1016/j.saa.2021.120812

3 Yoshida, T., Okabayashi, H., Takahashi, K., & Ueda, I. (1984). A proton nuclear magnetic resonance study on the release of bound water by inhalation anesthetic in water-in-oil emulsion. *Biochimica et Biophysica Acta (BBA)-Biomembranes*, 772(1), 102–107. https://doi.org/10.1016/0005-2736(84)90522-4

4 Khan, M. I. H., Wellard, R. M., Nagy, S. A., Joardder, M. U. H., & Karim, M. A. (2016). Investigation of bound and free water in plant-based food material using NMR T2 relaxometry. *Innovative food Science & emerging technologies*, 38, 252–261. https://doi.org/10.1016/j.ifset.2016.10.015

5 Hempel, N. J., Brede, K., Olesen, N. E., Genina, N., Knopp, M. M., & Löbmann, K. (2018). A fast and reliable DSC-based method to determine the monomolecular loading capacity of drugs with good glass-forming ability in mesoporous silica. *International journal of pharmaceutics*, 544(1), 153–157. https://doi.org/10.1016/j.ijpharm.2018.04.035

6 Mukasyan, A. S. (2017). DTA/TGA-based methods. In Concise Encyclopedia of Self-Propagating High-Temperature Synthesis (pp. 93–95). *Elsevier*. https://doi.org/10.1016/B978-0-12-804173-4.00040-5

7 Joyce, K., Rahmani, S., & Rochev, Y. (2020). Quasi-isothermal modulated DSC as a valuable characterization method for soft tissue biomaterial crosslinking reactions. Bioactive Materials, 5(2), 428–434. https://doi.org/10.1016/j.bioactmat.2020.03.002

8 Ma, C. Y., & Harwalkar, V. R. (1991). Thermal analysis of food proteins. In Advances in food and nutrition research (Vol. 35, pp. 317–366). *Academic Press*. https://doi.org/10.1016/S1043-4526(08)60067-4

9 Al-Hassan, A. A., & Norziah, M. H. (2012). Starch–gelatin edible films: Water vapor permeability and mechanical properties as affected by plasticizers. *Food hydrocolloids*, 26(1), 108-117. https://doi.org/10.1016/j.foodhyd.2011.04.015

10 Ismail, I. S., Singh, G., Smith, P., Kim, S., Yang, J. H., Joseph, S., & Vinu, A. (2020). Oxygen functionalized porous activated biocarbons with high surface area derived from grape marc for enhanced capture of CO2 at elevated-pressure. *Carbon*, 160, 113-124. https://doi.org/10.1016/j.carbon.2020.01.008

11 Deng, W., Li, X., Yan, J., Wang, F., Chi, Y., & Cen, K. (2011). Moisture distribution in sludges based on different testing methods. *Journal of Environmental Sciences*, 23(5), 875-880. https://doi.org/10.1016/S1001-0742(10)60518-9

12 Zvetkov, V. L., Simeonova-Ivanova, E., & Calado, V. (2014). Comparative DSC kinetics of the reaction of DGEBA with aromatic diamines IV. Iso-conversional kinetic analysis. *Thermochimica Acta*, 596, 42–48. https://doi.org/10.1016/j.tca.2014.09.014

13 Kramarenko, V. Yu. (2013). Nonisothermal kinetics in the thermal analysis of polymers. 1. Simple reactions. *Bulletin of the National Technical University KhPI. Series: Chemistry, chemical technology and ecology*, (64), 64–76.

14 Mahato, S., Zhu, Z., & Sun, D. W. (2019). Glass transitions as affected by food compositions and by conventional and novel freezing technologies: A review. *Trends in Food Science & Technology*, 94, 1–11. https://doi.org/10.1016/j.tifs.2019.09.010

Information about authors*

Saiko, Dmitry Sergeevich — Doctor of Physical and Mathematical Sciences, Professor, Professor of the Department of Higher Mathematics and Physical and Mathematical Modeling, Voronezh State Technical University, Moskovsky av, 14, 394006, Voronezh, Russian Federation; *e-mail:* imanovaa@mail.com; https://orcid.org/0000-0001-7116-4633;

Titov, Sergey Aleksandrovich — Doctor of Technical Sciences, Professor, Department of Physics of Heat Engineering and Heat Power Engineering, Federal State Budget Educational Institution of Higher Education "Voronezh State University of Engineering Technologies", Revolution av., 394036, Voronezh, Russian Federation; e-mail: 125titov@mail.ru; https://orcid.org/0000-0003-1612-0018;

Saranov, Igor Aleksandrovich (*corresponding author*) — Candidate of Technical Sciences, Senior Lecturer, Department of Information Security, Federal State Budget Educational Institution of Higher Education "Voronezh State University of Engineering Technologies", Revolution av., 394036, Voronezh, Russian Federation; e-mail: mr.saranov@mail.ru; https://orcid.org/0000-0002-9510-5168;

Andreev, Danila Gennadievich — Graduate student, Department of Physics of Heat Engineering and Heat Power Engineering, Federal State Budget Educational Institution of Higher Education "Voronezh State University of Engineering Technologies", Revolution av., 394036, Voronezh, Russian Federation; e-mail: peas_scalemodel@mail.ru; https://orcid.org/0000-0003-4720-8362;

Lobacheva, Natalja Nikolaevna — Candidate of Technical Sciences, Docent, Department of Foreign Languages, Federal State Budget Educational Institution of Higher Education "Voronezh State University of Engineering Technologies", 19, Revolution av., Voronezh, 394036, Russian Federation; e-mail: naloni@mail.ru; https://orcid.org/0000-0002-6561-7285

*The author's name is presented in the order: *Last Name, First and Middle Names*

How to Cite: Sarsenbekova, A.Zh., Burkeyev, M.Zh., Zhumanazarova, G.M., Kudaibergen, G.K., & Nasikhatuly, Ye. (2023) The Effect of Liquid Active Media on the Character of Equilibrium Swelling of Copolymers Based on Polypropylene Fumarate Phthalate with Acrylic Acid. *Eurasian Journal of Chemistry, 109(1), 51-58.* https://doi.org/10.31489/2959-0663/1-23-12

Article

Received: 01 December 2022 | Revised: 24 January 2023 | Accepted: 08 February 2023 | Published online: 06 March 2023

UDC 691.175.5/.8

https://doi.org/10.31489/2959-0663/1-23-12

Akmaral Zh. Sarsenbekova[1], Meyram Zh. Burkeyev[1], Gaziza M. Zhumanazarova[2*], Gulshakhar K. Kudaibergen[3], Yermauyt Nasikhatuly[1]

[1]Karagandy University of the name of academician E.A. Buketov, Kazakhstan;
[2]Karaganda Industrial University, Temirtau, Kazakhstan;
[3]Stem Cell Laboratory, National Center for Biotechnology, Astana, Kazakhstan
*(*Corresponding author`s e-mail: gaziza.zhumanazarova@mail.ru)*

The Effect of Liquid Active Media on the Character of Equilibrium Swelling of Copolymers Based on Polypropylene Fumarate Phthalate with Acrylic Acid

The article is devoted to the study of the influence of external factors on copolymers based on poly(propylene fumarate phthalate) with acrylic acid. In the present work, the effect of low-molecular salts on the swelling rate of the synthesized copolymers was studied. The surface morphology was examined using SEM. The swelling rate of the studied polymers depends on many factors, including the nature of the polymer and the solvent, the presence of electrolytes, changes in pH and ambient temperature, the molecular weight of the polymer, etc. It is assumed that the polymer network of copolymers mainly consists of links of unsaturated polyester resin. The results show that the ratio of monomer units in the copolymer significantly affects the susceptibility of the polymer gel to the presence of low-molecular salts. Changing the properties of the comonomer has been shown to produce hydrogels that can swell or collapse due to changes in ionic strength or the thermodynamic quality of the solution. By varying the ratio of the comonomeric units, the intervals of swelling and contraction of polymer meshes inherent in polyelectrolyte bodies with the same charges were adjusted. It was also found that the polymers under consideration belong to anionic meshes.

Keywords: polypropylene fumarate phthalate, low-molecular weight salts, discreteness, anionic meshes, acrylic acid, radical copolymerization, polar organic solvents, swelling, collapse, unsaturated polyester resin.

Introduction

Nowadays significant effort is made to study and synthesize copolymeric materials sensitive to ambient environment changes. Distinguishable compounds of this kind are “smart” polymers which are negatively sensitive to environment changes (pH, solution ionic strength, temperature, light, electromagnetic impact etc.) and are characterized by first stepped phase shift with rapid change of macromolecule volume fraction. Multiple researches have been dedicated to studying “smart” polymers; however, there is no information on unsaturated polyester resins-based copolymers study and synthesis prior to our research. That being said, unsaturated polyester resins-based copolymers study is of theoretical and practical interest because of their simplicity and efficiency as well as the presence of unsaturated ethylene bonds allows obtaining cross-linked polymers by reacting with ionogenic monomers. Such materials can keep their properties in high temperatures, aggressive environments, humidity and other destructive factors [1–4]. It is stated in [5] that the presence of a low-molecular salts component in the solution can cause either swelling or collapsing of the polymer network.

According to data [6–13], adding low-molecular salt has a significant influence on polyelectrolyte gels which leads to shielding of effects related to the charge state of the network. This suggests that the nature of the cross-linked polymer interaction with mono- and polyvalent salt ions depends on its chemical composition. This makes further work in this area promising.

The purpose of the research was to study the swelling process of p-PFPh:AA polymers depending on various aqueous solutions and properties of technological medium, to study the water-binding properties of p-PFPh:AA components during swelling at different temperatures.

Experimental

Synthesis of poly(propylene fumarate phtalate) and copolymers based on it was described in authors’ previous works [14–15].

Aqueous solutions of low-molecular weight salts (LMS) were prepared in calculated amounts to determine the swelling rate of copolymers in solutions.

$CuSO_4$, $FeCl_3$, and $Pb(NO_3)_2$ were used as low-molecular weight salts.

Table 1

Concentration of low-molecular weight salts solutions (per 100 ml)

Concentration, mol/l (100 ml)				
$CuSO_4$, g	$1.60 \cdot 10^{-3}$	$1.60 \cdot 10^{-2}$	$1.60 \cdot 10^{-1}$	1.60
$FeCl_3$, g	$1.62 \cdot 10^{-3}$	$1.62 \cdot 10^{-2}$	$1.62 \cdot 10^{-1}$	1.62
$Pb(NO_3)_2$	$3.31 \cdot 10^{-3}$	$3.31 \cdot 10^{-2}$	$3.31 \cdot 10^{-1}$	3.31

The equilibrium swelling rate of p-PFPh based copolymers with acrylic acid in the low-molecular salts solution was also determined gravimetrically [16].

The degree of polymer swelling was measured gravimetrically [17]. The dry polymers (m_0) were incubated in salt solution, and their swollen masses (m) were recorded after 24 h. All samples were taken in samples to reduce errors. The swelling ratio (α) of polymers was calculated by:

$$SR(\%) = \alpha = \frac{m_s - m_d}{m_d}.$$

The morphology of the polymers was observed using a scanning electron microscope (SEM, Auriga Crossbeam 540, Carl Zeiss).

Results and Discussion

The swelling rate of polymers (p-PFPh:AA) is important for studying the swelling processes. Knowing its value will allow predicting the behavior of polymers in various liquid media.

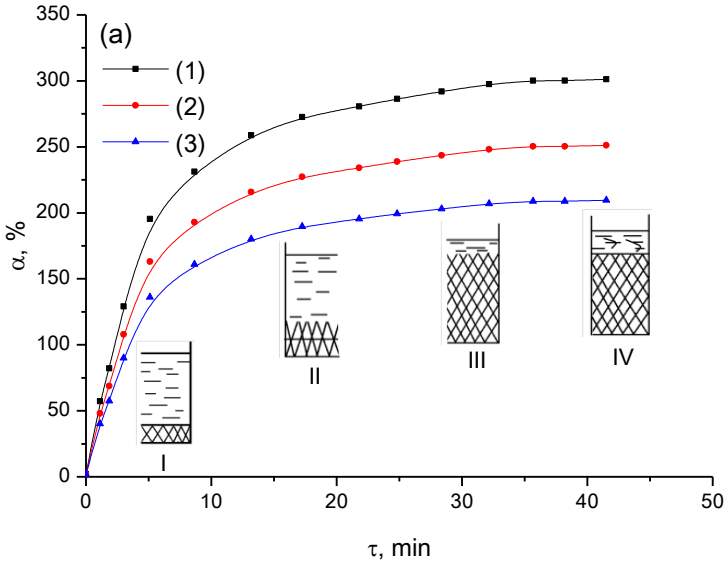

1 — 6.77:93.23; *2* — 44.17:55.17; *3* — 86.67:13.33

Figure 1. Dependence of the degree of swelling on the contact time of p-PFPh:AA copolymers with tap water (pH 7.1) at reference ratios M_1:M_2, mol. %

As can be seen from the data presented in Figure 1, the kinetic curves of the degree of swelling dependence on the contact time of p-PFP:AA copolymers with tap water (pH 7.1) corresponded to the process of limited swelling. The curves showed a linear increase in swelling during the first 5 minutes, which was characteristic of the hydration stage and formation of the bound water layer, further gradual increase in the degree of swelling up to the maximum value corresponded to the osmotic stage, when free water diffused into the polymer matrix until reaching equilibrium and the swelling limit.

The kinetic curves (Fig. 1) in the coordinates of the degree of swelling versus contact time of p-PFP:AA copolymers with tap water (pH 7.1) are described by the equation:

$$\alpha = \alpha_{max} \cdot \frac{i \cdot \tau}{1 + (i \cdot \tau)}, \quad (1)$$

where α_{max} is the maximum degree of swelling (%); τ is the time (min); i is the empirical constant.

To determine the constants included in the equation data (1), the dependence $\alpha = f(\tau)$ is approximated and then plotted in coordinates $d\alpha/d\tau$ from τ. The result is a dependence of the swelling rate on the swelling time (curve *a*, Fig. 2). Calculation of constants (α_{max} and i) is performed using a graphoanalytical method. To do this, the experimental data (Fig. 2, *a*) are reconstructed into coordinates $\frac{1}{\alpha} - \frac{1}{\tau}$ (curve *b*, Fig. 2) and described by the equation:

$$\frac{1}{\alpha} = \frac{1}{\alpha_{max}} + \frac{1}{\alpha \cdot i_{max}} \cdot \frac{1}{\tau}. \quad (2)$$

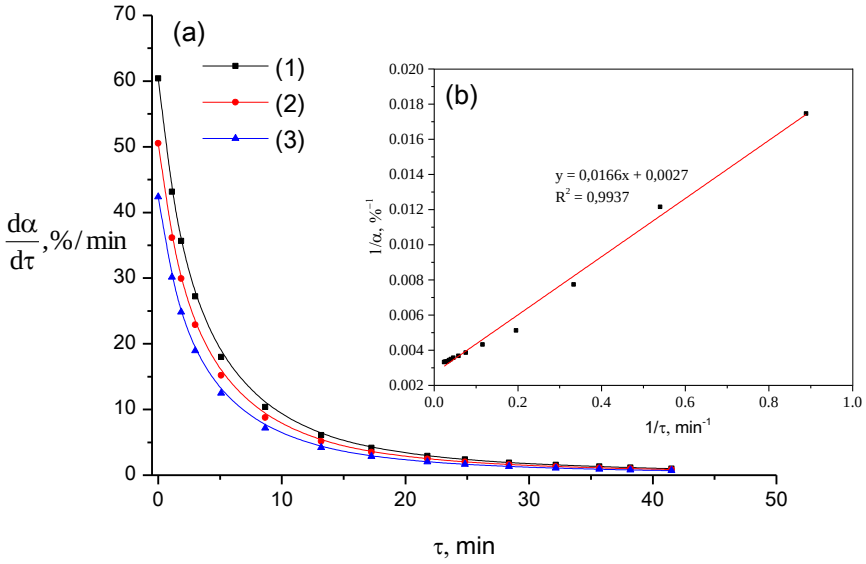

1 — 6.77:93.23; *2* — 44.17:55.17; *3* — 86.67:13.33

Figure 2. Diagram of constants determination for graphoanalytic approximation method p-PFPh:AA copolymers at initial ratios of M1:M2, mol.%

When extrapolating (Fig. 2, *b*) $\frac{1}{\tau} = 0$ the maximum swelling of the p-PFPh:AA copolymer is determined (6.77:93.23 mol.%) α_{max} = 370.34 %, and the tangent of the slope angle is a straight empirical constant i = 0.16. From the data presented in Figure 2, (curve, *a*) it can be seen that the swelling rate is determined by the diffusion of solvent molecules in the p-PFPh:AA copolymer, then swelling can be described by first-order kinetic equations analogous to chemical reactions of type A→B, that is, the rate of swelling $\frac{d\alpha}{d\tau}$ will be directly proportional to the degree of swelling $\frac{d\alpha}{d\tau} = k(\alpha_{max} - \alpha)$.

The average rate of the process was calculated using the formula obtained by differentiating Equation 1: $\frac{d\alpha}{d\tau} = \frac{\alpha_{max} \cdot i}{(1 + i \cdot \tau)^2}$ (Fig. 2, *a*). Analysis of the obtained data showed (Fig. 2, a) that with an increase in the contact time of the p-PFPh:AA copolymer (6.77:93.23 mol.%) with tap water (pH 7.1) the swelling rate decreased and after 17 minutes decreased significantly to 4.15 %/min. This indicated that during this time of contact $\frac{d\alpha}{d\tau}$ tends to zero and the process reaches equilibrium, and α becomes constant and reaches the

maximum value. Analysis of kinetic calculations showed (Fig. 3) that the swelling process of p-PFPh:AA copolymers in tap water proceeded at a sufficiently high rate ($\bar{k} = 9.72 \cdot 10^2$ s^{-1}). It should be noted (Fig. 1) that the contact time of the p-PFPh:AA copolymers with tap water, during which the maximum degree of swelling is achieved, is fast enough (5–10 minutes), which indicates the hydrophilic nature of the components included in the p-PFP: A copolymer in a ratio of 6.77:93.23 mol.%.

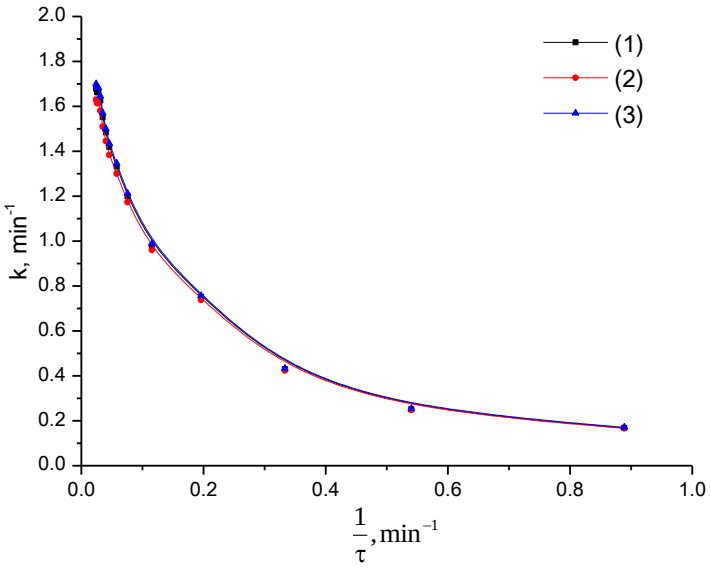

1 — 6.77:93.23; *2* — 44.17:55.17; *3* — 86.67:13.33

Figure 3. Dependence of swelling rate constant on time
for p-PFPh:AA copolymers at initial ratios of M_1:M_2, mol.%

In order to verify the correctness of the obtained data, we made an attempt to match experimental kinetic curves with calculated ones using mathematical technique. The possible form of kinetic curves, i.e. the dependence $\alpha = f(\tau)$ of the p-PFPh:AA copolymers (6.77:93.23 mol.%) is shown in Figure 4.

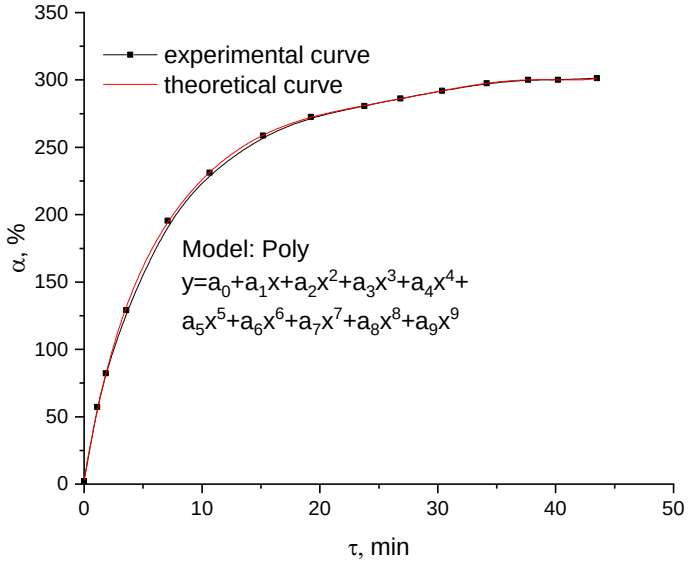

Figure 4. Experimental and calculated dependence of the degree of swelling on contact time
of p-PFPh:AA copolymer with tap water (pH 7.1) at initial ratios of 6.77:93.23 mol.%

As can be seen from Figure 4, the p-PFPh:AA (6.77:93.23 mol.%) swelling degree values calculated by model function — Poly(function type: $y = a_0 + a_1 x + a_2 x^2 + a_3 x^3 + a_4 x^4 + a_5 x^5 + a_6 x^6 + a_7 x^7 + a_8 x^8 + a_9 x^9$)

have satisfactory similarity with the experimental data, the same pattern is typical for other p-PFPh:AA copolymer with reference ratios of 44.17:55.17 mol.%; 86.67:13.33 mol.%.

As a further investigation of the swelling kinetics of p-PFPh:AA copolymers, we predicted swelling rates in the temperature range of 291, 295 and 303 K when exposed to salt and fresh water (Fig. 5, Table 1).

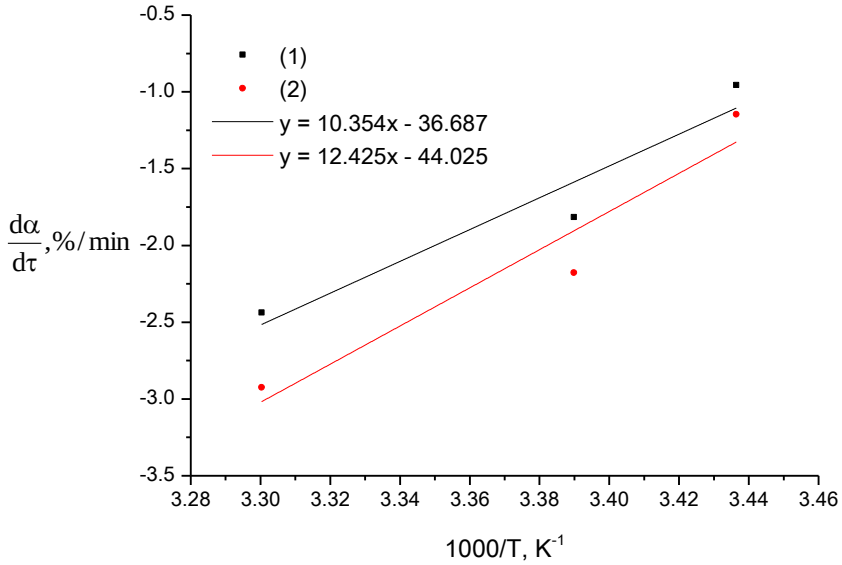

Figure 5. Dependence of swelling rate on inverse temperatures in fresh (1) and salty (2) water

Table 2

Values of physical constants of p-PFPh: AA copolymers

Ratio M_1:M_2, mol. %	Liquid medium	Type of impact	E, kJ mol^{-1}	A, min^{-1}
6.77:93.23	Fresh water	swelling	86.08	$8.57 \cdot 10^{15}$
	Salt water		103.30	$1.32 \cdot 10^{19}$
44.17:55.17	Fresh water		61.49	$6.12 \cdot 10^{15}$
	Salt water		77.67	$9.91 \cdot 10^{18}$
86.67:13.33	Fresh water		40.61	$4.04 \cdot 10^{15}$
	Salt water		44.34	$5.91\ 10^{18}$

Table 2 shows that the swelling characteristics of the p-PFPh:AA copolymers depend on the polymer mesh density and water composition. As shown in Table 2, when the p-PFPh:AA copolymer (at a ratio of 6.77:93.23 mol.%) swells in salt water, the invariant kinetic parameters have high values of E = 103.30 kJ·mol^{-1} and $A = 8.57 \cdot 10^{15}$, which indicates a greater rate of their swelling. For the p-PFPh:AA copolymer (at a ratio of 86.67:13.33 mol.%) the swelling activation energy is low.

For comparative analysis, the surface morphologies of the p-PFPh AA copolymers were investigated before (Fig. 6, (*a* and *b*)) and after swelling (Fig. 6, (*c* and *d*)) (Fig. 6).

The study of the surface morphology of the copolymer showed that the latter is a rather complex structurally morphological organization. During cryostructuring, copolymers with a characteristic openwork structure with a large pore content were formed (Fig. 6, *a* and *b*), and systems in a different phase of circulation — after swelling (Fig. 6, *c* and *d*), in the structure of which the main field of the pattern was occupied by a large number of smaller macropores.

Considering that the existing types of superabsorbents cannot be used effectively enough in the climatic conditions of arid zones, since they do not have sufficient thermal stability required for their use at temperatures above 35 °C, and at the same time, these products are highly sensitive to changes in ionic composition and soil pH, therefore, there has been a need to study the effect of inorganic salts on the swelling of p-PFPh:AA polymers.

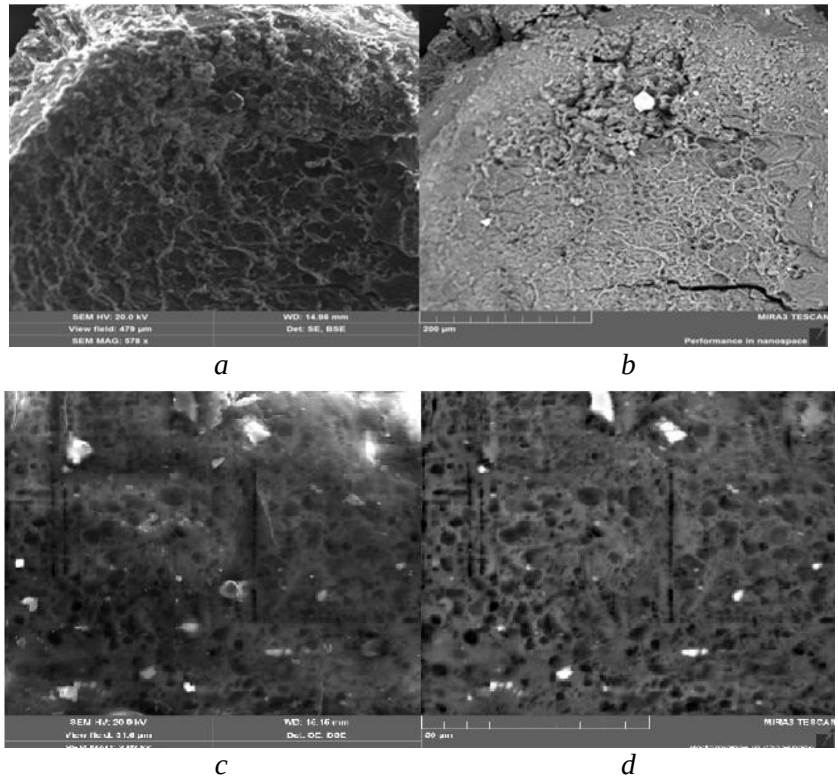

Figure 6. Micrographs of p-PFPh: AA copolymer structure at initial ratios of 6.77:93.23 mol % before (*a*, *b*) and after (*c*, *d*) swelling

Figure 7 shows the dependence of the external dimensions of the lattice on the concentration of the added low-molecular weight electrolyte, namely $Pb(NO_3)_2$, $CuSO_4$ and $FeCl_3$ for gels based on p-PFPh with AA of different molar composition. According to the presented experimental data, an increase in the ionic strength of the solution in the region from 0.001 to 1.0 mol/l has a significant effect on the external dimensions of the samples under consideration.

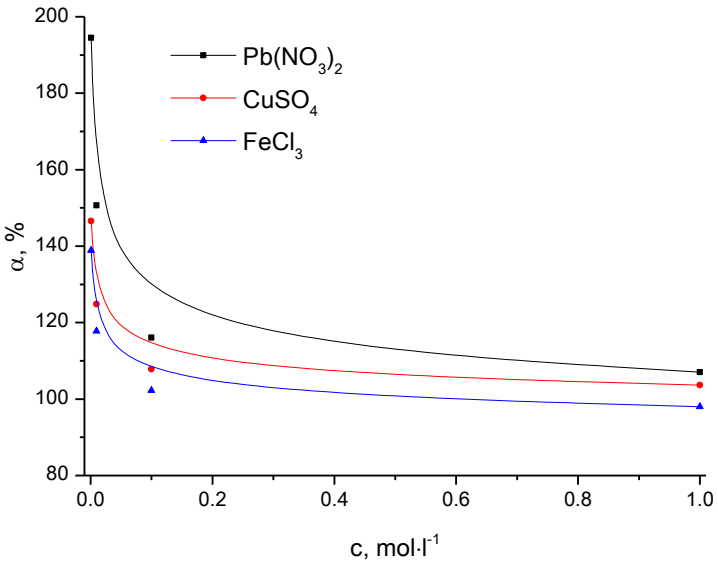

Figure 7. Effect of low molecular electrolyte ($Pb(NO_3)_2$, $CuSO_4$ and $FeCl_3$) on p-PFPh:AA copolymer swelling at initial ratios of 6.77:93.23 mol. %

The graphical dependencies (Fig. 7) show that at the lowest concentrations of added salt, the size of the gels varies slightly, a smooth contraction is observed. Further, at a certain critical concentration of the p-

PFPh used, a sharp collapse of the meshes is observed. A further increase in salt concentration does not affect the course of the curves. Based on the nature of the curves inherent in polyelectrolyte gels with the same charges, it can be concluded that the polymers we are considering should be attributed to anionic meshes. The shrinkage of the samples with increasing p-PFPh content in the mesh can be due to several reasons: first, the thermodynamic quality of the solvent — water, in which the samples are most swollen, deteriorates with increasing salt concentration; second, as low-molecular weight substrates are added to the surrounding solution, the polyelectrolyte effect may be suppressed as a result of shielding of charged ions by low-molecular weight ions.

As the proportion of p-PFPh units in the polymers increases, the sorption capacity of the gels decreases. The increase in the number of carboxyl groups in this series increases the sensitivity to additives of the low-molecular weight salt, while the concentration of the latter increases. The transition of hydrogels from the swollen state to the most contracted state is characterized by discreteness. It should be noted that for copolymers containing AA units, this phenomenon is observed at lower p-PFPh concentrations.

Conclusions

The results obtained demonstrate the possibilities of controlling the physicochemical properties of copolymers based on poly(propylene fumarate phthalate) and acrylic acid induced by the polymer composition, which allows creating new materials with a predetermined program of behavior. The swelling rate of the polymers we studied depends on many factors, including the nature of the polymer and solvent, the presence of electrolytes, ambient temperature, the molecular weight of the polymer, etc. It is assumed that the polymer network of copolymers mainly consists of links of unsaturated polyester resin.

The results show that the ratio of monomer units in the copolymer significantly affects the susceptibility of the polymer gel to the presence of low-molecular weight salts. It has been proved that changing the properties of the comonomer allows obtaining hydrogels capable of swelling or collapsing under the influence of changes in the ionic strength or thermodynamic quality of the solution. By varying the ratio of the comonomeric units, the swelling and contraction intervals of the polymer meshes inherent in polyelectrolyte bodies with the same charges were adjusted. It was also found that the polymers in question belonged to the anionic meshes.

Acknowledgments

The work was carried out within the project of the grant funding program for fundamental and applied scientific research of young postdoctoral scholarly of the Committee of Science of the Ministry of Science and Higher Education of the Republic of Kazakhstan for 2022-2024. “Application of computational methods for effective study of thermal decomposition of copolymers based on poly(propylene glycol fumarate phthalate)” AP15473241.

References

1 Kandelbauer, A., Tondi, G., Zaske, O. C., & Goodman, S. H. (2014). Unsaturated Polyesters and Vinyl Esters. *Handbook of Thermoset Plastics.* San Diego: William Andrew, 111–172. https://doi.org/10.1016/B978-1-4557-3107-7.00006-3

2 Guo X, Park H, Liu G, Liu W, Cao Y, Tabata Y, Kasper FK, & Mikos A. G. (2009). In vitro generation of an osteochondral construct using injectable hydrogel composites encapsulating rabbit marrow mesenchymal stem cells. *Biomaterials*, 30, 2741–2752. https://doi.org/10.1016/j.biomaterials.2009.01.048

3 Pagliaro, M. (2017). Esters, Ethers, Polyglycerols, and Polyesters. Glycerol, 59–90. https://doi.org/10.1016/b978-0-12-812205-1.00003-5

4 Yasko, A. W., He, S., Engel, P. S., Yaszemski, J. M., & Mikos, A. G. (2000). Injectable biodegradable polymer composites based on poly(propylenefumarate) with poly(ethylene glycol)-dimethacrylate. Biomaterials, 21, 2389–2394. https://doi.org/10.1016/S0142-9612(00)00106-X

5 Sarsenbekova, A. Zh., Kudaibergen, G. K., & Burkeev, M. Zh. (2019). Comparative analysis of the Thermal Decomposition Kinetics of Polyethylene Glycol Fumarate-Acrylic Acid Copolymers. *Russian journal of physical chemistry, 7, 93,* 1252–1257. https://doi.org/10.1134/S0036024419060281

6 Pot, U. (2009). *Poliefiry i alkidnyesmoly [Polyesters and alkyd resins]*. Moscow: KTC [in Russian].

7 Koliago, G. G., & Struk, V. A. (1990). *Materialy na osnove nenasytchennykh poliefirov [Materials based on unsaturated polyesters]*. Minsk: Nauka i tekhnika [in Russian].

8 Filippova, O. E. (2000). “Vospriimchivye” polimernyegeli [“Susceptible” polymer gels]. *Vysokomolekuliarnye soedineniia. — Polymer Science,* 42, 12, 2328–2352 [in Russian].

9 Holland, T. A., Tabata, Y., & Mikos, A. G. (2003). In vitro release of transforming growth factor-beta 1 from gelatin microparticles encapsulated in biodegradable, injectable oligo(poly(ethylene glycol) fumarate) hydrogels. *J Control Release*, 91, 299–313. https://doi.org/10.1016/S0168-3659(03)00258-X

10 Tazhbayev, E. M., Mustafin, E. S., & Burkeev, M. Zh. et al. (2006). Enthalpy of swelling of crosslinked copolymers of acrylic acid beta-vinyloxyethylamide in water and ethanol. *Russian journal of physical chemistry, 8*, 80, 1300–1304. https://doi.org/10.1134/S0036024406080231

11 Burkeev, M. Zh., Tazhbaev, E. M., Burkeeva, G. K., & Kovaleva, A. K. (2015). Nanocatalytic Systems Based on Poly(ethylene glycol maleate) — Acrylamide Copolymers. *Russian Journal of Applied Chemistry, 2*, 88, 314–319. https://doi.org/10.1134/S1070427215020202

12 Burkeev, M. Zh., & Tazhbayev, Ye. M. et al. (2019). Constants and parameters of radical copolymerization of poly(propylene glycol fumarate) with acrylic acid. *Bulletin of the University of Karaganda — Chemistry*, 1(93), 32–37. https://doi.org/10.31489/2019Ch1/25-31

13 Burkeev, M. Zh., Kudaibergen, G. K., & Burkeeva, G. K. et al. (2018). The number average and mass average molar masses of polyethylene (propylene)glycol fumarates. *Bulletin of the University of Karaganda — Chemistry*, 2(90), 17–22. https://doi.org/10.31489/2018ch2/17-22

14 Burkeev, M. Zh., Zhumanazarova G. K., & Zhakupbekova E. Zh. et al. (2020). Research of the influence of external factors on copolymersbased on unsaturated polyester resins. *Bulletin of the University of Karaganda — Chemistry*, 2(98), 51–57. https://doi.org/10.31489/2020Ch2/51-57

15 Burkeev, M. Zh., Zhumanazarova G. K., & Zhakupbekova E. Zh. et al. (2020). Poly(propylene fumarate phthalate) and acrylic acid radical copolymerization constants and parameters. *Bulletin of the University of Karaganda — Chemistry*, 1(97), 68–74. https://doi.org/10.31489/2020Ch1/68-74

16 Zolotov, Yu. A., Dorokhova, E. N., & Fadeeva, V. I. (2000). Fiziko-khimicheskiye metody analiza [Physico-chemical methods of analysis]. M.: Vysshaya shkola [in Russian].

17 Burkeev, M. Zh., Tazhbaev, E. M., & Burkeeva G. K. et al. (2013). Effect of External Factors on the Swelling of Hydrogels Based on Poly(ethylene glycol) Maleate with Some vinyl Monomers. *Russian Journal of Applied Chemistry*, 1(86), 63–68. https://doi.org/10.1134/S1070427213010114

Information about authors*

Sarsenbekova, Akmaral Zhakanovna — PhD of Chemistry, Associate Professor, Karagandy University of the name of academician E.A. Buketov, Universitetskaya street, 28, 100024, Karaganda, Kazakhstan; e-mail: chem_akmaral@mail.ru; https://orcid.org/0000-0002-8951-3616;

Burkeyev, Meyram Zhunusovich — Full Professor, Doctor of Chemical Sciences, Karagandy University of the name of academician E.A. Buketov, Universitetskaya street, 28, 100024, Karaganda, Kazakhstan; e-mail: m_burkeev@mail.ru; https://orcid.org/0000-0001-8084-4825;

Zhumanazarova, Gaziza Mustafaevna *(corresponding author)* —PhD student, Karaganda Industrial University, Republic Ave. 30, 101400, Temirtau, Karagandy Province, Kazakhstan; e-mail: gaziza.zhumanazarova@mail.ru; https://orcid.org/0000-0002-1793-0488;

Kudaibergen, Gulshakhar Kudaibergenkyzy — PhD of Chemistry, Senior Researcher, National Center for Biotechnology, Korgalzhynhighway 13/5, 100000, Astana, Kazakhstan; e-mail: kudaibergen@biocenter.kz; https://orcid.org/0000-0002-0779-4099;

Nasikhatuly, Yermauyt — Master of technical sciences, Karagandy University of the name of academician E.A. Buketov, Universitetskaya street, 28, 100024, Karaganda, Kazakhstan; e-mail: ermauit@gmail.com; https://orcid.org/0000-0003-4574-0902.

*The author's name is presented in the order: *Last Name, First and Middle Names*

How to Cite: Rakhymbay, L., Shugay, B., Karlykan, M., Namazbay, A., Konarov A., & Bakenov, Zh. (2023) Recent Advances in Layered $Na_2Mn_3O_7$ Cathode Materials for Sodium-Ion Batteries. *Eurasian Journal of Chemistry, 109(1), 59-67.* https://doi.org/10.31489/2959-0663/1-23-5

INORGANIC CHEMISTRY

Review

Received: 06 October 2022 | Revised: 26 October 2022 |
Accepted: 01 November 2022 | Published online: 06 March 2023

UDC 544.42+519.242.7

https://doi.org/10.31489/2959-0663/1-23-5

Lunara Rakhymbay, Bagdaulet Shugay, Maksat Karlykan,
Alibi Namazbay, Aishuak Konarov*, Zhumabay Bakenov

Department of Chemical and Materials Engineering, School of Engineering and Digital Sciences, Nazarbayev University, Astana, Kazakhstan
*(*Corresponding author's e-mail: aishuak.konarov@nu.edu.kz)*

Recent Advances in Layered $Na_2Mn_3O_7$ Cathode Materials for Sodium-Ion Batteries

There has been an increasing amount of attention paid to the different technologies that are used in energy production and storage in the context of day-to-day operations, which range from small-scale applications to large-scale applications, which are all equally important. As far as energy storage systems are concerned, Li-ion batteries are the market leader due to their high energy and power density, making them one of the most popular choices. Despite this, a significant concern is the scarcity of lithium resources and other metals that are needed for cathode material, such as cobalt and nickel, in the long run. Recent research has focused on alternative energy storage systems to mitigate these concerns. Due to sodium's widespread availability and similar chemistry to lithium-ion batteries (LIBs), sodium-ion batteries (SIBs) are considered the most promising next-generation alternatives. Being competitive in the market today requires the development of cathode materials that are of high performance. Among the studied materials, the $Na_2Mn_3O_7$ electrode displayed high capacity. In addition, the low price of sodium and manganese makes it even more attractive. In this work, we summarized the recent progress in studying and enhancing the $Na_2Mn_3O_7$ cathode material.

Keywords: rechargeable batteries, sodium-ion battery, redox reaction, layered structure, cathode, low voltage, high voltage, oxygen redox.

Content

List of abbreviations

ESS: energy storage systems
BES: battery energy storage
SIBs: sodium-ion batteries
LIBs: lithium-ion batteries
SHE: standard hydrogen electrode

EES: electrical energy storage
HC: hard carbon
CV: cyclic voltammetry
GITT: galvanostatic intermittent titration technique
XANES: X-ray absorption near edge structure

Review Plan

Inclusion and Exclusion Criteria: The present review discussed the current progress in the sodium cathode materials, specifically the $Na_2Mn_3O_7$. The review data are based on very recent scientific publications from 2017 to 2022. Some older literature sources (2001–2013) provide information about the first attempts to synthesize $Na_2Mn_3O_7$ and other materials with oxygen redox. A large-scale study of diazonium sulfonate salts began with the work of Barbero (1998) and continues now. We searched and analyzed articles from Scopus, and Web of Science. The keywords used for the search were "sodium cathodes", "$Na_2Mn_3O_7$", "layered structure", "oxygen redox", "Manganese based", etc. The resultant data were discussed in this work. No statistical methods were used in this review.

Introduction

Modern generations use rechargeable batteries to supply power and power any modern electronics (such as mobile phones, laptops, etc.) that require electricity to function without the need for an external source of electricity [1–6]. When compared to other rechargeable battery technologies, LIBs combine the advantages of high energy density, a compact, and lightweight design, and excellent cycle life compared to other rechargeable battery technologies. However, due to the increasing number of applications, from small to a larger scale, the pressure for the production of LIBs is getting tougher every year since the resources of lithium and other transition metals such as cobalt and nickel are limited, which negatively affects the price [7–11]. This has led to an extensive study of a variety of different types of rechargeable batteries, such as the Na-, K-, Zn-, Ca-, and Mg-ion batteries, to take advantage of their availability of resources over LIBs so that they may serve as alternatives to LIBs.

In this regard, sodium-ion batteries (SIBs) possess distinct advantages over LIBs, namely relative abundance and low electrochemical potential standing at –2.71 V compared to a standard hydrogen electrode (SHE) negligibly above that of LIBs (330 mV); thus, enabling SIBs to fulfill demands for large-scale electrical energy storage (EES) [12]. The SIBs commercialized by the Faradion company can be an example of a successful trial that could surpass the energy densities of Li-ion batteries ($LiFePO_4$/graphite) with a quickly convergent cycle lifetime, comparable rate performance and charge acceptance [13]. Additionally, laminated batteries and coin cells were exemplified by Sumitomo Chemical Co. Ltd. employing O3-type $NaFe_{0.4}Mn_{0.3}Ni_{0.3}O_2$ cathode and hard carbon (HC) anode. When the laminated battery was charged beyond 200 percent of its functional capacity and reached 12 V, neither explosion nor ignition occurred. Even though these SIBs demonstrate high-rate capabilities and cycle life, they perform worse than their LIBs counterparts. Then, Faradion produced storage with an aimed capacity of 418 Wh utilizing 48 cells and a 3 Ah pouch prototype SIB to charge an electric bicycle [14]. Despite the weaknesses of SIBs lacking in LIBs, such as insufficient energy density due to low operation voltage, SIBs are still considered a prospective alternative to surpass high-cost LIBs in a large-scale application. The energy density of the battery can be enhanced by utilizing cathode materials with high redox potentials using electrode materials that possess a high specific capacity. Since most cathode materials store sodium ions through intercalation, the number of sites for storage is limited, leading to the challenge of increasing the specific capacity of cathode materials. In addition, the utilization of cathode materials with high redox potentials is restricted due to the decomposition of electrolytes at high potentials.

In this review, we have focused on $Na_2Mn_3O_7$-based cathode materials since they displayed high capacity (>200 mAh g^{-1}). Moreover, sodium and manganese are cheap elements. However, the material suffered from rapid capacity fading, which hindered its commercialization. Many approaches have been addressed, such as doping to stabilize the structure. A detailed look into these approaches will be discussed in this work.

1. A low voltage cathode: based only on Mn^{4+}/Mn^{3+} redox

The electrochemical activity of Na-Mn-O ternary layered metal oxide ($Na_2Mn_3O_7$) is an important phenomenon in the research of Mn-based cathode materials for SIBs as manganese-based cathodes have gained some attention because of its effective environmental-friendly aspect and low price. As a cathode material,

$Na_2Mn_3O_7$ possesses a layered structure where layers build by Mn-O bonds in each corner of the octahedra. As redox reaction is central chemistry, it is critical to investigate whether the intercalation and deintercalation process only with Mn^{4+} oxidation surrounded by octahedral oxygen or whether SIBs are accompanied by the release of oxygen.

As Adamczyk et al. [15] the first well-studied counterpart of sodium cathode was $Li_2Mn_3O_7$ prepared by the ionic exchange method by Raekelboom et al. [16] from $Na_2Mn_3O_7$. As synthesized material was crystallized in the layered structure with the space group of *R*3*m*. The assembled half-cell with $Li_2Mn_3O_7$ cathode material delivered an initial capacity of 160 mAh g^{-1}, where a plateau appears at 3.0 V. However, due to the unstable crystal structure where layered structure transferred to the spinal structure, the long-term cycling displayed poor performance. On the other hand, this phase transition is not noticed in the SIBs systems, and because of this given novelty, researchers synthesized $Na_2Mn_3O_7$ by the conventional solid-state method [15]. By sintering at 600 °C for 4 hours, they obtain the material with triclinic space group P1. Figure 1 illustrates the galvanostatic charge and discharge curves of the given material for the initial five cycles, where detected the main plateau at 2.1 V, which provides the 160 mAh g^{-1} capacity. The cyclic voltammetry peaks prove the above-detected plateau region which is consistent with the Mn^{4+}/Mn^{3+} couple. The polarization degree of described peaks was around 20 mV which was 2.1 V for the reduction peak and 2.2 V for the oxidation peak. As well known, the layers of the cathode material consist of transition metals with *d* orbitals. During the redox reactions, the *d*-orbitals mentioned above start to convert to degenerate states and, at the low voltage, lead to the asymmetrical location of transition metal layers. In the degenerate states, electrons of the *d*-orbital may occupy XY, XZ, or YZ orbitals. In simple words, the geometry of equatorial and axial bonds alters and leads to the shortening or elongation of axial bonds compared with equatorial bonds. Due to these changes during the cycling, the performance was not satisfying.

Recent studies by Sada et al. [17] used $Na_2Mn_3O_7$ as an appropriate positive carrier for reversible redox reactions of Li, K, and Na batteries. They cut the voltage window to 3.0 V and excluded the oxygen release. As illustrated in Figure 2, the galvanostatic experiments in the shortened voltage window started with the discharge cycle of the coin cell batteries as the oxidation state of the Mn in the cathode obtained the highest (4+) state. Figure 2 demonstrates the specific capacities where specific discharge capacities reached 160 mAh g^{-1} for Li and 140 mAh g^{-1} for Na and K batteries. Interestingly, compared to Na, and K, Li-ion exhibited a jumping of the working voltage almost to 1 V, which boosts the energy density of the lithium-based half-cell battery. However, LIBs systems exhibit irreversible phase transitions, which lead to a fast decline of the irreversible capacity in the following cycles [18].

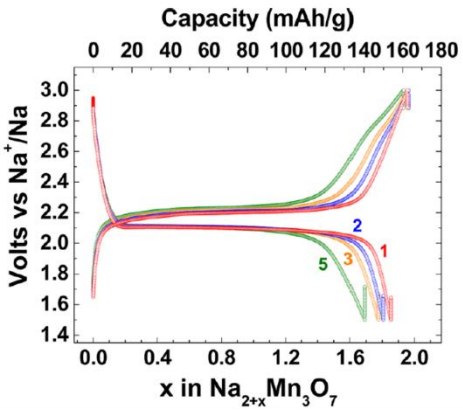

Figure 1. Galvanostatic charge and discharge profile of SIBs. Reprinted with permission from [15]. Copyright {2017} American Chemical Society

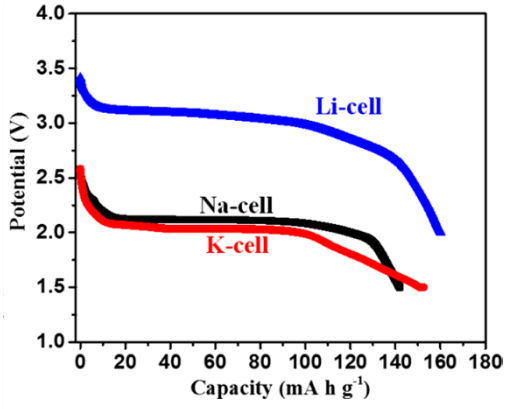

Figure 2. Comparison of the first discharge curves of $Na_2Mn_3O_7$ with Li^+, Na^+, and K^+ half-cells. Reprinted with permission from [19]. Copyright {2018} American Chemical Society

The studies mentioned above concerned the possibility of using Mn-based material for non-aqueous electrolyte systems where electrolytes are toxic and have safety problems because of exothermic reactions. By considering aqueous Zn-ion batteries, researchers proposed an alternative way to exclude such issues in developing $Na_2Mn_3O_7$ materials as a cathode for aqueous Zn-ion batteries [19]. In their preparation, they use

600 °C for the tablets prepared by the solid-state method. Figure 3 demonstrates the interesting phenomenon with initial discharge capacity and following increase upon cycling. This phenomenon can be explained by the low wettability degree of active material and activation of $Na_2Mn_3O_7$, followed by phase transformations illustrated in Figure 4. The characteristic peaks appeared at 1.3 and 1.44 V in the reduction reaction and symmetric peaks at 1.5 and 1.5 V in the oxidation reaction. These peaks match with the Mn^{4+}/Mn^{3+} redox reaction and provide overlapped symmetric peaks. Further cycling until 400 cycles provide a retention rate of around 65 % of the initial capacity. If we compare the energy density of non-aqueous and aqueous electrolytes for SIBs and Zn-ion batteries, we detect comparable 300-350 Wh kg^{-1} results.

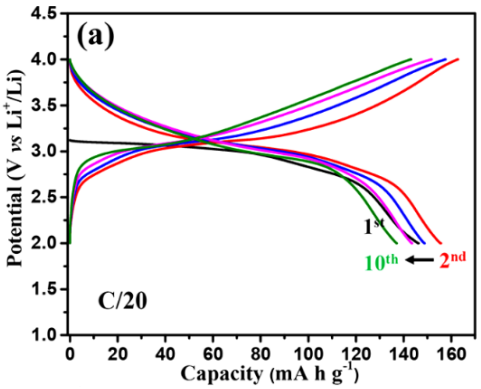

Figure 3. Galvanostatic charge and discharge curves at C/20 rate. Reprinted with permission from [19]. Copyright {2018} American Chemical Society

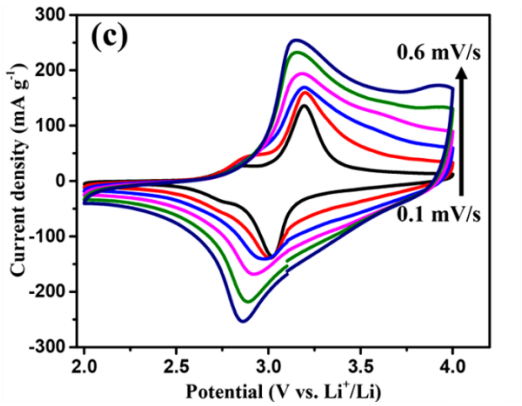

Figure 4. Cyclic voltammograms with six different scan rates from 0.1 to 0.6 mV s^{-1}. Reprinted with permission from [19]. Copyright {2018} American Chemical Society

To sum up, research on cathode for SIBs field proves the capabilities of the $Na_2Mn_3O_7$ to use as a promising candidate. The capacity of redox reaction at shortened cut-off voltage window came from reversible intercalation and deintercalation of two sodium ions through a so-called biphasic process where material structure can be explained by the formula $Na_{4.2}Mn_3O_7$ with Na^+ state. As described above, a long plateau at 2.1 V for the galvanostatic test and a peak with a low polarization in the cyclic voltammetry test provide the 160 mAh g^{-1}. With an average working voltage of 2.1 V and energy density of 330 Wh kg^{-1}, other properties such as non-toxicity, low price, and simple preparation ways increase the interest in a given material.

2. A high voltage cathode: based on the combination of Mn^{4+}/Mn^{3+} and Oxygen redox

Another interesting study indicates that when the theoretical limit of the M-redox reaction is exceeded in alkali metal excess transition metal oxides ($A_{1+x}M_{1-x}O_2$), additional capacity can be obtained as a result of additional oxygen redox reactions. [20]. A good example of this is the material $Li_{1.2}Ni_{0.13}Co_{0.13}Mn_{0.54}O_2$, where $0.2Li^+$ are located in the transition metal layer. This material delivered a specific capacity of 270 mAh·g^{-1}, of which 150 mAh·g^{-1} of capacity was derived via oxygen redox. [21]. Ceder's research group provided a theoretical explanation for reversible oxygen-redox reactions. The redox activity of oxygen in layered materials with an excess of lithium arises from Li-O-Li bonding, which creates orphan states of oxygen that rise from the oxygen-binding manifold [22]. There is still some uncertainty regarding oxygen-redox reactions, but it is generally accepted that in AMO_2, oxygen is coordinated by three transition metals, and its 2p orbitals are primarily involved in bonding states located below Fermi's level. Consequently, oxygen oxidation removes a bonding electron from an M-O bond. On the other hand, it is important to note that two transition metal atoms are coordinated by two oxygen atoms in $A_{1+x}M_{1-x}O_2$, unlike in the case of AMO_2. By having a nonbonding 2p orbital along the A-O-A axis and a position below the Fermi level, this oxygen contributes to the oxygen-redox reaction without causing M-O bonds to become easily broken [23, 24].

In 2018 Prof. Yamada's research group studied the reversible oxygen redox capacity of $Na_2Mn_3O_7$ at ≈4.1 V versus Na/Na^+, and DFT calculations were used to confirm nonbonding oxygen 2p orbitals [25, 26]. The authors predicted that oxygen has so-called nonbonding 2p orbitals in manganese vacancy, which delivers this extra capacity. As shown in Figure 5*a*, during the initial cycle, there were no changes in Mn L-edge, which indicates that the Mn does not contribute to the capacity. On the other hand, the O K-edge (Fig. 5*b* and 5*c*) displays that during charge, the intensity of the shoulder peak increased, and during discharge, it returned back to the initial state. These changes are associated with reversible oxygen redox. In addition to the exper-

imental data, it was confirmed by the theoretical calculations, which are shown in Figures 5d and 5e [25]. The charge-discharge curve between 1.5–3.0 V verified that reaction occurred due to $Mn^{4+/3+}$ redox, which corresponds to previous French scientist's investigations [15]. However, in this paper, they observed another part of the cut-off voltage (3.0–4.7 V) where an extra 75 mAh g^{-1} capacity (at ≈4.1 V versus Na/Na^+) is obtained (Fig. 6). Considering that Mn can not be oxidized upper 4+, considered that it happened due to reversible oxygen redox. Combining Mn and O redox $Na_2Mn_3O_7$ can deliver a high reversible capacity (>200 mAh·g^{-1}) [27].

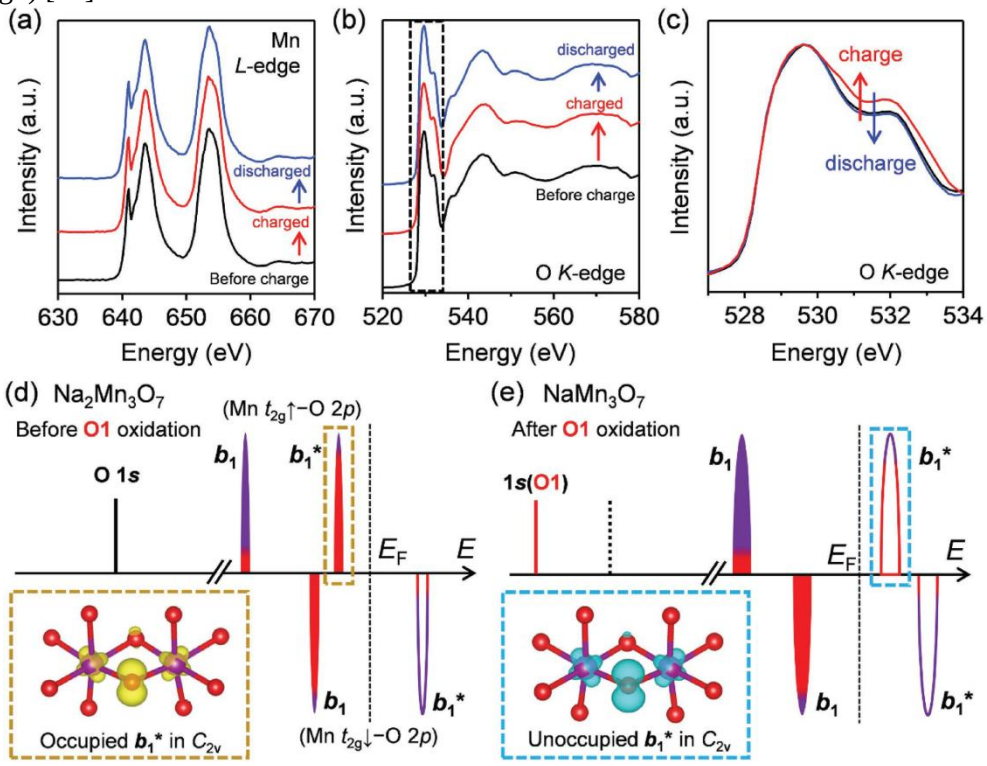

Figure 5. Electronic structure changes of $Na_2Mn_3O_7$ during the charge and discharge. a) Ex situ X-ray absorption spectra for Mn L3-edge. b) Ex situ X-ray absorption spectra for O K-edge. c) Enlarged part of X-ray absorption spectra for O K-edge. Schematic illustration of the electronic structures of d) $Na_2Mn_3O_7$ and e) $NaMn_3O_7$. Densities of states are labelled based on the molecular orbitals of OMn_2 in a C_{2v} symmetry. Reprinted with permission from [25]. Copyright {2018} Wiley

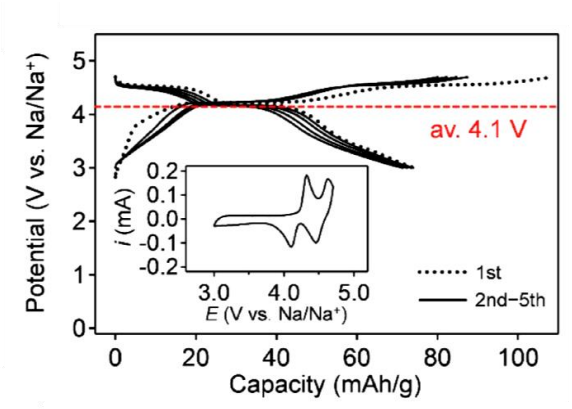

Figure 6. Galvanostatic charge/discharge curves between 3.0 and 4.7 V versus Na/Na^+ Reprinted with permission from [25]. Copyright {2018} Wiley

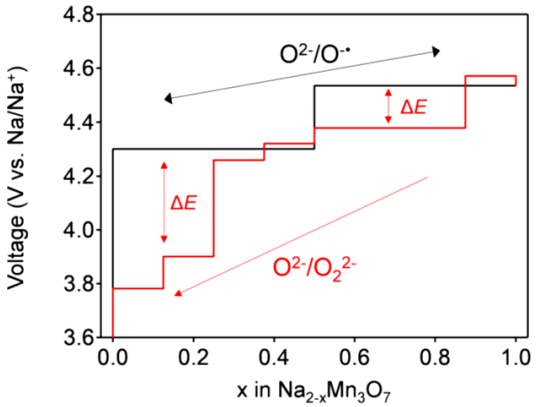

Figure 7. Predicted voltage hysteresis of $Na_{2-x}Mn_3O_7$ with hypothetical peroxide-like O_2^{2-} dimers. Reprinted with permission from [26]. Copyright {2021} Springer Nature

Even so, the chemical state of oxidized oxygen in this material is still debatable. Because of the high voltage hysteresis (|rGox | |rGred |), oxidized oxide ions (O•) form stable peroxide-like O_2^{2-} dimers when

charged. Following discharge, the O_2^{2-} dimer may be reduced to O_2^{4-} and then decomposed to O_2. In addition, this hysteresis, when transition-metal migration and/or surface cation densification happen simultaneously, the overlapping kinetic hysteresis caused by concentration overpotential, makes overall mechanisms challenging [28].

The $Na_{2-x}Mn_3O_7$ was recently investigated to exhibit a high reversible oxygen-redox capacity with little voltage hysteresis (0.04 V) and thus a good counterpart (Fig.7), |rGox | |rGred |) for gaining an understanding of the cause of the normally high voltage hysteresis observed following oxygen redox. Why $Na_{2-x}Mn_3O_7$ exhibits the reversible oxygen-redox reaction in this mechanism $O^{2-/}O^{-\bullet}$? To answer this question, Prof. Yamada's group again investigated this material and aimed to confirm the existence of $O^{-\bullet}$ in $Na_{2-x}Mn_3O_7$ as the dominant state in the reversible oxygen redox in the thermodynamical view of analysis. By the DFT calculation, it was confirmed that the calculated magnetic moments of Mn and O gradually appear on O atoms during dissociation, which indicates the formation of $O^{-\bullet}$. In comparison, the multiorbital Mn-O bond ($(\sigma + \pi)$ helps to stabilize the formed $O^{-\bullet}$ in the structure $Na_{2-x}Mn_3O_7$ [26].

Partially substituting the Mn^{4+} with other elements with different oxidation states, such as Mg^{2+}, Al^{3+}, Ti^{4+}, etc., is one efficient method for further deeply studying the redox-active oxygen atoms. For efficient substitution, Mn and element should have similar ionic radii [24].

P. Siriwardena et al. studied a series of Mg^{2+} doped $Na_2Mn_3O_7$. The results imply that Mg^{2+} doping can positively affect capacity enhancement and rate capability. 2 mol. % Mg^{2+} doped material exhibited the best specific capacity of 143 mAh g^{-1} after 30 cycles. However, with long-term electrochemical cycling, a somewhat negative effect on capacity retention was observed, which was associated with increasing Mn^{4+} in the system. As we know that Mn^{4+} can form Mn^{2+} in an acidic solution, which can easily dissolve in the electrolyte, which causes structural instability. In addition, GITT and CV studies for NaMnO, $NaMnMg_{0.5}O$, and $NaMnMg_2O$ materials have shown that Mg^{2+} doping can reduce the Na^+ vacancy ordering, resulting in improved diffusion. Also, a $NaMnMg_{0.5}O$/ HC anode full cell was investigated that exhibited 80 mAh g^{-1} [29].

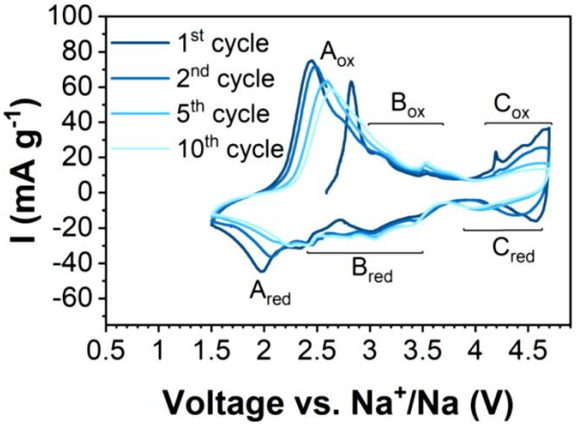

Figure 8. CV curves of $Na_{2.4}Mn_{2.6}Al_{0.4}O_7$ at a scan rate of 0.1 mV s^{-1} in the voltage range 1.5–4.7 V vs. Na+/Na. Reprinted with permission from [30]. Copyright {2021} Royal Society of Chemistry

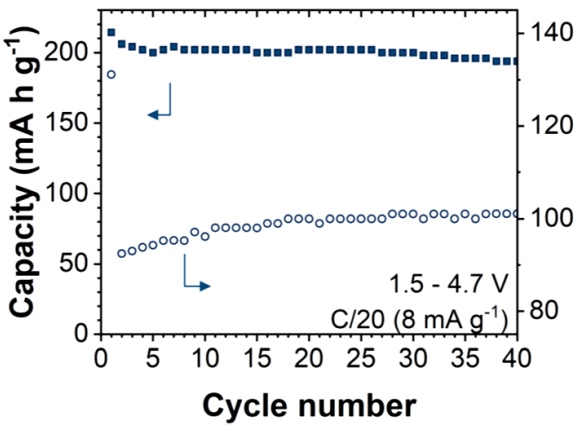

Figure 9. Cycle performance of Al-doped NaMnO in the voltage range 1.5–4.7 V. Reprinted with permission from [30]. Copyright {2021} Royal Society of Chemistry

Soares et al. have studied the effects of partial substitution of Al^{3+} ions in the $Na_2Mn_3O_7$ cathode material. During experiments (Fig. 8), two redox couple of Mn^{3+}/Mn^{4+} and O^2/O^{n-} was confirmed on CV, XANES, and computational studies. The electrochemical characteristics showed the 215 mAh g^{-1} initial capacity between the voltage range 1.5–4.7 at C/20 and 90 % capacity retention after 40 cycles, as shown in Figure 9. Modeled structure gave observation that Al^{3+} is more electronegative than Mn^{4+} which can let diffusion of Na^+ in various directions. And diffusion kinetics can be improved through the shorter length Al-O bond that helps widener the Na^+ pathway [30].

Redox-inactive Ti^{4+} chemistry was investigated by Liu et al. and used to partially substitute Mn^{4+} to form $Na_2Ti_{0.5}Mn_{2.5}O_7$. The results indicate that Ti^{4+} can reduce objectionable interlayer gliding at a high voltage, and this material showed ultra-slow volume change (0.11 %), revealing structure stability. $Na_2Ti_{0.5}Mn_{2.5}O_7$ delivered good cycling performance with 79.1 % capacity retention after 60 cycles at

50 $mA \cdot g^{-1}$. Moreover, after storing in the air for 60 days, the cyclic stability of $Na_2Ti_{0.5}Mn_{2.5}O_7$ showed 77.0 % capacity retention after 60 cycles which indicates the air stability of doped material [31].

Conclusions

In summary, $Na_2Mn_3O_7$ material is very attractive as a cathode material not only for SIBs due to the low price and high capacity. The manganese redox can be used if the cutoff voltage is limited up to 3V and the capacity of about 160 mAh g^{-1} is delivered. However, due to the Jahn-Telle distortion associated with Mn^{3+}, the cycling performance still needs to be improved. When the cut-off voltage increased over 3 V (up to 4.7 V), the participation of the oxygen redox increased the capacity to over 200 mAh g^{-1}. The enhancement of the cycling performance was done by partial substitution of the manganese with other metals such as Mg, Al, and Ti. Furthermore, coating the material with carbon or other materials is one of the ways to improve cycling performance.

Acknowledgment

This work was supported by the Ministry of Education and Science of the Republic of Kazakhstan Grant (AP08856179) and the Nazarbayev University Faculty-Development Competitive Research Grant (080420FD1914). A.K. thanks the Social Policy Grant awarded to him by the NU.

References

1 Dunn, B., Kamath, H., & Tarascon, J. M. (2011). Electrical energy storage for the grid: A battery of choices. *Science*, 334, 6058. https://doi.org/10.1126/science.1212741

2 Delmas, C. (2018). Sodium and Sodium-Ion Batteries: 50 Years of Research. *Advanced Energy Materials*, 8, 1703137. https://doi.org/10.1002/aenm.201703137

3 Pan, H., Hu, Y. S., & Chen, L. (2013). Room-temperature stationary sodium-ion batteries for large-scale electric energy storage. *Energy and Environmental Science*, 6, 2338-2360. https://doi.org/10.1039/c3ee40847g

4 Guney, M. S., & Tepe, Y. (2017). Classification and assessment of energy storage systems. *Renewable and Sustainable Energy Reviews*, 75, 1187-1197. https://doi.org/10.1016/j.rser.2016.11.102

5 Amiryar, M. E., & Pullen, K. R. (2017). A review of flywheel energy storage system technologies and their applications. *Applied Sciences*, 7, 3. https://doi.org/10.3390/app7030286

6 Kiehne, H. A. (2003). Battery Technology Handbook. *Battery Technology Handbook*. https://doi.org/10.1201/9780203911853

7 Dehghani-Sanij, A. R., Tharumalingam, E., Dusseault, M. B., & Fraser, R. (2019). Study of energy storage systems and environmental challenges of batteries. *Renewable and Sustainable Energy Reviews*, 104, 192-208. https://doi.org/10.1016/j.rser.2019.01.023

8 May, G. J., Davidson, A., & Monahov, B. (2018). Lead batteries for utility energy storage: A review. *Journal of Energy Storage*, 15, 145-157. https://doi.org/10.1016/j.est.2017.11.008

9 Fang, Y., Xiao, L., Chen, Z., Ai, X., Cao, Y., & Yang, H. (2018). Recent Advances in Sodium-Ion Battery Materials. In *Electrochemical Energy Reviews*, 1, 294–323. https://doi.org/10.1007/s41918-018-0008-x

10 Wood Mac. Site. Features. Shared. View Models. Metadata. Publisher. (2018, August 6). *U.S. Energy Storage Monitor*. Wood Mackenzie. Retrieved August 16, 2022, from https://www.woodmac.com/industry/power-and-renewables/us-energy-storage-monitor/

11 *Energy storage*. Energy. (n.d.). Retrieved September 5, 2022, from https://energy.ec.europa.eu/topics/research-and-technology/energy-storage_en

12 Monconduit, L. (2021). *Na-Ion Batteries*. Wiley-ISTE. https://doi.org/10.1002/9781119818069

13 Rudola, A., Rennie, A. J. R., Heap, R., Meysami, S. S., Lowbridge, A., Mazzali, F., Sayers, R., Wright, C. J., & Barker, J. (2021). Commercialization of high energy density sodium-ion batteries: Faradion's journey and outlook. *Journal of Materials Chemistry A*, 9, 8279-8302. https://doi.org/10.1039/d1ta00376c

14 Deng, J., Luo, W. bin, Chou, S. L., Liu, H. K., & Dou, S. X. (2018). Sodium-Ion Batteries: From Academic Research to Practical Commercialization. *Advanced Energy Materials*, 8, 1701428. https://doi.org/10.1002/aenm.201701428

15 Adamczyk, E., & Pralong, V. (2017). $Na_2Mn_3O_7$: A Suitable Electrode Material for Na-Ion Batteries? *Chemistry of Materials*, *29*(11), 4645–4648.

16 Raekelboom, E. A., Hector, A. L., Owen, J., Vitins, G., & Weller, M. T. (2001). Syntheses, structures, and preliminary electrochemistry of the layered lithium and sodium manganese (IV) oxides, $A_2Mn_3O_7$. *Chemistry of Materials*, *13*(12), 4618–4623. https://doi.org/10.1002/chin.200208006

17 Sada, K., & Barpanda Prabeer, B. (2019). Layered Sodium Manganese Oxide $Na_2Mn_3O_7$ as an Insertion Host for Aqueous Zinc-ion Batteries. *MRS Advances*, *4*(49), 2651-2657. https://doi.org/10.1557/adv.2019.297

18 Sada, K., Senthilkumar, Baskar Ritambhara Gond, S., Pralong, V., & Barpanda, P. B. (2021). Layered $Na_2Mn_3O_7$: A Robust Cathode for Na, K, and Li-Ion Batteries. *Recent Research Trends in Energy Storage Devices*. https://doi.org/10.1007/978-981-15-6394-2

19 Sada, K., Senthilkumar, B., & Barpanda, P. (2018). Layered $Na_2Mn_3O_7$ as a 3.1 V Insertion Material for Li-Ion Batteries. *ACS Applied Energy Materials*, *1*(12), 6719–6724.

20 Yabuuchi, N., Takeuchi, M., Nakayama, M., Shiiba, H., Ogawa, M., Nakayama, K., Ohta, T., Endo, D., Ozaki, T., Inamasu, T., Sato, K., & Komaba, S. (2015). High-capacity electrode materials for rechargeable lithium batteries: Li_3NbO_4-based system with cation-disordered rocksalt structure. *Proceedings of the National Academy of Sciences of the United States of America*, *112*(25). https://doi.org/10.1073/pnas.1504901112

21 Koga, H., Croguennec, L., Ménétrier, M., Douhil, K., Belin, S., Bourgeois, L., Suard, E., Weill, F., & Delmas, C. (2013). Reversible Oxygen Participation to the Redox Processes Revealed for $Li_{1.20}Mn_{0.54}Co_{0.13}Ni_{0.13}O_2$. *Journal of The Electrochemical Society*, *160*(6). https://doi.org/10.1149/2.038306jes

22 Seo, D. H., Lee, J., Urban, A., Malik, R., Kang, S., & Ceder, G. (2016). The structural and chemical origin of the oxygen redox activity in layered and cation-disordered Li-excess cathode materials. *Nature Chemistry*, *8*(7). https://doi.org/10.1038/nchem.2524

23 Mortemard De Boisse, B., Liu, G., Ma, J., Nishimura, S. I., Chung, S. C., Kiuchi, H., Harada, Y., Kikkawa, J., Kobayashi, Y., Okubo, M., & Yamada, A. (2016). Intermediate honeycomb ordering to trigger oxygen redox chemistry in layered battery electrode. *Nature Communications*, *7*. https://doi.org/10.1038/ncomms11397

24 Yabuuchi, N., Nakayama, M., Takeuchi, M., Komaba, S., Hashimoto, Y., Mukai, T., Shiiba, H., Sato, K., Kobayashi, Y., Nakao, A., Yonemura, M., Yamanaka, K., Mitsuhara, K., & Ohta, T. (2016). Origin of stabilization and destabilization in solid-state redox reaction of oxide ions for lithium-ion batteries. *Nature Communications*, *7*. https://doi.org/10.1038/ncomms13814

25 Mortemard de Boisse, B., Nishimura, S., Watanabe, E., Lander, L., Tsuchimoto, A., Kikkawa, J., & Yamada, A. (2018). Highly Reversible Oxygen-Redox Chemistry at 4.1 V in Na4/7− x [□1/7 Mn6/7]O2 (□: Mn Vacancy). *Advanced Energy Materials*, 8(20), 1800409. http://doi:10.1002/aenm.201800409

26 Tsuchimoto, A., Shi, X. M., Kawai, K., Mortemard de Boisse, B., Kikkawa, J., Asakura, D., Okubo, M., & Yamada, A. (2021). Nonpolarizing oxygen-redox capacity without O-O dimerization in $Na_2Mn_3O_7$. *Nature Communications*, *12*(1). https://doi.org/10.1038/s41467-020-20643-w

27 House, R. A., Maitra, U., Pérez-Osorio, M. A., Lozano, J. G., Jin, L., Somerville, J. W., Duda, L. C., Nag, A., Walters, A., Zhou, K. J., Roberts, M. R., & Bruce, P. G. (2020). Superstructure control of first-cycle voltage hysteresis in oxygen-redox cathodes. *Nature*, *577*(7791). https://doi.org/10.1038/s41586-019-1854-3

28 Tran, N., Croguennec, L., Ménétrier, M., Weill, F., Biensan, P., Jordy, C., & Delmas, C. (2008). Mechanisms associated with the "plateau" observed at high voltage for the overlithiated $Li_{1.12}(Ni_{0.425}Mn_{0.425}Co_{0.15})_{0.88}O_2$ system. *Chemistry of Materials*, *20*(15). https://doi.org/10.1021/cm070435m

29 Siriwardena, D. P., Fernando, J. F. S., Wang, T., Firestein, K. L., Zhang, C., Brand, H. E. A., Jones, M. W. M., Kewish, C. M., Berntsen, P., Jenkins, T., Lewis, C. E. M., von Treifeldt, J. E., Dubal, D. P., & Golberg, D. v. (2021). Probing the effect of Mg doping on triclinic $Na_2Mn_3O_7$ transition metal oxide as cathode material for sodium-ion batteries. *Electrochimica Acta*, *394*. https://doi.org/10.1016/j.electacta.2021.139139

30 Soares, C., Silván, B., Choi, Y. S., Celorrio, V., Seymour, V. R., Cibin, G., Griffin, J. M., Scanlon, D. O., & Tapia-Ruiz, N. (2021). $Na_{2.4}Al_{0.4}Mn_{2.6}O_7$ anionic redox cathode material for sodium-ion batteries — a combined experimental and theoretical approach to elucidate its charge storage mechanism. *Journal of Materials Chemistry A*, *10*(13). https://doi.org/10.1039/d1ta05137g

31 Liu, Y., Wang, C., Ren, M., Fang, H., Jiang, Z., & Li, F. (2021). Ultralow-strain Ti substituted Mn-vacancy layered oxides with enhanced stability for sodium-ion batteries. *Journal of Energy Chemistry*, *63*. https://doi.org/10.1016/j.jechem.2021.07.024

Information about authors*

Rakhymbay, Lunara — PhD student, School of Engineering and Digital Sciences, Nazarbayev University, Kabanbay Batyr Ave., 53, Astana, Kazakhstan; *e-mail:* lunara.rakhymbay@nu.edu.kz; https://orcid.org/0000-0002-7924-837X;

Shugay, Bagdaulet — Research Assistant, School of Engineering and Digital Sciences, Nazarbayev University, Kabanbay Batyr Ave., 53, Astana, Kazakhstan; e-mail: bagdaulet.shugay@alumni.nu.edu.kz; https://orcid.org/0000-0002-3564-432X;

Karlykan, Maksat — Undergraduate student, Department of Chemical and Materials Engineering, School of Engineering and Digital Sciences, Nazarbayev University, Kabanbay Batyr Ave., 53, Astana, Kazakhstan; e-mail: maksat.karlykan@nu.edu.kz;

Namazbay, Alibi — Undergraduate student, Department of Chemical and Materials Engineering, School of Engineering and Digital Sciences, Nazarbayev University, Kabanbay Batyr Ave., 53, Astana, Kazakhstan; e-mail: alibi.namazbay@nu.edu.kz;

Konarov, Aishuak (*corresponding author*) — Assistant Professor, Department of Chemical and Materials Engineering, School of Engineering and Digital Sciences, Nazarbayev University, Kabanbay Batyr Ave., 53, Astana, Kazakhstan; e-mail: aishuak.konarov@nu.edu.kz; https://orcid.org/0000-0001-9352-8602;

Bakenov, Zhumabay — Professor, Department of Chemical and Materials Engineering, School of Engineering and Digital Sciences, Nazarbayev University, Kabanbay Batyr Ave., 53, Astana, Kazakhstan; e-mail: zbakenov@nu.edu.kz; https://orcid.org/0000-0003-2781-4955

*The author's name is presented in the order: *Last Name, First and Middle Names*

How to Cite: Burkeyeva, G.K., Kovaleva, A.K., Tazhbayev, Ye.M., Ibrayeva, Zh.M., & Plocek, J. (2023) Development of Energy-Efficient "Cold" Curing Method for Polypropylene Glycol Fumarate Using an Optimized Initiating System. *Eurasian Journal of Chemistry, 109(1), 68-77*. https://doi.org/10.31489/2959-0663/1-23-10

CHEMICAL TECHNOLOGY

Article

Received: 01 December 2022 | Revised: 26 January 2023 |
Accepted: 09 February 2023 | Published online: 06 March 2023

UDC 541.64

https://doi.org/10.31489/2959-0663/1-23-10

Gulsym K. Burkeyeva[1], Anna K. Kovaleva[1*], Yerkeblan M. Tazhbayev[1], Zhansaya M. Ibrayeva[1], Jiri Plocek[2]

[1]Karagandy University of the name of academician E.A. Buketov, Kazakhstan;
[2]Institute of Inorganic Chemistry of the Czech Academy of Sciences, Husinec-Rez, Czech Republic
*(*Corresponding author`s e-mail: cherry-girl1899@mail.ru)*

Development of Energy-Efficient "Cold" Curing Method for Polypropylene Glycol Fumarate Using an Optimized Initiating System

The possibility of using the polymeric matrix obtained as a result of "cold" polymerization of polypropylene glycol fumarate (p-PGF) with methacrylic acid (MAA) as a polymeric base for obtaining new adhesives of domestic production was demonstrated. The starting reagent (p-PGF) was synthesized by condensation polymerization of fumaric acid with propylene glycol in the presence of a catalyst, which reduced the temperature and shortened the process time. A number of solutions of p-PGF in MAA of different mass compositions were obtained and their rheological properties were determined. Curing of the studied solutions was carried out by radical polymerization at room temperature in the presence of the "cold curing" initiating system. The optimum composition and amount of components of the "cold" curing initiating system consisting of an initiator (benzoyl peroxide) and a promoter (dimethylaniline) were established. Technological parameters of curing (temperature, lifetime and curing time, the value of volume shrinkage) were determined. The obtained compounds were identified by infrared spectroscopy. The surface morphology of the cured samples was studied by scanning electron microscopy. It was found that varying the composition of the initial polymer-monomer mixture allows controlling the physicochemical properties.

Keywords: sealant, unsaturated polyester, polypropylene glycol fumarate, unsaturated carboxylic acid, methacrylic acid, radical copolymerization, "cold" curing, initiating system.

Introduction

With the widespread increase in the rate of construction, sealants and adhesives derived from polymer matrices by incorporating various fillers, plasticizers and others have gained great importance [1, 2]. At the same time, the polymer matrix-base has meet a number of requirements, namely optimal size of polymer network cells, structure stability under the influence of negative external factors, including the effect of UV radiation, resistance to organic solvents and alkalis, heat and cold resistance, resistance to mechanical loading and other deformation changes, low shrinkage and a sufficiently long lifetime and curing time [3, 4]. It is more preferable that the system is capable of curing with air oxygen [5] at room temperature or under low-temperature conditions without using additional curing conditions (increased pressure, photo or UV initiation, etc.).

Thus, promising co-reagents for obtaining a polymeric matrix are unsaturated polyesters of various compositions, which cure with vinyl monomers to form a polymer network with good elastic properties [6]. The undoubted advantages of the solutions of unsaturated polyesters in vinyl monomers before curing include the ability to control the consistency of solutions in a wide concentration range by varying the composition of the initial polymer-monomer mixture [7]. With their sufficiently low viscosity and ability to enter

into reaction of radical copolymerization with reactive vinyl monomers of hydrophilic and hydrophobic nature both when heated and at room temperature, the unsaturated polyesters become suitable co-reagents for obtaining polymer bases for sealants and adhesives. Thus, the resulting cured products have abrasion resistance and high resistance to mechanical stress, high resistance to aggressive environments, UV- and frost-resistance and heat resistance, and as a result of the absence of by-products in the curing process their operation is environmentally friendly and safe. Given the wide range of co-reagents used for the synthesis of initial unsaturated polyesters and their good compatibility with vinyl monomers due to the presence of a highly reactive double bond, it is possible to obtain final products with the required physicochemical and mechanical properties and performance characteristics [6].

Previously, the physicochemical characteristics of polymer bases obtained from polyethylene glycol maleate and acrylic acid solutions were studied, and the parameters of “cold” curing kinetics depending on the initial composition of co-reagent solutions were established [7].

The aim of this work is to study a number of rheological properties of the solutions of polypropylene glycol fumarate with methacrylic acid, to select the optimal composition of the initiating system and to establish technological parameters (temperature, lifetime and curing time, volume shrinkage) of the “cold” curing of the solutions of above said co-reagents.

Experimental

The reagents used in the study were propylene glycol, methacrylic acid, benzoyl peroxide, dimethylaniline (“Sigma-Aldrich”), fumaric acid (“Vekon”), aluminium chloride (“Reachem”). All reagents were used without additional purification.

Synthesis of the initial unsaturated polyester, namely polypropylene glycol fumarate (p-PGF) was carried out by polycondensation reaction of propylene glycol with fumaric acid at 423-433 K in a four-neck flask equipped with a stirring shaft, two reflux condensers, thermometer to control reaction temperature, Dean-Stark trap to collect water removed during the process and a tube to supply nitrogen. Polycondensation was carried out according to the procedure given in [8] under constant stirring in the presence of aluminum chloride catalyst in an inert nitrogen environment, which was fed into the system to avoid undesirable gelatinization processes.

Determination of the molecular weight of the obtained p-PGF in dioxane solution was performed by gel permeation chromatography on a VISCOTEK 270 DUAL DETECTOR MALVERN chromatograph, where polystyrene was used as a standard. Molecular mass was M_w ~1488 Da.

Radical copolymerization of p-PGF with methacrylic acid (MAA) was carried out in bulk at various initial mass ratio of co-monomers at 293 K in the presence of “cold” curing initiation system consisting of benzoyl peroxide (BPO) initiator and dimethylaniline (DMA) promoter.

The dynamic viscosity of the initial p-PGF-MAA solutions was determined at 293K using a vibrating viscometer SV-10 equipped with a liquid thermostat VT3, which allows to maintain the set temperature during the entire process [9].

Density values of the initial solutions and p-PGF-MAA copolymers were studied by pycnometric and hydrostatic methods according to all-Union State Standard 18329-2014 [10].

The total volumetric shrinkage was determined by calculation, according to State Standard 18616-80 [11] based on the difference in density of the initial solution and the mixture in the cured state:

$$X = \left(1 - \frac{\rho_0}{\rho}\right) \cdot 100\ \% \quad (1)$$

where ρ_0 is the density of initial solution; ρ is the density of cured solution.

The gelatinization time (lifetime) of p-PGF-MAA solutions was recorded automatically on a GelTimer Gelnorm GT-S instrument according to ISO 57884-2017 [12]. Curing time was measured according to ISO 2535-2017 [13].

The presence of functional groups in the cured p-PGF-MAA samples was determined by analyzing infrared spectra performed in KBr tablets on a FSM 1201 spectrometer [14].

The surface morphology of p-PGF-MAA samples was studied using a MIRA 3 TESCAN scanning electron microscope at an accelerating voltage of 20 kV [15].

Results and Discussion

The field of application of sealants is determined by their physicochemical and mechanical properties and is not limited to the construction industry only. Thus, sealing materials are also used for sealing aquariums, in engines and gearboxes. However, the main consumers are organizations engaged in repair and finishing and repair-decorative works.

Not depending on the composition of sealing materials and direct field of application there are general operational requirements, among which are good adhesion to different surfaces and other physico-mechanical properties (according to regulatory standards): gas and vapor permeability [16], water resistance, the ability to retain sealing properties under the influence of negative external factors for a long period of time [17]. From an economic point of view, important indicators are also quite low price and availability of initial reagents for their production [18].

Given the ability of unsaturated polyesters to interact with vinyl monomers to form a three-dimensional polymer network, the resulting products are called thermosetting composites [19]. This implies the need for a number of conditions for their curing. Thus, the curing process of thermosetting plastics to form a three-dimensional network of copolymer occurs as a result of exposure to elevated temperature, radioactive or UV radiation, or in the presence of curing agents and catalysts — when the curing occurs in air [20].

Therefore, the development of techniques and research of new polymer sealants curing at room temperature (so-called "cold" curing) should take place in stages, including the following tasks:

1. Synthesis of one of the reagents used as a p-PGF filler;
2. Preparation of the solutions of p-PGF in vinyl monomer of different composition and study of their rheological properties;
3. Optimization of technological parameters (temperature, solution lifetime, and curing time) of curing process for the unsaturated polyester-vinyl monomer (p-PGF-MAA) binary system by selecting the composition and concentration of the "cold" curing initiating system;
4. Curing of the studied solutions at room temperature by radical copolymerization in the presence of an optimized "cold" curing initiating system;
5. Identification of reaction products and study of a number of their physicochemical properties.

According to earlier studies [7], it was found that the most optimal compositions for obtaining adhesion materials were solutions of unsaturated polyesters in vinyl monomer with the amount of the first co-reagent 30-45 mass. %. In this study, p-PGF-MAA ratios where the unsaturated polyester content was in the above range were chosen as test samples.

Rheological properties are the main physicochemical characteristics of polymer compounds the knowledge of which is of great importance for improving the technologies of preparation and operation processes of the final polymer product. Knowledge of rheological characteristics is necessary in the chemical engineering industry to control the kinetics of chemical reactions, phase transitions, etc. [21]. In this regard, the dynamic viscosity and density of initial solutions of unsaturated polyester (p-PGF) in MAA of different compositions were studied. The results obtained are presented in Table 1.

Table 1

Rheological properties of initial solutions of p-PGF-MAA, T = 293 K

Composition of initial solution, mass.%		Dynamic viscosity (η), mPa·s	Density of solution (ρ), g/cm^3
p-PGF	MAA		
30.32	69.68	48.2±0.2	1.3019±0.075
34.96	65.04	59.3±0.2	1.3193±0.066
41.27	58.73	107.9±0.2	1.3301±0.073
45.14	54.86	213.7±0.3	1.3405±0.077

Analyzing the data presented in Table 1, it should be noted that the obtained values of dynamic viscosity and density correlate well with each other, as well as with what p-PGF contains in the solution. Thus, the results obtained indicate rather low values of dynamic viscosity and density, which are 48.2 mPa·s and 1.3019 g/cm^3, respectively for the ratio with the minimum amount of p-PGF (~30:70 mass. %), whereas increasing its content in the initial polymer-monomer mixture to ~45 mass.% leads to increasing the values of the studied parameters to 213.7 mPa·s and 1.3405 g/cm^3, respectively. This can be explained by the high viscosity values of p-PGF, the increase in the content of which in the studied solutions provokes a jump in their

viscosity and density values. Dependence of the dynamic viscosity and density of the studied solutions on the p-PGF content is shown in Fig. 1.

Currently, in automobile and construction structures, as well as in technological processes for repairing equipment in oil-gas-, mining and mountain fields there are used synthetic sealants based on phenol formaldehyde, epoxy and polyester resins, which can be divided into two classes, namely containing solvent and solvent-free. Despite the good adhesion properties to metals and other surfaces, sealants containing solvent (phenol formaldehyde), have a number of drawbacks, the most important of which is the presence of traces of solvents (water or organic solvents) in the adhesive composition. In this regard in many cases there are empty spaces, micro pores and micro cracks in the sealing seam. They are formed during evaporation of solvent and water eliminated as a result of polycondensation of phenol formaldehyde resin. Therefore, this type of packing seams cannot always provide a high degree of sealing the compounds. Another disadvantage of similar sealants containing a solvent is often the high curing temperature and the high degree of shrinkage of a polymer layer, which is also due to the evaporation process.

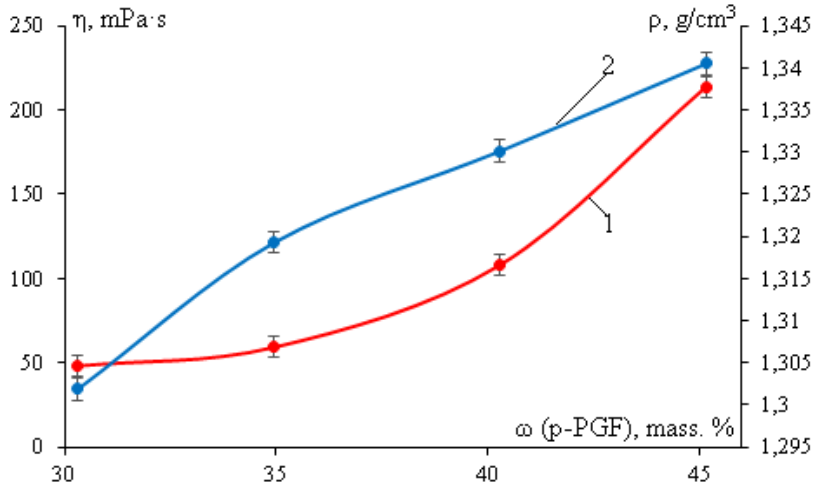

1 — dependence of the dynamic viscosity of the solution on the content of p-PGF in it;
2 — dependence of solution density on the content of p-PGF in it

Figure 1. Dependence of rheological properties of initial solutions of p-PGF-MAA on the content of p-PGF in them

The above disadvantages are absent in sealants that do not contain solvent, have high adhesive properties and can cure without heating or at rather low temperatures. Sealants based on epoxy oligomers, polyurethanes and unsaturated polyesters are widely used.

The curing of sealants of this group (without solvents) occurs during the polymerization reaction of the oligomers or monomers contained in its composition. It is not accompanied by elimination of by-products such as low molecular compounds unlike in polycondensation.

At the end of the curing process, the reaction product is a monolithic polymer with high cohesive hardness. The curing process of a solvent-free sealant is accompanied by negligible shrinkage. Sealants of this type by their characteristics meet the operating conditions in the construction industry, as well as in the car and tool building, so their use for the repair of technological devices is more promising [5]. Another characteristic indicator of sealant quality is its lifetime (the gelation time and gelatinization time), i.e. the time interval during which the thermosetting polymer retains the ability to be applied and processed in viscous-flow state after the introduction of compounds that facilitate its transition to a cured state.

In this regard, the main technological parameters for obtaining high-quality adhesive polymer bases are temperature, gelation time and curing time, the control of which is possible by using an optimally selected initiator system. Considering the possibility of interaction of unsaturated polyesters with vinyl monomers at low temperatures in the presence of an initiator and a promoter, a number of studies were carried out to select the optimal ratio of the components of the initiating system consisting of benzoyl peroxide (BPO) and dimethylaniline (DMA).

The results are presented in Table 2.

Table 2

Dependence of the influence of a promoter on gelatinization time and curing time of the solution of p-PGF-MAA (30.32:69.68 mass. %) (BP + DMA, T = 293 K)

Content, %		Gelatinization time ($\tau_{gelat.}$), min.	Curing time ($\tau_{curing.}$), min.
BPO	DMA		
1	0.05	141.24±5.37	207.18±8.70
1	0.1	98.31±3.74	169.06±7.10
1	0.15	82.36±3.13	145.13±6.09
1	0.2	49.15±1.87	78.17±3.28
1	0.25	14.25±0.54	26.03±1.09

Thus, the activity of the "cold" curing initiating system consisting of BPO as an initiator and DMA as a promoter is preserved over a wide temperature range, which allows varying the gelatinization and curing times of the binary p-PGF-MAA system in order to identify the most optimal values. It should be noted that when choosing the quantitative content of the components of the initiating system, only the amount of the DMA promoter was varied (from 0.05 to 0.2 % by mass of the initial solution of the p-PGF-MAA mixture), while the amount of the initiator was constant and equal to 1 %.

The choice of this amount of BPO was based on the analysis of a number of works [6, 22] and literature sources [23–25]. At the same time, as noted above [7], the BPO concentration affects a number of mechanical properties of the final product, in particular, at its high content the cured polymer is capable of a partial or a complete loss of elasticity and reduction of the numerical values of stress-strain indicators.

Analyzing the data in Table 2, we can say that with the minimum amount of DMA in the initiating system, which is 0.05 %, the gelatinization time ($\tau_{gelat.}$) and curing time (τ_{curing}) of the initial solution of p-PGF-MAA of 30.32:69.68 mass.% are 141 min and 207 min, respectively, whereas increasing the amount of the promoter to 0.25 % reduces the parameters under study to 14 min ($\tau_{gelat.}$) and 26 min (τ_{curing}): in the first case the curing time is rather long, while in the second case it is very short, which may cause significant difficulties during operation.

According to the data given in Table 2, the most suitable values of gelatinization and curing times of the p-PGF-MAA binary systems under consideration are 49 min and 78 min, respectively, which determines an optimal composition of initiating system in the amount of 1 % of initiator and 0.2 % of promoter (out of mass of initial solution of p-PGF in MAA).

The dependence of the effect of the amount of the DMA promoter on gelatinization time and curing time for the p-PGF-MAA binary system of the composition of 30.32:69.68 mass.% in the presence of the BPO initiator at 293 K is clearly presented in Fig. 2.

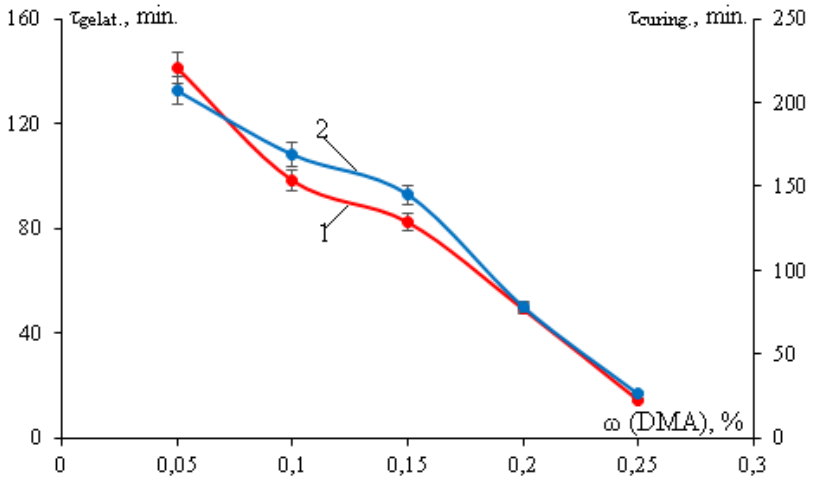

1 — the effect of the amount of the DMA promoter on gelatinization time of the solution of p-PGF in MAA;
2 — the effect of the amount of the DMA promoter on curing time of the solution of p-PGF in MAA

Figure 2. The effect of the amount of the DMA promoter on curing time of p-PGF-MAA in the presence of BPO at 293 K

To continue the research, a radical copolymerization reaction of initial solutions of p-PGF in MAA was performed at 293 K in the presence of a “cold” curing initiating system with a BPO content of 1 % and DMA of 0.2 % (of the mass of the initial curing solutions). Thus, a promoter DMA (0.2 %) was added to the studied p-PGF-MAA solutions of various mass ratios (Table 1) and the mixture was stirred until homogeneous mass was obtained. After that, the initiator was added with constant vigorous stirring for 1 min and then the gelatinization and curing times were determined according to ISO 57884-2017 [11] and ISO 2535-2017 [12].

Schematically the copolymerization process of p-PGF in MAA with the formation of three-dimensional cross-linked products is shown in Fig. 3.

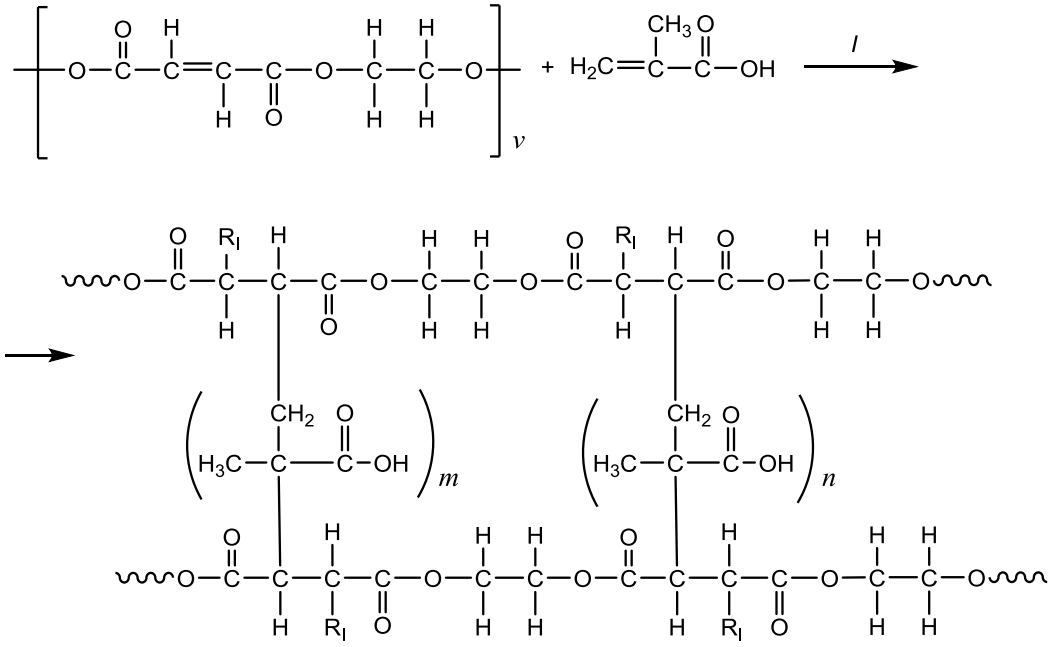

Figure 3. Scheme of p-PGF-MAA synthesis

Identification of the cured p-PGF-MAA binary systems with different mass ratios was carried out by analyzing the corresponding IR spectra. Figure 4 shows the IR spectrum of the solidified reaction product of p-PGF with MAA at the initial ratio of the co-reagents in the solution of 45.14:54.86 mass.%, respectively.

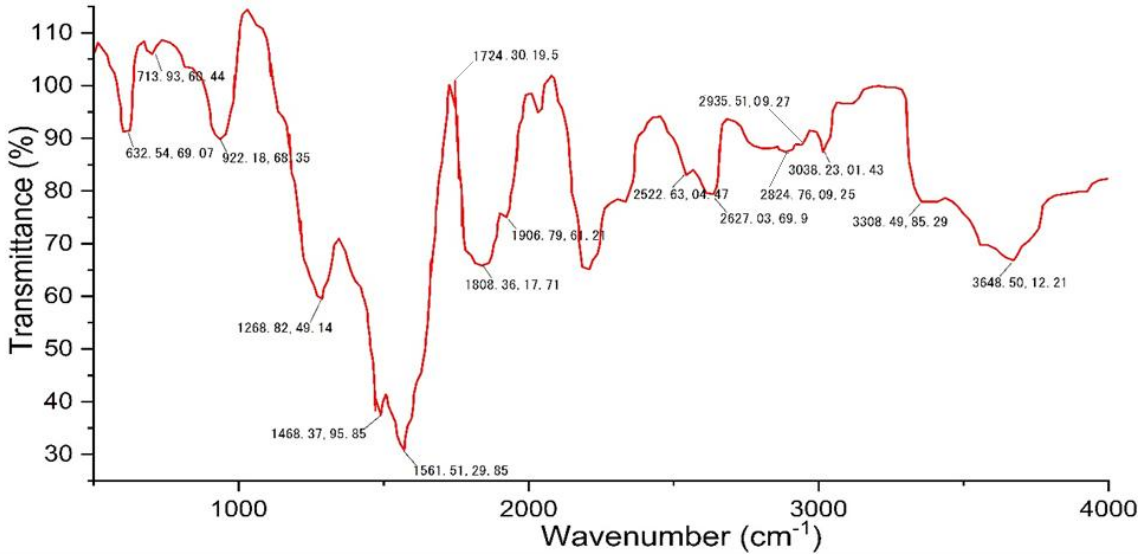

Figure 4. IR-spectra of the cured p-PGF-MAA system with an initial ratio of co-reagents in solution 45.14:54.86 mass. %

Hence, there are absorption bands in the 1720–1740 cm^{-1} (1724 cm^{-1}) and 3300-3600 cm^{-1} (3308 cm^{-1}) ranges in the IR spectra, which is a confirmation of the presence of –COOH groups. The presence of absorption bands at 2935 cm^{-1} is characteristic of MAA methylene groups. Also in the IR spectra there are characteristic stretching vibrations of ether groups C–O–C and –C=C– characteristic of fumarate (1268 and 1468 cm^{-1}) as well as C-H groups at 2824 cm^{-1}.

Further, Table 3 shows the data for determining the gelatinization time ($\tau_{gelat.}$) and curing time (τ_{curing}), as well as the densities of the obtained cured p-PGF-MAA products of different mass composition in the presence of the initial "cold" curing system (BPO 1 % and DMA 0.2 %).

Table 3

Dependence of kinetic curing parameters and properties of cured reaction products on the mass composition of p-PGF-MAA, BPO+DMA (1 % +0.2 %), T = 293 K

Composition of initial solutions, mass. %		Density (ρ), g/cm^3	Gelatinization time ($\tau_{gelat.}$), min.	Curing time (τ_{curing}), min.	Volume shrinkage, %
30.32	69.68	1.4485±0.074	49.15±1.87	78.17±3.28	10.1
34.96	65.04	1.4594±0.074	58.36±2.22	90.43±3.71	9.6
41.27	58.73	1.4802±0.075	68.04±2.59	102.08±4.19	10.1
45.14	54.86	1.4889±0.076	77.13±2.93	118.14±4.84	10.0

Therefore, analyzing the data obtained, it can be noted that with the increase of p-PGF content in the initial mixture the density value of the cured reaction product increases, hence, the gelatinization time (working life) and curing time increase. This dependence can be explained by comparing the activities of the initial co-reagents p-PGF and MAA. Thus, according to earlier studies [20], the copolymerization constant r_1 (p-PGF) in the p-PGF-MAA system is 0.72, and the constant r_2 (MAA) is 1.33. The obtained data correlate well with the studies of the copolymerization kinetics of the considered binary system at T = 333 K, which allowed to establish an inverse dependence of the reaction rate on the unsaturated polyester content in the initial polymer-monomer mixture.

Analyzing the data in Table 3, it should be noted that, despite the difference in gelatinization and curing time of solutions, this difference is not significant and varies in the range of 25-30 minutes.

According to the data in Table 3, we can conclude that the density of the cured product increases depending on the amount of p-PGF in it, which also correlates well with the indicators of the dynamic viscosity of the initial solutions. In particular, the highest value of dynamic viscosity was determined in the solution of p-PGF in MAA of 45.14:54.86 mass.% (with the maximum content of the first co-reagent — p-PGF) and was 213.7 mPa·s, which was characterized by the minimum curing rate.

Based on the obtained values of final product densities, the total volumetric shrinkage of the solutions of p-PGF in MAA during curing was calculated. So, a significant disadvantage of most polymeric materials is their high shrinkage during curing [23], which is characterized by a change in linear dimensions as a result of system curing and which causes a decrease in their adhesion strength. During the operation of sealants, this indicator becomes particularly important because of not only a decrease in the level of tightness of the seam during curing, but also the appearance of additional adhesions directly in places of contact of the sealing material with the product surface. In this regard, the permissible range of the value of the volume shrinkage indicator for sealants is 4–10 %.

Thus, the data presented in Table 3 indicate that the volume shrinkage values of the solutions of p-PGF in MAA during transition to the cured state are within the acceptable limits used for sealants. It should be taken into account that the cured products were obtained for the purpose of their use as a polymer base for the creation of filled sealant materials. Inclusion of fillers, plasticizers and other additives in polymer matrix contributes to significant reduction of volume shrinkage value of the final product, i.e. highly filled sealant, which will give an opportunity to obtain sealing material with low volume shrinkage, not exceeding 3 %.

Then, the dependence of gelatinization time ($\tau_{gelat.}$) and curing time (τ_{curing}) on the p-PGF content in the stock solution in the presence of the initiating system (BPO+DMA) at 293K was plotted based on the data in Table 3 (Fig. 5).

The surface morphology of the cured p-PGF-MAA binary systems of different mass composition was studied by scanning electron microscopy (Fig. 6). SEM image analysis (Fig. 6, b) shows some differences in surface morphology, i.e., a denser structure of the cured sample with the maximum p-PGF content was ob-

tained, while the SEM image of the sample with the lowest amount of unsaturated polyester has a more cellular structure (Fig. 6, a).

The figures show that the copolymers with a higher p-PGF content of 46.04:53.96 mass. % (in the right) are characterized by a denser structure, which correlates well with the results of dynamic viscosity and density of cured samples.

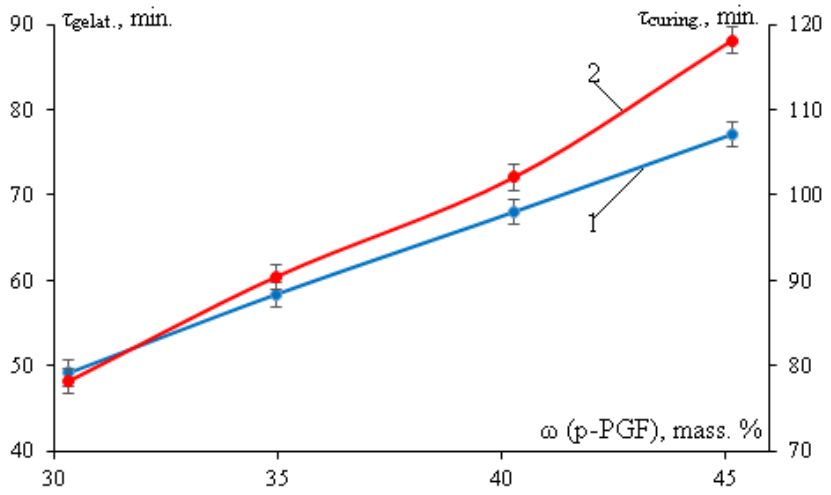

1 — the effect of p-PGF content on gelatinization time of the solution of p-PGF in MAA;
2 — the effect of p-PGF content on curing time of the solution of p-PGF in MAA.

Figure 5. Dependence of gelatinization and curing time on the content of p-PGF in the stock solution in the presence of BPO+DMA initiating system at 293 K

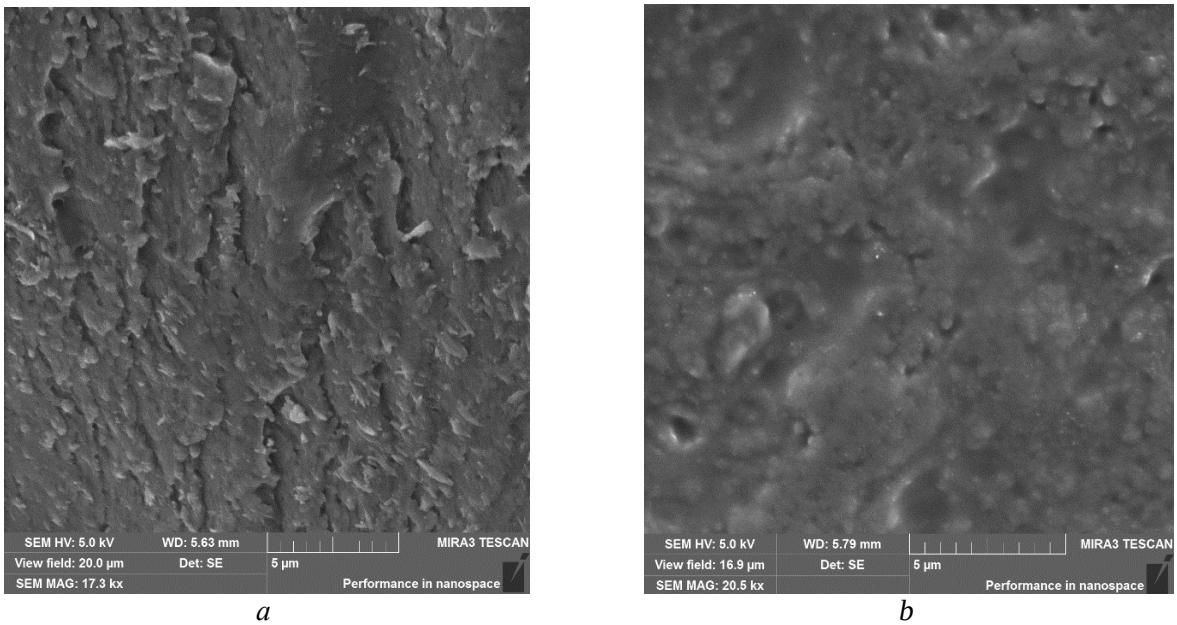

a *b*

Figure 6. SEM images of surfaces of cured samples of p-PGF-MAA of the following compositions: *a* — 30.32:69.68 mass. %; *b* — 45.14:55.86 mass. %

The established rheological and some other physico-chemical properties of the initial solutions of polypropylene glycol fumarate in methacrylic acid at different mass ratios of co-reagents and cured reaction products justify the prospects of using the considered p-PGF-MAA binary system as an adhesive polymer base. The study found that by varying the content of co-reagents in the initial solutions of polypropylene glycol fumarate in methacrylic acid, it is possible to control the rheological properties of the cured mixture and the kinetic parameters of the curing reaction. In particular, increasing the amount of p-PGF in the stock solution from 30.32 mass.% to 45.14 mass. % leads to a more than 4-fold increase in the dynamic viscosity index

from 48.2 mPa·s to 213.7 mPa·s. It should be noted that all the results obtained during the study correlate well with each other. Therefore, the values of the dynamic viscosity of the solutions of p-PGF in MAA of different mass composition are in good agreement with the values of the densities of both these initial solutions and the cured reaction products. The gelatinization time (lifetime) as well as curing time of the p-PGF-MAA binary system increased from 49 to 77 min. ($\tau_{gelat.}$) and from 78 to 118 min (τ_{curing}), respectively, when the amount of p-PGF in the stock solution was increased from 30.32 mass.% to 45.14 mass. %.

Analysis of IR-spectra and SEM images showed qualitative and quantitative "cold" curing of the solutions of p-PGF in MAA in the presence of BPO+DMA initiating system (1 % and 0.2 % by mass of the cured solution, respectively).

Conclusions

The optimized composition and concentrations of the components of the "cold" curing initiating system BPO+DMA (1 % and 0.2 % by mass of the curing solution, respectively) is the most energy-efficient for curing p-PGF-MAA solutions, not requiring additional reaction conditions (UV-emitter, high temperature, expensive catalysts, etc.). The resulting polymerization products can later be used as a polymer base for the production of filled sealing composites.

Acknowledgments

The work was carried out under the results-oriented budgeting of the Ministry of Science and Higher Education of RK № BR10965249 "Development of new sealants and adhesives based on unsaturated polyester resins for the construction and defense industries".

References

1 Lubis, M. A. R., Sari, F. P., Laksana, R. P. B., Fatriasari, W. & Hermiati, E. (2006). Ambient curable natural rubber latex adhesive cross-linked with polymeric isocyanate for bonding wood. *Polymer Bulletin, 79*(8). 6745–6757. https://doi.org/10.1007/s00289-021-03845-0

2 Sancaktar, E. (2011). *Constitutive Adhesive and Sealant Models* [Electronic resource]. Handbook of adhesion technology, 1–2. 553–595. https://doi:10.1007/978-3-642-01169-6_23

3 Chew, M. Y. L. & Zhou, X. (2002). Enhanced resistance of polyurethane sealants against cohesive failure under prolonged combination of water and heat. *Polymer Testing, 21*(2). 187-193. https://doi.org/10.1016/S0142-9418(01)00068-X

4 Zhang, J., Shen, H. Z., Zhang, X. & Li, H. Y. (2021). Experimental and theoretical investigation of mechanical behavior related to temperature, humidity and strain rate on silane-modified polyurethane sealant. *Polymer Testing, 103*(107370). https://doi.org/10.1016/j.polymertesting.2021.107370

5 Ma, J. T., Chen, S. S., Zhou. W. & Wang S. (2004). Effects on silicone sealant adhesion buildup on float glass substrates. *Durability of Building and Construction Sealants and Adhesives, 1453*. 97–112. https://doi.org/10.1520/stp12558s

6 Burkeyev, M. Zh., Tazhbayev, E. M. & Burkeyeva, G. K. (2016). *Nenasyshchennye poliefirnye smoly v reaktsiiakh radikalnoi sopolimerizatsii [Unsaturated polyesters in radical copolymerization reactions]* [Monograph]. Karaganda: NRIC «Parasat–M», 96 [in Russian].

7 Burkeyeva, G. K., Tazhbayev, Ye. M., Muslimova, D. M., Nurseiit, G. D. & Zhaparova, L. Zh. (2022). "Cold curing" of polyethylene glycol maleate with acrylic acid and some physicochemical properties of their solutions. *Bulletin of the University of Karaganda Chemistry, 106*(2). 25–31. https://doi.org/10.31489/2022Ch2/2-22-22

8 Burkeyev, M. Zh., Kovaleva, A. K., & Tazhbayev, E. M. (2018). Patent No. 33266 RK. Publ. C08G63/00, 8 [in Russian].

9 GOST 29226-91 (1991). *Zhidkostnye viskozimetry. Obshchie tekhnicheskie trebovaniia i metody ispytanii [Viscometers for liquids. General technical requirements and test methods]*. Moscow: IPK Publishing House of Standards, P. 12. https://docs.cntd.ru/document/1200023960 [in Russian].

10 GOST 18329-2014 (ISO 1675:1985). (2015). *Smoly i plastifikatory zhidkie. Metody opredeleniia plotnosti [Liquid resins and plasticizers. Methods for determining density]*. Moscow: Standart inform, 9. https://docs.cntd.ru/document/1200127491 [in Russian].

11 GOST 18616-80. (1980). *Plastmassy. Metod opredeleniia usadki [Plastics. Shrinkage determination method]*. Moscow: USSR State Committee of Standards, 20. https://docs.cntd.ru/document/1200020831 [in Russian].

12 GOST 22181-91 (ISO 2535:74). (1991). *Nenasyshchennye poliefirnye smoly. Metody opredeleniia vremeni zhelatinizatsii. [Unsaturated polyester resins. Methods for determining the time of gelatinization]*. Moscow: Committee of Standards, 20. https://docs.cntd.ru/document/1200020853 [in Russian].

13 GOST 22181-2015 (ISO 2535:2001) (2017). *Plastmassy — Nenasyshchennye poliefirnye smoly — Izmerenie vremeni geleobrazovaniia pri temperature okruzhaiushchei sredy [Plastics — Unsaturated polyester resins — Measurement of gel time at ambient temperature]*. Minsk: Eurasian Council for Standardization, Metrology and Certification, 15. http://standarts.nism.gov.kg/uploads/demo/pdf/bf20e738030a640ba87b4ade58d40f5d.pdf [in Russian].

14 Brostow, W. & Glass N. M. (2003). Cure progress in epoxy systems: dependence on temperature and time. *Materials Research Innovation, 7*(3). 125–132. https://doi.org/10.1007/s10019-002-0222-2

15 Eichhoff, U. & Simon, A. (2004). Dynamic infrared spectroscopy with a step-scan FT-IR for the characterization of polymers. *XVI international conference on spectroscopy of molecules and crystals, 5507*. 396–402. https://doi.org/10.1117/12.570020

16 Osterberg, M. & Khursheed, A. (2008). Initial results on the spectroscopic SEM concept. *Physics Procedia, 1*(1). 529–535. https://doi.org/10.1016/j.phpro.2008.07.135

17 Anoop, V., Sankaraiah, S., Chakraborty, S. & Mary N. L. (2022). Enhanced mechanical, thermal and adhesion properties of addition cured polydimethylsiloxane nanocomposite adhesives. *International Journal of Adhesion and Adhesives, 117*. 666–674. https://doi.org/10.1016/j.ijadhadh.2022.103177

18 Dal Lago, B., Biondini, F., Toniolo, G. & Lamperti-Tornaghi, M. (2017). Experimental investigation on the influence of silicone sealant on the seismic behaviour of precast facades. *Bulletin of Earthquake Engineering, 15*(4). 1771–1781. https://doi.org/10.1007/s10518-016-0045-y

19 Hutchinson, A. R. &Iglauer, S. (2006). Adhesion of construction sealants to polymer foam backer rod used in building construction. *International Journal of Adhesion and Adhesives, 26*(7). 555–566. https://doi.org/10.1016/j.ijadhadh.2005.09.001

20 Kovaleva, A. K., Burkeyeva, G. K., Tazhbayev, Ye. M., Muslimova, D. M. (2022). Issledovanie reaktsii radikalnoi sopolimerizatsii nenasyshchennykh poliefirov s akrilovoi kislotoi [Study of radical copolymerization reaction of unsaturated polyesters with acrylic acid]. *Himicheskii Zhurnal Kazakhstana — Chemical Journal of Kazakhstan, 79*(3). 130–140. https://doi.org/10.51580/2022-3/2710-1185.86 [in Russian].

21 Rusu, M. C., Block, C., Van-Assche, G. & Van-Mele B. (2012). Influence of temperature and UV intensity on photopolymerization reaction studied by photo-DSC. *Journal of Thermal Analysis and Calorimetry, 110*(1). 287–294. https://doi.org/10.1007/s10973-012-2465-5

22 Burkeev, M. Zh., Magzumova, A. K., Tazhbaev, E. M., Burkeeva, G. K., Kovaleva, A. K., Khamitova, T. O., & Mataev, M. M. (2013). Effect of external factors on the swelling of hydrogels based on poly(ethylene glycol) maleate with some vinyl monomers. *Russian Journal of Applied Chemistry, 86*(1). 63–68. https://doi.org/10.1134/s1070427213010114

23 Comyn, J. (2006). Adhesives and sealants: general knowledge, application techniques, new curing techniques. *Handbook of Adhesives and Sealants, 2*, 1–50. https://doi.org/10.1016/s1874-5695(06)x8001-6

24 Verner, D. (2011). Modifikatsiia reologicheskikh kharakteristik polisulfidnykh germetikov s pomoshchiu funktsionalnykh napolnitelei Hakuenka [Modifying the Rheological Characteristics of Polysulfide Sealants Using Hakuenka Functional Fillers]. *Lakokrasochnaia promyshlennost — Paint industry, 10*, 31–34 [in Russian].

25 Sharma, A. K., Kumar, R., Canteenwala, T. C., Parmar, V. S., Patkar, S., Kumar, J. & Watterson, A. C. (2005). Biocatalytic synthesis and characterization of copolymers based on poly(ethylene glycol) and unsaturated methyl esters. *Journal of Macromolecular Science-Pure and Applied Chemistry, A42*(11). 1515–1521. https://doi.org/10.1080/10601320500229061

Information about authors*

Burkeyeva, Gulsym Kabayevna — PhD, Associate Professor of Chemical Sciences, Karagandy University of the name of academician E.A. Buketov, Universitetskaya street, 28, 100024, Karaganda, Kazakhstan; e-mail: guls_b@mail.ru; https://orcid.org/0000-0003-1993-7648;

Kovaleva, Anna Konstantinovna — PhD, Senior Researcher, Karagandy University of the name of academician E.A. Buketov, Universitetskaya street, 28, 100024, Karaganda, Kazakhstan; e-mail: cherry-girl1899@mail.ru; https://orcid.org/0000-0001-9758-648X;

Tazhbayev, Yerkeblan Muratovich — Doctor of Chemical Sciences, Professor, Karagandy University of the name of academician E.A. Buketov, Universitetskaya street, 28, 100024, Karaganda, Kazakhstan; e-mail: tazhbaev@mail.ru; https://orcid.org/0000-0003-4828-2521;

Ibrayeva, Zhansaya Mirkhankyzy – Doctoral student of 1st year; Karagandy University of the name of academician E.A. Buketov, Universitetskaya street, 28, 100024, Karaganda, Kazakhstan; e-mail: zhansaya.ibraieva@mail.ru; https://orcid.org/0000-0002-1419-1384;

Plocek, Jiri — PhD, CSc. Institute of Inorganic Chemistry of the Czech Academy of Sciences, Czech Republic, Husinec-Rez 1001 25068 Rez; e-mail: plocek@iic.cas.cz; https://orcid.org/0000-0001-6082-5766

*The author's name is presented in the order: *Last Name, First and Middle Names*

How to Cite: Tulasi, S.L., Sumalatha, P., Rani, N.U., Peddi, P. (2023) Green Synthesis, Characterization and Environmental Application of Copper Oxide Nanoparticle obtained Using Aqueous Extract of *Schrebera Swietenioides Roxb*. *Eurasian Journal of Chemistry, 109(1), 78-89.* https://doi.org/10.31489/2959-0663/1-23-2

Article

Received: 24 November 2022 | Revised: 26 January 2023 | Accepted: 07 February 2023 | Published online: 06 March 2023

UDC 54.057; 542.8

https://doi.org/10.31489/2959-0663/1-23-2

S. Lakshmi Tulasi[*1], P. Sumalatha [2], N. Usha Rani[1], Pavani Peddi[1]

[1]*PVP Siddhartha Institute of Technology, Kanuru, Vijayawada, Andhra Pradesh, India;*
[2]*Seshadri Rao Gudlavalleru Engineering college, Gudlavalleru. Andhra Pradesh, India*
*(*Corresponding author's e-mail: tulasi13111986@gmail.com)*

Green Synthesis, Characterization and Environmental Application of Copper Oxide Nanoparticle obtained Using Aqueous Extract of *Schrebera Swietenioides Roxb.*

The goal of the present study was to synthesize the nanoparticles using green methodology with the use of the aqueous plant extract of *S. swietenioides*. The copper oxide nanoparticle has been synthesized using aqueous root extract of *S. swietenioides* as a green reducing agent and copper sulfate as source of the metal ions. Formation of the nanoparticles in the reaction mixture was preliminary confirmed by the UV-Vis spectroscopy method. The FT-IR analysis of the synthesized nanoparticles shows the involvement of various bioactive functional groups in the formation of nanoparticles. The UV–Vis absorption spectra indicate the characteristic maximum absorption peak at a wavelength of 340 nm. This confirms the formation of nano-sized copper particles. The SEM analysis of the synthesized copper oxide nanoparticles confirms that the particles have mostly spherical shape with rough surfaces and the size of 21-43 nm. The copper nanoparticles in the media of the aqueous root extract of *S swietenioides* have been studied for their applications in the photo catalytic reduction of pollutant dyes and metals. The synthesized nanoparticles have been characterized and it was proved that the particles were nano-sized and contained high metal percentage.

Keywords: green synthesis, plant extract, *S. Swietenioides*, copper oxide nanoparticle, UV–visible spectrophotometer, FT-IR, SEM, Photo catalytic activity.

Introduction

Plants are considered as cost-efficient and eco-friendly chemical reagents. Plants act as potential heavy metal detoxificants and are being to overcome the problems caused by various environmental pollutants. These pollutants are very toxic even at the trace levels [1]. The synthesis of NPs using plant extracts considered as clean and environmentally accepted "green chemistry" concept [2].

The synthesis of NPs using plant extracts has considerable advantage on the synthesis with the use of microorganisms due to the complex preservation process of the microbial strains as well as contamination-free maintenance of the culture [3]. The kinetics of the NPs synthesis using plant extracts was higher than in the other green synthesis approaches and equal to the NPs synthesis using chemical methods. The different parts of the plant such as seeds, fruits, leaves, stem, bark, roots etc., are widely used in the synthesis of NPs due to the excellent phytochemicals they produce [4]. A wide range of metal NPs, such as silver, gold, iron, zinc, copper etc. have been synthesized using green approach.

Plant extracts are widely used in the synthesis of CuO NPs nowadays. The synthesis of CuO NPs using plant extracts involves simple, convenient and easy procedure with low energy consumption that produces more stable NPs. During the synthesis of CuO NPs by green methodology, cupric acetate, copper chloride dihydrate, and copper sulphate pentahydrate were generally used as metal ions source [5]. In the process of synthesis and storage of copper NPs, copper tends to oxidize easily and hence stabilizing or capping agent is needed for preventing oxidation and agglomeration. Various properties of NPs such as light absorption, surface morphology, size, shape, crystalline nature etc., were characterized using various techniques. The diverse properties of the NPs were greatly influenced by their shape which was determined by the microscopy techniques. The morphology, surface information and dispersion of the NPs were determined with scanning electron microscope (SEM). Formation of the nanoparticles in the reaction mixture was preliminary confirmed by the UV-Vis spectroscopy method. The UV-vis absorption spectra shows the characteristic maximum absorption peak at a wavelength of 379 nm, which confirms that the nanoparticles are mono-dispersed and narrow in size. The copper and CuO NPs are multifunctional in nature and hence are having wide range

of applications in varies field. The photo catalytic activity of the copper nanoparticles in the media of the aqueous root extract of *S swietenioides* were determined using different pollutant, carcinogenic dyes and heavy metals. The copper nanoparticles in the media of the aqueous root extract of *S swietenioides* were studied for their photo catalytic degradation efficiency on pollutant dyes (sudan red (III) and azure A) and pollutant metal lead. These NPs were applied as antimicrobial agents, photo catalytic agent for degradation of pollutants, anticarcinogenic agent and were used in the formation of biofilms [6, 7]. These NPs can be successfully applied for the improvement of agriculture [8, 9] and food packaging.

Experimental

Chemicals and reagents:

The chemicals used in the study such as copper sulphate pentahydrate, sodium hydroxide, hydrogen peroxide, dibasic disodium phosphate, monobasic sodium di-hydrogen phosphate, sudan red dye, azure A dye, lead nitrate were of analytical reagent grade and were purchased from Merck chemicals and SD fisher scientific, Mumbai.

Collection of plant material:

The roots of the plant *Schrebera swietenioides* Roxb., were collected in the hill area located in Tirumala, Tirupati, Andhra Pradesh. The collected plant sample was authenticated by Dr.Ch. Srinivasa Reddy, Assistant Professor, Department of Botany, SRR & CVR Government Degree College (A) Vijayawada with plant authentication number SRR-CVR/ 2019-20/Bot/31. The collected roots surface was cleaned using sterile cotton and distilled water in order to remove the sand and dirt. Then the water particles on the cleaned material were removed using tissue paper and the plant material was cut onto the small pieces, which were dried up under the shade and preserved.

Extractions of plant materials:

An accurately weighed 10 grams of plant powder was put in a 250 mL beaker containing 100 mL of double distilled water. The plant material with water was boiled on a hot plate at 40 °C for 80 min. The phytochemical constituents present in the plant material were extracted to the water solvent. Then the extract was filtered, the plant material obtained as sediment was discarded and the clear filtrate was made up to 100 mL with distilled water. The clear filtrate obtained was used for the synthesis of nanoparticles [10].

Root Extract Mediated Copper oxide Nanoparticles:

The synthesis of copper oxide nanoparticles using aqueous root extract of *S swietenioides* was carried based on the methodology [11] with minor modifications. After the addition of the 400 mL of 5 mM copper sulphate and 50 mL of aqueous root extract into the 500 mL volumetric flask, the pH of the solution was adjusted to 7 with the 1N sodium hydroxide solution. The change in the colour of the reaction mixture and the formation of particles was observed as an indication of the formation of copper nanoparticles. Then it was centrifuged, supernatant was discarded and precipitate was collected carefully. Residual plant extract was removed by washing the precipitate with excess distilled water. The purified precipitate was collected and dried at 60 °C for 2 h in a hot air oven. Dark brown colour copper nanoparticles were obtained and characterized (Fig. 1).

Copper sulphate | Plant extract | Formation of nanoparticles

Figure 1. Colour changing observed during the synthesis of copper oxide nanoparticles

Characterization of nanoparticles:

The synthesized copper nanoparticles were characterized using various characterization techniques such as UV-vis spectroscopy (JASCO spectrometer, Japan), FT-IR(Bruker, USA), SEM (NOVA NANOSEM450, FEI USA), XRD(Rigaku Corporation, Japan). The size, shape, surface morphology, functional groups and chemical composition of the copper nanoparticles in the media of the aqueous root extract of *S swietenioides* were also determined [12, 13].

Photo catalytic activity of nanoparticles:

The photo catalytic activity of the copper nanoparticles in the media of the aqueous root extract of *S swietenioides* were determined using different pollutant, carcinogenic dyes and heavy metals. Copper nanoparticles in the media of the aqueous root extract of *S swietenioides* were studied for their photo catalytic degradation efficiency on pollutant dyes (sudan red (III) and azure A) and pollutant metal lead [14–16].

UV-visible spectrophotometer:

The UV-vis spectroscopy analysis of the colour change observed during the addition of aqueous root extract of *S. swietenioides* and copper metal solution was carried out. The UV–Vis absorption spectra shows the characteristic maximum absorption peak at a wavelength of 340 nm. This confirms the formation of nano-sized copper particles [17]. The similar type of absorption peak was not identified in the absorption spectra of plant root extract as well as the aqueous copper metal solution. Hence it can be confirmed the characteristic wavelength maximum is due to the formation of copper oxide nanoparticles. Figure 2 shows the absorption spectra of synthesized copper oxide nanoparticles.

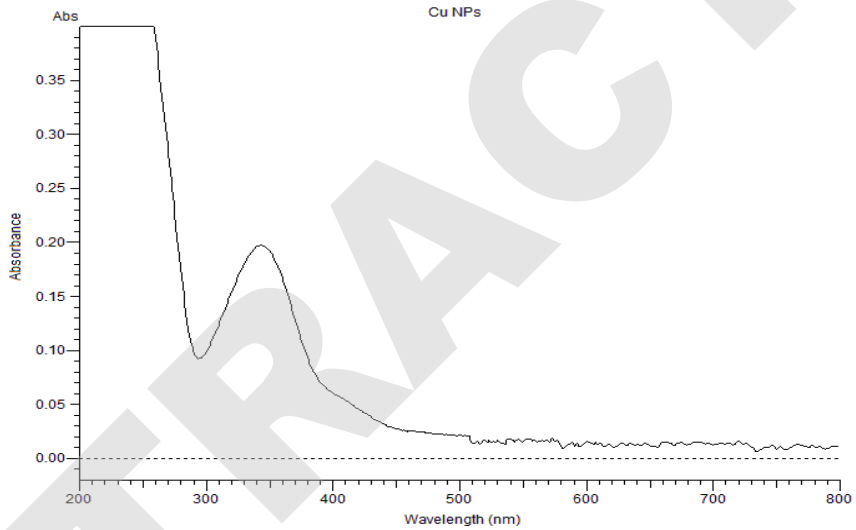

Figure 2. UV-visible absorption spectra of copper oxide nanoparticles

FT-IR analysis of synthesized nanoparticles:

The FT-IR analysis of the copper nanoparticles in the media of the aqueous root extract of *S swietenioides* was conducted in order to identify the bioactive functional groups in the root extract that are responsible for the reduction of metallic copper to the copper oxide nanoparticles. The FT-IR spectrum is given in Figure 3 and the functional groups that were identified by the FT-IR are given in Table 1.

Table 1

Bioactive functional groups identified by the FT-IR spectrum

S No	Absorption, cm^{-1}	Functional group
1	3667 & 3616	O-H bond in free and intermolecular bonded alcohols
2	3500	N-H bond in primary amines
3	3395	O-H bond in carboxylic acid
4	3330	N-H bond in aliphatic primary amines
5	1655	C-H bond in aromatic compounds
6	1317	C-O bond in aromatic esters

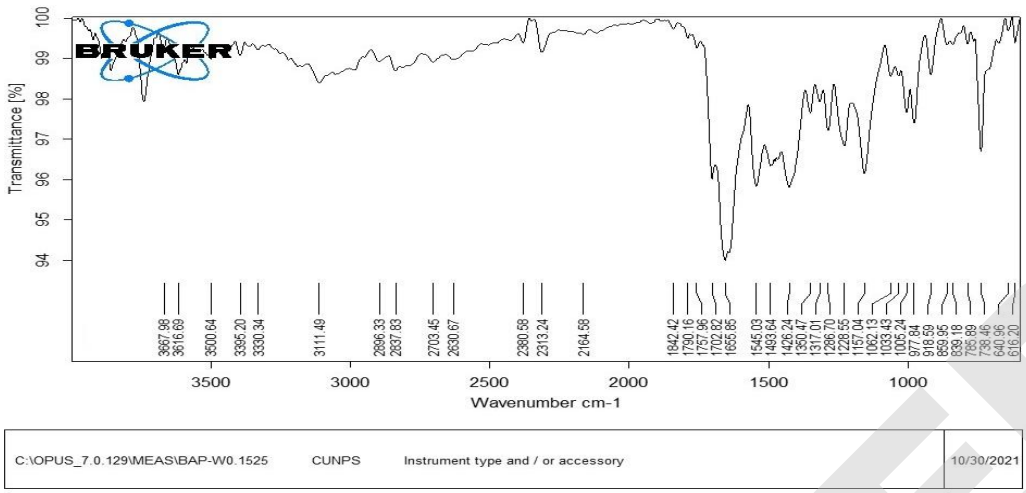

Figure 3. FT-IR spectrum of copper oxide nanoparticles synthesized using aqueous root extract of *S. swietenioides*

The functional groups determined by the FT-IR analysis of copper oxide nanoparticles were in correlation with the phytochemical solvent extracts of *S swietenioides* leaves. Hence the results confirm the involvement of the plant based biomolecules in the formed nanoparticles.

SEM analysis:

The SEM analysis was performed to determine the size and shape of the copper oxide nanoparticles synthesized using aqueous root extract of *S swietenioides*. The SEM analysis of the copper nanoparticles in the media of the aqueous root extract of *S swietenioides* gives the information about their shape and the size. The FE-SEM analysis was conducted to determine the morphology of Cu NPs. Analysis results are given in Figure 4. The particles were observed to be aggregates with spherical shape and some of them were undefined shape nanoparticles.

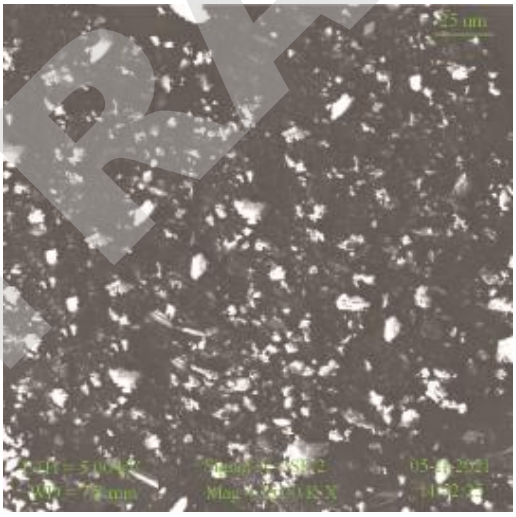

Figure 4. SEM micrograph of the copper nanoparticles in the media of the aqueous root extract of *S swietenioides*

TEM analysis:

TEM is the perfect analytical tool for the chemical and structural characterization of the nano-scale materials. Diffraction, imaging and micro analytical information was obtained from the TEM analysis. The combination of these results describes the behaviour of the nano-sized and nanostructured materials. Thus, TEM analysis of the copper oxide nanoparticles synthesized using aqueous leaf and root extract of *S swietenioides* was carried out.

The TEM analysis of the copper nanoparticles in the media of the aqueous root extract of *S swietenioides* confirms the synthesized nanoparticles were spherical shape. The surface of the individual particle was also studied and it was confirmed the surface of the nanoparticles is smooth. The average parti-

cle size was observed to be 75 nm. The size of the nanoparticles was distributed broadly in the range of 20-95 nm. The result achieved in the TEM analysis was in correlation with the results reported for the same sample in SEM. The TEM micrograph observed for the synthesized copper oxide nanoparticles is given in Figure 5

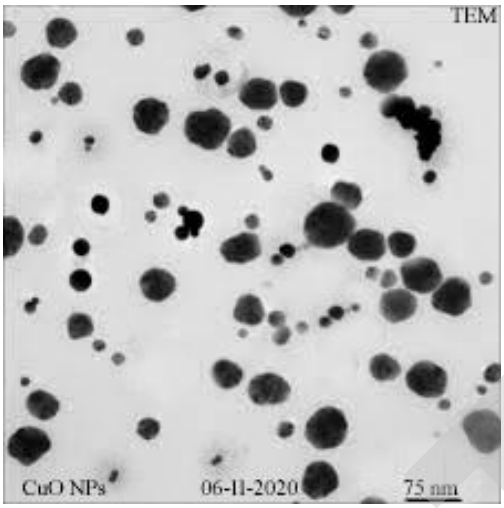

Figure 5. TEM micrograph of the the copper nanoparticles in the media of the aqueous root extract of S swietenioides

XRD analysis:

The lattice phase, crystalline structure, crystalline particle size and crystal lattice parameters of the synthesized nanoparticles were determined by the XRD analysis. Scherrer equation was used for the calculation of the lattice parameters of nanoparticles. The XRD analysis of the copper oxide nanoparticles synthesized using aqueous root extract of *S swietenioides* was carried out.

The XRD spectra of the copper oxide nanoparticles synthesized using aqueous root extract of *S swietenioides* shows the 2θ characteristic peaks corresponds to planes as same as the crystal lattice structure. The peaks identified at 2θ value of 16.38°, 32.15°, 39.81°, 49.87° and 53.20°, which corresponds to (110), (111), (220), (800) and (713) planes of the crystal lattice. Identified peaks and their corresponding planes confirm that the nanoparticles are in monoclinic configuration and their identified planes are in good correlation with the JCPDS standard card number 89-5899. The Scherrer formula ($D = 0.9\ \lambda/\beta \cos\theta$, where β = full width at half maximum at the θ angle and λ = wavelength) was used in calculation of the average crystalline size of the CuNPs and obtained results were at 32±4 nm on the (111) plane. The results achieved in the XRD analysis for the copper oxide nanoparticles synthesized in the study were in good correlation with the results achieved for the same sample in SEM and TEM analysis. The XRD spectra of the copper oxide nanoparticles synthesized in the study is given in Figure 6.

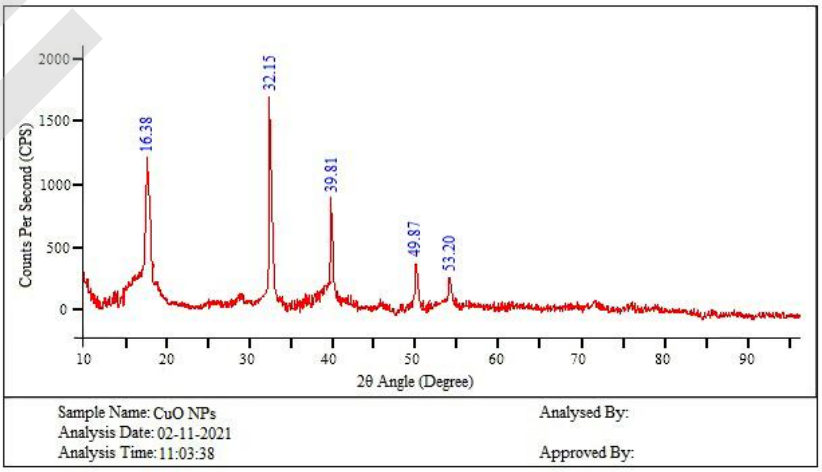

Figure 6. XRD spectrum of the copper nanoparticles in the media of the aqueous root extract of S *swietenioides*

Results and Discussion

Photo catalytic Reduction of Sudan Red (III) Dye Using Copper Oxide Nanoparticles:

The reduction study was performed at various strengths of nano-catalyst and at optimized 10 ppm concentration of Sudan red dye. The result confirms that dose dependent catalytic activity was observed and the reduction activity was increased with the growth in dose of the nano-catalyst. The reduction efficiency was also observed to be increasing with increase in contact time. The reduction efficiency was observed to be high in the initial time of the study and maximum reduction was completed within 45 min of time. The % of reduction at the contact time of 45 min was observed to be 61.23±0.060, 54.28±0.153, 38.13±0.028 and 20.50±0.036 % respectively at nano-catalyst dose of 1.0, 0.75, 0.50 and 0.25 g/L. The reduction time was increased up to 2 h and at the longest studied time the % of reduction was observed to be 84.22±0.051, 79.83±0.062, 54.54±0.576 and 44.44±0.071 respectively at nano-catalyst dose of 1.0, 0.75, 0.50 and 0.25 g/L. Table 2 shows the reduction study of sudan red at various strengths of *S swietenioides* mediated copper oxide nanoparticles and its comparison graph is shown in Figure 7. Comparative UV-visible absorption spectra before and after treatment of Sudan red solution with nanoparticles are presented in Figure 8.

Table 2

Reduction study of Sudan red at various strengths of *S swietenioides* mediated copper oxide nanoparticles

S No	Time in min	% of Sudan red reduction at nano-catalyst strength of			
		0.25 g/L	0.50 g/L	0.75 g/L	1.0 g/L
1	15	17.19±0.060	18.26±0.042	26.86±0.061	29.52±0.071
2	30	21.44±0.031	27.45±0.020	43.09±0.053	54.23±0.067
3	45	39.32±0.065	42.65±0.029	59.64±0.059	69.71±0.025
4	60	42.10±0.042	48.26±0.035	76.19±0.053	81.11±0.044
5	75	43.23±0.038	53.63±0.026	76.90±0.042	82.28±0.075
6	90	43.96±0.070	54.24±0.042	78.49±0.074	82.72±0.040
7	105	44.14±0.062	54.95±0.025	79.18±0.057	83.10±0.075
8	120	44.44±0.071	54.54±0.576	79.83±0.062	84.22±0.051

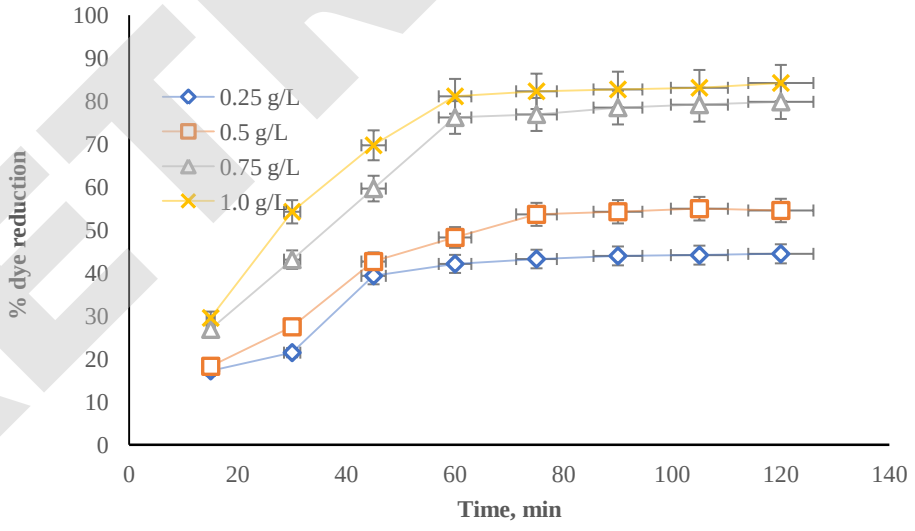

Figure 7. Comparative reduction study results of Sudan red at various strengths of *S swietenioides* mediated copper oxide nanoparticles

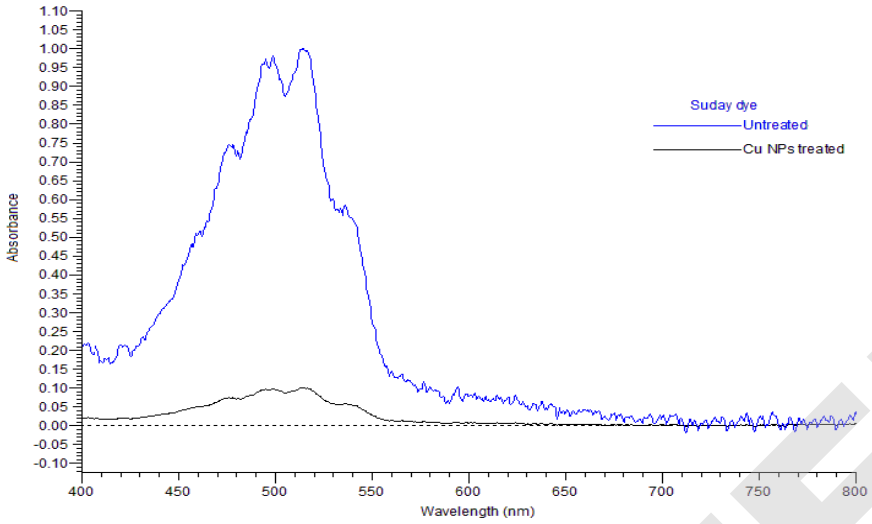

Figure 8. Comparative UV-visible absorption spectra before and after treatment of Sudan red solution with nanoparticles

The rate constant of the catalytic degradation of Sudan red using the synthesized copper oxide nanoparticles was calculated by plotting the graph with the time of reduction study in minutes on *x-axis* and $\ln(A_0/A_t)$ on the *y*-axis. The results confirm that the degradation of Sudan red using copper oxide nanoparticles follows the pseudo first order reaction mechanism for all the doses of nano-catalyst studied. The rate constant (k) of the studied strengths of nanoparticles was calculated and the k was obtained as 1.37×10^{-2}, 1.27×10^{-2}, 5.85×10^{-3} and 3.77×10^{-3} for the reduction using the nanoparticles at 1.0, 0.75, 0.5 and 0.25 g/L strength respectively. The degradation time profile of treatment of Sudan red solution with copper oxide nanoparticles is given in Figure 9.

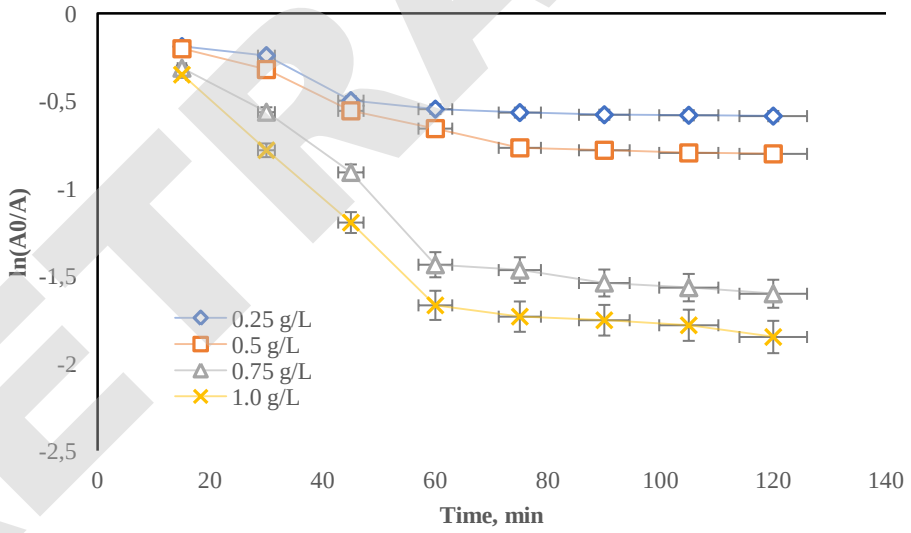

Figure 9. Photo degradation time profile of A_t/A_0 for sudan red dye

Photo Catalytic Reduction of Azure A Dye Using Copper Oxide Nanoparticles:

The reduction study was performed at various strengths of nano-catalyst and at optimized 50 ppm concentration of Azure A dye. The result confirms that dose dependent catalytic activity was observed and the reduction activity was raised with an increase in dose of the nano-catalyst [18]. The reduction efficiency was also observed to be growing with an increase in contact time. The reduction efficiency was observed to be high in the initial time of the study and maximum reduction was completed within 45 min of time. The % of reduction at the contact of 45 min was observed to be 64.00±0.566, 46.71±0.020, 34.24±0.026 and

29.32±0.050 % respectively at nano-catalyst dose of 1.0, 0.75, 0.50 and 0.25 g/L. The reduction time was increased up to 2 h and at the longest studied time the % of reduction was observed to be 81.62±0.663, 80.65±0.040, 60.54±0.032 and 39.70±0.044 respectively at nano-catalyst dose of 1.0, 0.75, 0.50 and 0.25 g/L. Table 3 shows the reduction study of azure A at various strengths of *S swietenioides* mediated copper oxide nanoparticles and its comparison graph is shown in Figure 10. Comparative UV-visible absorption spectra before and after treatment of Azure A solution with nanoparticles are presented in Figure 11.

T a b l e 3

Reduction study of Azure A at various strengths of *S swietenioides* mediated copper oxide nanoparticles

S No	Time in min	% of Azure A reduction at nano-catalyst strength of			
		0.25 g/L	0.50 g/L	0.75 g/L	1.0 g/L
1	15	8.24±0.031	9.67±0.060	17.35±0.035	38.40±4.505
2	30	15.35±0.049	21.62±0.036	35.13±0.057	49.76±0.451
3	45	29.32±0.050	34.24±0.026	46.71±0.020	64.00±0.566
4	60	36.81±0.040	41.11±0.025	69.43±0.020	73.38±0.606
5	75	37.12±0.031	58.71±0.084	78.35±0.023	79.36±0.636
6	90	38.18±0.040	59.24±0.042	79.67±0.060	80.08±0.678
7	105	39.15±0.072	59.86±0.050	80.12±0.030	80.93±0.655
8	120	39.70±0.044	60.54±0.032	80.65±0.040	81.62±0.663

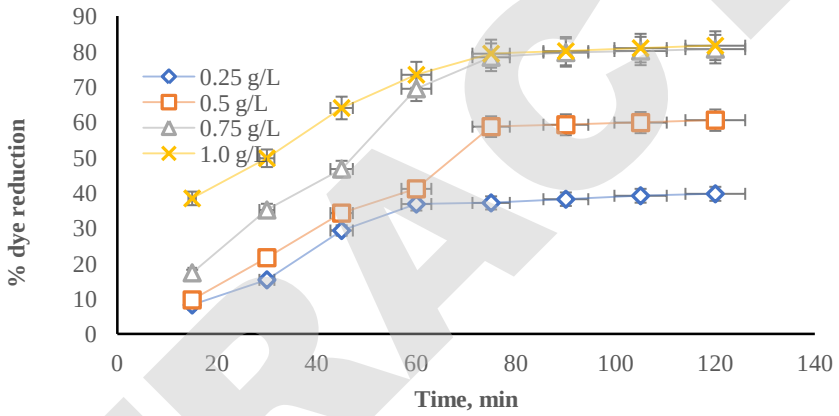

Figure 10. Comparative reduction study results of Azure A at various strengths of *S swietenioides* mediated copper oxide nanoparticles

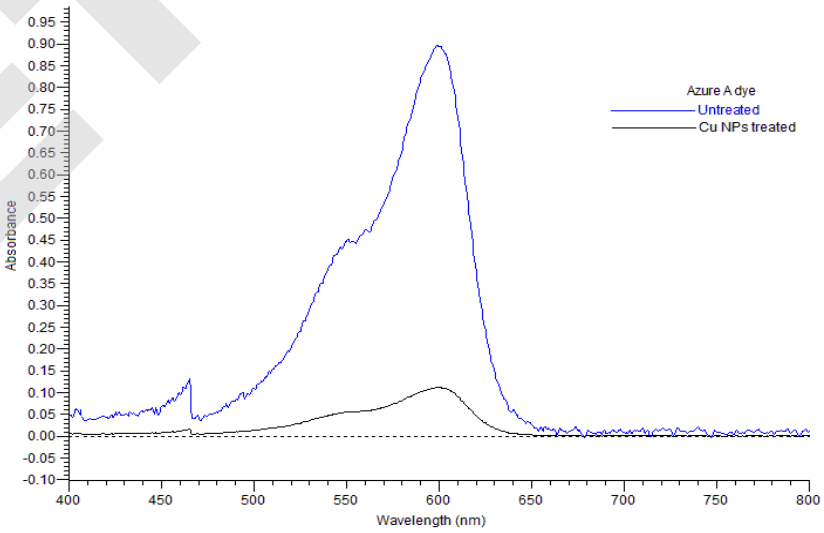

Figure 11. Comparative UV-visible absorption spectra before and after treatment of Azure A solution with nanoparticles

The rate constant of the catalytic degradation of Sudan red using the synthesized copper oxide nanoparticles was calculated by plotting the graph with the time of reduction study in minutes on *x-axis* and $\ln(A_0/A_t)$ on the *y*-axis. The results confirm that the degradation of Sudan red using copper oxide nanoparticles follows the pseudo first order reaction mechanism for all the doses of nano-catalyst studied. The rate constant (*k*) of the studied strengths of nanoparticles was calculated and the *k* was obtained as 1.28×10^{-2}, 1.53×10^{-2}, 8.69×10^{-3} and 3.96×10^{-3} for the reduction using the nanoparticles at 1.0, 0.75, 0.5 and 0.25 g/L strength respectively. The degradation time profile of treatment of Azure A solution with copper oxide nanoparticles is given in Figure 12.

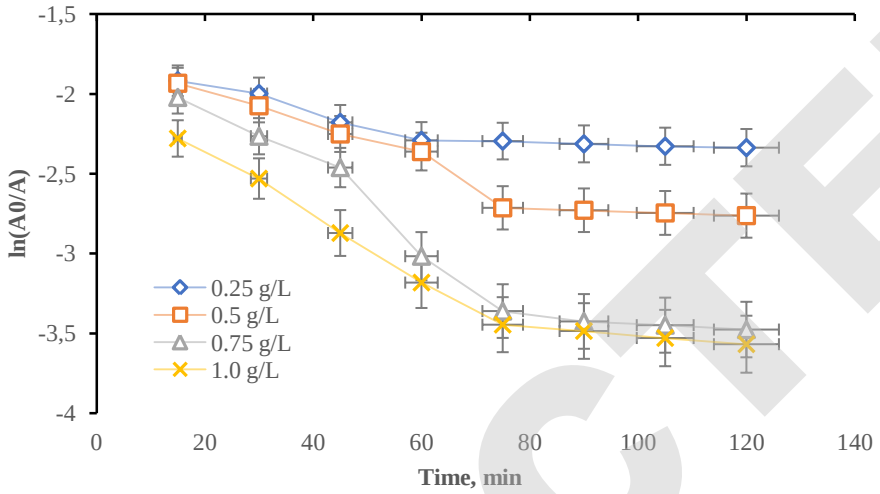

Figure 12. Photo degradation time profile of A_t/A_0 for azure A dye

Photo catalytic Reduction of Lead Metal Using Copper Oxide Nanoparticles:

The reduction study was performed at various strengths of nano-catalyst and at optimized 50 µg/mL concentration of lead metal. The result confirms that dose dependent catalytic activity was observed and the reduction activity was raised with an increase in dose of the nano-catalyst [19]. The reduction efficiency was also observed to be increasing with an increase in contact time. More than 50 % of the reduction was observed within the time of 45 min at a nano catalyst-dose of 0.75 and 1.0 g/L and the observed degradation was at 54.28±0.153 and 61.23±0.060 % respectively. The reduction time was increased up to 2 h and at the longest studied time the % of reduction was observed to be 88.94±0.026, 81.02±0.127, 66.15±0.023 and 39.60±0.048 % respectively at nano-catalyst dose of 1.0, 0.75, 0.50 and 0.25 g/L. Table 4 shows the reduction study of lead metal at various strengths of *S swietenioides* aqueous root extracts mediated copper oxide nanoparticles and its comparison graph is shown in Figure 13. The comparative UV-vis absorption spectra obtained for before and after treatment of lead — dithizone complex solution with nanoparticles are given in Figure 14.

Table 4

Reduction study of lead metal at various strengths of *S swietenioides* mediated copper oxide nanoparticles

S No	Time in min	% of lead reduction at Nano catalyst strength of			
		0.25 g/L	0.50 g/L	0.75 g/L	1.0 g/L
1	15	8.04±0.016	13.46±0.055	20.77±0.062	24.48±0.076
2	30	13.73±0.026	27.22±0.041	34.82±0.039	39.18±0.540
3	45	20.50±0.036	38.13±0.028	54.28±0.153	61.23±0.060
4	60	29.91±0.029	51.59±0.070	73.11±0.088	82.45±0.059
5	75	36.24±0.039	64.98±0.055	78.57±0.039	87.60±0.061
6	90	38.06±0.023	65.35±0.032	79.62±0.129	85.86±4.027
7	105	39.07±0.024	65.50±0.044	80.20±0.098	88.72±0.046
8	120	39.60±0.048	66.15±0.023	81.02±0.127	88.94±0.026

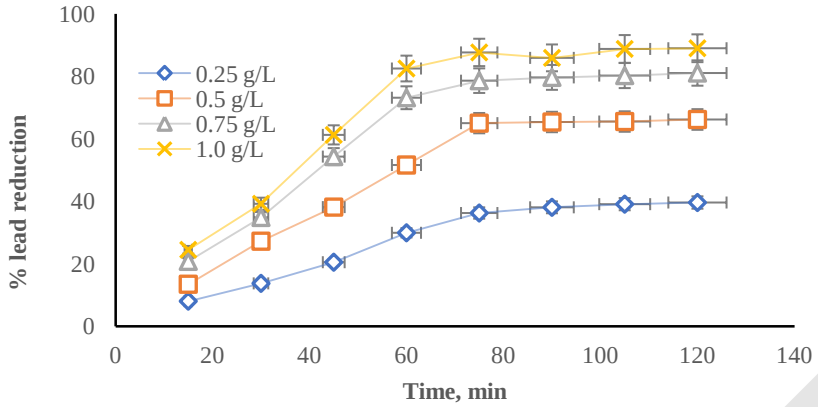

Figure 13. Comparative reduction study results of lead metal at various strengths of *S swietenioides* mediated copper oxide nanoparticle

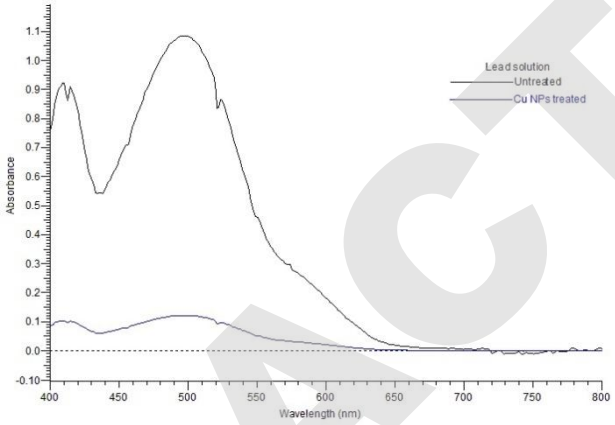

Figure 14. Comparative UV visible absorption spectra before and after treatment of lead – dithizone complex solution with nanoparticles

The rate constant of the catalytic degradation of lead metal using the synthesized copper oxide nanoparticles was calculated by plotting the graph with the time of reduction study in minutes on *x-axis* and $\ln(A_0/A_t)$ on the *y*-axis. The results confirm that the degradation of Sudan red using copper oxide nanoparticles follows the pseudo first order reaction mechanism for all the doses of nano-catalyst studied. The rate constant (k) of the studied strengths of nanoparticles was calculated and the k was obtained as 2.04×10^{-2}, 1.47×10^{-2}, 9.80×10^{-3} and 4.38×10^{-3} for the reduction using the nanoparticles at 1.0, 0.75, 0.5 and 0.25 g/L strength respectively. The degradation time profile of treatment of lead metal with copper oxide nanoparticles is given in Figure 15.

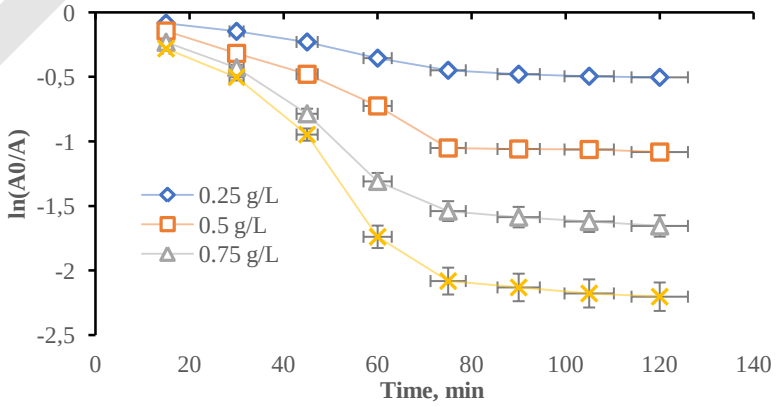

Figure 15. Photo degradation time profile of A_t/A_0 for lead metal

Conclusions

To sum up, it can be concluded that the study confirms the green synthesis of copper oxide nanoparticles using aqueous root extract of *Schrebera swietenioides* Roxb. The synthesized nanoparticles have been characterized and it was proved the particles were nano-sized and contained high metal percentage. The obtained nanoparticles were effective in the photo catalytic degradation of various carcinogenic pollutant dyes and metals and they can be used in the photo catalytic reduction of various pollutant dyes and metals, such as Sudan red (III), Azure A and lead metal) and were proven to be effective. The synthesized copper nanoparticles were found to be stable up to five cycles of the photo catalytic reduction process in all the dyes and metal in the study.

Acknowledgments

The authors of the article are thankful to Siddhartha Academy for providing the research facilities.

References

1 Shahid, M., Dumat, C., Khalid, S. et al. (2017). Foliar heavy metal uptake, toxicity and detoxification in plants: a comparison of foliar and root metal uptake. *J Hazardous Mater, 325*, 36–58. https://doi.org/10.1016/j.jhazmat.2016.11.063

2 Pal, G., Rai, P., & Pandey, A. (2019). Chapter 1 — Green synthesis of nanoparticles: a greener approach for a cleaner future. In: Shukla AK, Iravani (eds.). *Characterization and applications of nanoparticles SBT-GS micro and nano technologies*, Elsevier, Amsterdam, 1–26. https://doi.org/10.1016/B978-0-08-102579-6.00001-0

3 Gahlawat, G., & Roy, C. A. (2019). A review on the biosynthesis of metal and metal salt nanoparticles by microbes, *RSC Adv, 9*(23), 12944–12967. https://doi.org/10.1039/c8ra10483b

4 Iravani, S. (2011). Green synthesis of metal nanoparticles using plants. *Green Chem, 13*, 2638–2650. http://dx.doi.org/10.1039/c1gc15386b

5 Singh, J., Kumar, V., Kim, K. H., & Rawat M. (2019). Biogenic synthesis of copper oxide nanoparticles using plant extract and its prodigious potential for photocatalytic degradation of dyes. *Environmental research, 177*, 108569. https://doi.org/10.1016/j.envres.2019.108569

6 Ismail, N. A., Shameli, K., Che, J. N. W., Rasit, A. R., Mohamad, S. N. A. & Mohamed, I. E. D. (2021). Preparation of Copper Nanoparticles by Green Biosynthesis Method: A Short Review. *IOP Conf. Series: Materials Science and Engineering, 1051*, 012084. https://doi.org/10.1088/1757-899X/1051/1/012084

7 Ananda, M. H. C., Buzuayehu, A., Prakash, C. H. & Kumar, S. (2018). A Review on Green Synthesis of Cu and CuO Nanomaterials for Multifunctional Applications, *Mat Sci Res India, 15*(3), 279–295. http://dx.doi.org/10.13005/msri/150311

8 Elsy, R. L. V., Hortensia, O. O., Gregorio, C. P., Karim, A. R., Marcelino, C. F., Adalberto, B. M. & Antonio, J. M. (2018). Application of Copper Nanoparticles Increases the Fruit Quality and the Content of Bioactive Compounds in Tomatoes. *Appl Sci, 8*, 1020. https://doi.org/10.3390/app8071020

9 Kandasamy, S., Anbazhagan, S., Arokia, V. A. M., Hu, X., & Myeong, H. W. (2020). Physical and bioactivities of biopolymeric films incorporated with cellulose, sodium alginate and copper oxide nanoparticles for food packaging application. *International Journal of Biological Macromolecules, 153*, 207–214. https://doi.org/10.1016/j.ijbiomac.2020.02.250

10 Ghosh, M. K., Sahu, S., Gupta, I. & Ghorai, T. K. (2020). Green synthesis of copper nanoparticles from an extract of Jatropha curcas leaves: characterization, optical properties, CT-DNA binding and photocatalytic activity. *RSC Adv, 10*(37), 22027–22035. https://doi.org/10.1039/d0ra03186k

11 Suresh, C. M., Anita, D., Chanda, K. G., & Rohini, T. (2020). Green synthesis of copper nanoparticles using Celastrus paniculatus Willd. leaf extract and their photocatalytic and antifungal properties. *Biotechnology Reports, 27*, 00518. https://doi.org/10.1016/j.btre.2020.e00518

12 Peddi, P., Rao, P., Rani, N. U., & Lakshmi Tulasi, S. (2021). Green synthesis, characterization, antioxidant, antibacterial, and photocatalytic activity of Suaeda maritima (L.) Dumort aqueous extract-mediated copper oxide nanoparticles. *J Genet Eng Biotechnol., 19*, 1–11. https://doi.org/10.1186/s43141-021-00229-9

13 Siddique, M., Fayaz, N., & Saeed, M. (2021). Synthesis, characterization, photocatalytic activity and gas sensing properties of zinc doped manganese oxide nanoparticles. *Physica B: Condensed Matter, 602*, 412504. https://doi.org/10.1016/j.physb.2020.412504

14 Khan, I., Saeed, K., & Khan, I. (2019). Nanoparticles: Properties, applications and toxicities. *Arabian Journal of Chemistry, 12*(7), 908–931. https://doi.org/10.1016/j.arabjc.2017.05.011

15 Kulkarni, N., & Muddapur, U. (2014). Biosynthesis of metal nanoparticles: a review. *J. Nanotechnol*, 510246. https://doi.org/10.1007/978-3-642-18312-6_3

16 Mohammod, A., Leong, M. K., & Wong, H. L. (2017). Green synthesis of copper oxide (CuO) nanoparticles using banana peel extract and their photocatalytic activities. *AIP Conference Proceedings, 1828*, 020016. https://doi.org/10.1063/1.4979387

17 Shraddha, P., Sridevi, H., Thivaharan, V., Ramesh, V. & Raja, S. (2019). Photocatalytic zinc oxide nanoparticles synthesis using Peltophorum pterocarpum leaf extract and their characterization. *Optik, 185*, 248–255. https://doi.org/10.1016/j.ijleo.2019.03.101

18 Ozge, C., Emre, N., Umut, K., Sirous, K. A., Cleva, W. O. & Havva, Y. A. (2020). Synthesis of stable gold nanoparticles using linear polyethyleneimines and catalysis of both anionic and cationic azo dye degradation. *Mater. Adv, 1*, 2407–2417. https://doi.org/10.1039/d0ma00404a

19 Khoso, W. A.., Haleem, N., Baig, M. A. et al. (2021). Synthesis, characterization and heavy metal removal efficiency of nickel ferrite nanoparticles (NFN's). Sci Rep, 11, 3790–3799. https://doi.org/10.1038/s41598-021-83363-1

Information about authors*

Tulasi, Lakshmi S. (*corresponding author*) — Assistant Professor, Department of Freshman Engineering, PVP Siddhartha Institute of Technology, Kanuru-52007, Vijayawada, Andhra Pradesh, India; e-mail: tulasi13111986@gmail.com; https://orcid.org/0000-0001-6130-7215;

Sumalatha, P. — Assistant Professor, BS&H Department, Seshadri Rao Gudlavalleru Engineering college, Gudlavalleru. Andhra Pradesh, India; e-mail: sumasobhan@gmail.com; https://orcid.org/0000-0001-7230-4976

Rani, Nannapaneni Usha — Assistant Professor Dept. of Freshman Engineering, PVP Siddhartha Institute of Technology, Kanuru, 52007 Vijayawada, Andhra Pradesh, India. e-mail: nannapaneniusharani73@gmail.com;

Peddi, Pavani — Assistant Professor, Department of Freshman Engineering, PVP Siddhartha Institute of Technology, Kanuru-520007 Vijayawada, Andhra Pradesh, India, e-mail: pavanipeddi7@gmail.com; https://orcid.org/0000-0003-0712-8907

*The author's name is presented in the order: *Last Name, First and Middle Names*